HYDROGENATION AND DEHYDROGENATION CHARACTERISTICS OF ELECTRODEPOSITED MG-AL ALLOYS

By

MAHESH TANNIRU

A DISSERTATION PRESENTED TO THE GRADUATE SCHOOL
OF THE UNIVERSITY OF FLORIDA IN PARTIAL FULFILLMENT
OF THE REQUIREMENTS FOR THE DEGREE OF
DOCTOR OF PHILOSOPHY

UNIVERSITY OF FLORIDA

2009

To Family

ACKNOWLEDGMENTS

I would like to sincerely express my gratitude and appreciation for my advisor, Dr. Fereshteh Ebrahimi, for her constant encouragement and thought-provoking ideas that helped me in the development of this dissertation. Her enthusiasm towards research, the time and energy she spends on each student to develop their project was always a source of motivation for me to progress in my research.

I thank all my committee members, Dr. Sinnott, Dr. Bourne, Dr. Singh, Dr. Slattery and Dr. Wu for their interest and expert advice towards my research. Special thanks are due to Dr. Slattery for conducting part of the experiments carried out in this dissertation at Florida Solar Energy Center. I am grateful to Dr. Wu for providing me the necessary equipment to build an experimental set up at University of Florida. The support provided by Dr. Bourne for carrying out TEM characterization, sample preparation using FIB and discussions about the research is invaluable. I express my sincere thanks to Dr. Bourne for his time and co-operation. Meetings with Dr. Craciun, Dr. Jacob Jones, Dr. Nino to discuss the XRD results were very helpful in carrying out this research and I thank them for their co-operation. The generosity of Dr. Jacob Jones to help me conducting experiments on the Insitu-XRD in his laboratory is appreciated.

Many thanks are due to Wayne, Kerry and Dr. Dempere for their sincere suggestions regarding the characterization techniques and their timely help in carrying out the analysis using EPMA, HRTEM. The characterization facilities provided by MAIC at University of Florida are greatly appreciated. I am grateful to my master's advisor Dr. Devesh Misra, at University of Louisiana for his continued support and motivation during my graduate study. Particularly his strong will towards research and welfare of the students working in his group is incredible. I take this opportunity to thank him for introducing me to research in materials science and providing me an opportunity to learn various new techniques.

I would like to thank Dr. Ebrahimi's former and current group members: Dr. Tatiparti, Dr. Wang, Dr. Rios, Dr. Damian, Mike, Ian, Sonalika and Daniel for being helpful and providing a wonderful working environment. I take this moment to thank all the friends I have made during the graduate study at University of Florida and University of Louisiana. Dr. Ganesan, Dr. Behera, Dr. Nerikar, Dr. Katira, Dr. Omar, Harish, Badri, Dr. Pramanick, Dr. Aidhy, Dr. Ravinuthala, Dr. Kannan, and Pravin to name a few. Special thanks to Soujanya Ponnada (sony), BV Srikanth, Janardhan Singaraju and all other friends in India and other parts of the world for their support throughout these years. Lastly but not the least, I would like to express my sincere love and gratitude to my parents, brother, sisters, sister in law, and brother in law for their blessings, inspiration and continued support, without which this work would be impossible. This project is funded by NSF under the contract number: DMR-0605406.

TABLE OF CONTENTS

page

LIST OF TABLES

LIST OF FIGURES

Abstract of Dissertation Presented to the Graduate School
of the University of Florida in Partial Fulfillment of the
Requirements for the Degree of Doctor of Philosophy

HYDROGENATION AND DEHYDROGENATION CHARACTERISTICS OF ELECTRODEPOSITED MG-AL ALLOYS

By

Mahesh Tanniru

December 2009

Chair: Fereshteh Ebrahimi
Major: Materials Science and Engineering

Magnesium hydride with theoretical hydrogen capacity of 7.6wt% is one of the promising solid-state hydrogen storage materials. However, the main shortcoming of this hydride is its high hydrogen release temperature owing to its large negative energy of formation. Alloying of magnesium to form either solid solutions or intermetallic compounds is one of the solutions for reduction of the thermodynamic stability of MgH_2. In this study, we have fabricated Mg-Al alloy powders with low Al content via electrodeposition route and coated the powders with Ni as catalyst. To investigate the effect of Al addition on de/hydrogenation characteristics of electrodeposited powders, experiments were carried out in the temperature range of 180-400ºC.

The results of pressure composition isotherms developed under equilibrium conditions and temperatures at and above 300ºC elucidated that the enthalpy of formation/dissociation is not significantly changed by the addition of Al. Detailed microstructural and chemical analyses revealed that Al is rejected by the MgH_2 upon its formation from hcp-Mg during hydrogenation at high temperatures. The lack of influence of alloying on the stability of MgH_2 formed under equilibrium conditions is attributed to the absence of Al in its structure.

Hydrogen absorption tests under 1 MPa pressure at low temperatures in the range of 180-280ºC illustrated that under non-equilibrium conditions Al is trapped in the MgH_2 phase. The

desorption of hydrogen in Al containing hydride was found to take place in 2 stages; in the temperature ranges of 90-150ºC and 250-320ºC, respectively. These results suggest that the entrapment of Al destabilizes MgH_2 and hence hydrogen can be released at much low temperatures. Detailed analysis of microstructure suggests that the release of hydrogen in 2 stages is associated with the inhomogeneous distribution of Ni catalyst on the surface of the particles. Addition of Al to hcp-Mg reduced the total capacity of the hydrogen absorbed in the powder. Furthermore, the kinetics of hydride formation is high initially but slowed down due to the diffusion of Al in hcp-Mg. Interestingly, a phenomenon of hydrogen absorption at low temperatures (40-100ºC) is noticed in Mg-Al alloy powders and is attributed to the porosity present in the powder.

CHAPTER 1
INTRODUCTION

Over the past two centuries the major source of energy for the humankind has been based on fossil fuels like coal, crude oil, and natural gas. The continuous increase in demand for fuels along with a limited reserve of fossil fuels has led researchers to focus on alternative sources of energy [1]. Transportation sector is a major consumer of fossil fuels [2]. Fuel cells are one of the promising technologies that can be used in the transportation sector [3]. Among the various fuel cells available, the proton exchange membrane (PEM) fuel cells based on hydrogen oxidation are ideal for the on-board vehicular applications due to their operational conditions [2]. The major issue faced by this technology is to find a means of storing hydrogen and significant research is being carried out to address this issue [4].

Hydrogen can be stored on-board of vehicles either in gaseous, liquid or solid form [2, 5]. However, when stored in gaseous form its volumetric capacity is very low and safety is also an important issue as hydrogen should be compressed to higher pressures to store enough volume [6, 7]. Liqudification of hydrogen is not economically feasible as it needs to be cooled below -251°C [6]. Hence, hydrogen absorbed in a solid material is considered to be a viable solution for storing hydrogen on-board of vehicles [8]. Among the various materials available for hydrogen storage, metal hydrides or complex metal hydrides offer several advantages like high gravimetric and volumetric capacities [9].

Hydrogen reacts with almost all metals and forms metal hydrides [10]. However, alkali metals and alkaline earth metals like aluminum and magnesium offer high gravimetric capacity of hydrogen due to their low density [11]. Magnesium hydride with theoretical gravimetric capacity of 7.6 wt% is one of the ideal hydrides that can be used for hydrogen storage application. The major drawback of MgH_2 is its high thermodynamic stability (enthalpy of

formation of -76kJ/molH_2) and hence requires high temperature of about 350°C to release hydrogen [12-14]. In addition, the hydrogen absorption and desorption kinetics are also slow for MgH_2 [14, 15]. Several solutions have been proposed to surmount these challenges [9, 16]. Alloying has been identified as a potential mechanism for improving the hydrogen release temperature of magnesium hydride. For example, an experimental study on Mg-Ni alloys has revealed that the dehydrogenation temperature is decreased from 320°C to 250°C owing to alloying with Ni [17]. Theoretical calculations have shown that alloying of MgH_2 with certain metals can reduce the Mg-H bond strength and lowers its enthalpy of formation and dissociation [18].

The kinetics of hydrogen absorption and desorption in Mg-based alloys are improved by adding catalysts, fabricating materials with nanostructure, and/or creating high surface area to volume ratio powders [19-21]. It is shown that addition of catalysts helps in the dissociation of hydrogen molecule, which is one of the rate limiting steps during the hydrogenation process [22]. Nanocrystalline materials offer faster paths for diffusion and it is reported that a Mg-5mol%Pd material with 30nm grain size absorbed ~ 6 wt% hydrogen while the same material with 1 μm grain size absorbed only 0.2 wt% of hydrogen in 120 minutes [23]. Thus, from the above discussion it can be concluded that nanocrystalline MgH_2 with a suitable alloying element that can reduce its stability plus some catalyst for faster hydrogen absorption/desorption kinetics will be an ideal candidate for storage of hydrogen.

Aluminum when added as an alloying element to MgH_2 is calculated to have significant destabilizing effect on the Mg-H bond strength [24]. The light weight nature of Al also helps in retaining the gravimetric capacity of hydrogen in MgH_2 [25]. Additionally, the high thermal conductivity of Al is advantageous during the desorption of hydrogen as it involves heat transfer

and its affinity towards oxygen also protects Mg from forming MgO, which is very detrimental to the dissociation/recombination of hydrogen [26]. Due to the low solubility of Al in hcp-Mg phase below 300°C, alloys of Mg-Al with high concentration of Al form the intermetallic compound $Mg_{17}Al_{12}$ which is very stable. This intermetallic phase requires high temperatures (> 300°C) to absorb hydrogen [27]. In addition, the total capacity of hydrogen reduces with increasing the Al content as it does not form the hydride to store hydrogen. Therefore, with all these advantages, nanocrystalline powder of Mg with small amounts of Al is a potential material for hydrogen storage in PEM Fuel cells. Despite the apparent benefits of Al addition to Mg, limited work has been reported on this system. Most of the hydrogenation studies conducted on Mg-Al powders are for the compositions close to that of intermetallic compounds of Al_3Mg_2 and $Mg_{17}Al_{12}$, which require high temperatures for hydrogenation due to their high stability [25, 28-30]. Although theoretical calculations suggest that the incorporation of Al in MgH_2 structure should significantly reduce the stability of this hydride [30], no experimental verification of this phenomenon has been conducted. In addition, there have been no reported studies on the microstructural evolution during the hydrogenation and dehydrogenation processes. Based on the discussion so far, there is a need for a fundamental understanding of the hydrogenation and dehydrogenation characteristics of Mg-Al alloy powders.

The objective of this study was to investigate the effect of Al addition on the hydrogenation and dehydrogenation characteristics of hcp-Mg. The Mg-Al alloy powders can be synthesized using various techniques like ball milling and rapid solidification [31-33]. In our group we have been able to fabricate nanocrystalline Mg-Al alloys. This method can produce relatively pure alloy powders when compared to other processes such as ball milling [34]. In addition, it has been shown that the morphology, composition and microstructure of the alloys

can also be controlled using this technique [34]. A commercially available pure Mg powder was also studied to understand the effect of Al addition.

The hydrogen absorption and desorption characteristics of electrodeposited Mg-Al and pure Mg powders were evaluated using two methods. The thermodynamic properties of enthalpy and entropy were measured by developing Pressure Composition Temperature (PCT) curves under equilibrium conditions at different temperatures in the range of 300-400°C. High temperatures were chosen to dissolve Al in the hcp-Mg phase and thereby understand the effect of Al addition on the enthalpy and entropy of hydride formation/dissociation. The hydrogen absorption behavior of both the Mg-Al and pure Mg powders below 300°C were evaluated using an in house built absorption unit. The hydrogen release temperature for the powders was established using a Thermogravimetric analyzer (TGA). X-ray diffraction (XRD), scanning electron microscopy (SEM), energy dispersive spectroscopy (EDS) were employed to investigate the various phase transformations, to understand microstructural evolution and to conduct compositional analysis at different stages of hydrogenation tests, respectively. Precise compositional measurements were made using Electron Probe Micro Analyzer (EPMA) to identify the concentration of Al in different phases. The initial microstructure of both the pure Mg and Mg-Al powders was characterized using the transmission electron microscopy (TEM).

In this dissertation, Chapter 2 presents the relevant background and includes a brief overview of the fundamentals of hydrogenation and dehydrogenation experiments employed to study materials along with the fabrication techniques and the characteristics of Mg-Al alloy powders before and after hydrogenation tests. The experimental details of the fabrication of alloy powders and the different hydrogenation tests carried out in this study are reported in Chapter 3. Chapter 4 discusses the characteristics of the initial powders before hydrogenation. PCT curves

and the effect of Al addition on the thermodynamic stability of the MgH_2 are presented in the Chapter 5. Microstructural analyses, along with compositions of various phases at different stages of PCT curves for Mg-Al powders are discussed in this chapter. The hydrogenation and dehydrogenation studies of Mg-Al alloy powders as functions of time, temperature and composition along with the details of the microstructural evolution are presented in Chapters 6 and 7. An interesting phenomenon of hydrogen absorption at low temperatures and high pressures observed in the electrodeposited nanocrystalline Mg-Al powders is illustrated in Chapter 8. Finally, general conclusions that can be made out of this study along with the future outlook are made in Chapter 9.

CHAPTER 2
BACKGROUND

Among the various materials available, magnesium hydride (MgH_2) is considered to be one of the most attractive material for hydrogen storage for on-board vehicular applications due to its high hydrogen capacity and cheap cost [3, 9, 35]. However, the practical application of MgH_2 is mainly limited due to its high hydrogen release temperature [8]. Various studies have been carried out to improve the hydrogen absorption and desorption properties of magnesium [14, 21, 36-38]. In particular, the alloying of MgH_2 with different metals is explored as a solution to reduce its thermodynamic stability [38]. Furthermore, new fabrication techniques like high energy ball milling have been developed to synthesize nanocrystalline structures that improve the kinetics [39, 40]. Even though, efforts have been carried out in improving the properties of MgH_2, the practical realization of this material is still not achieved. Therefore, the hydrogenation and dehydrogenation characteristics of magnesium hydride are studied in this dissertation.

The goal of this chapter is to provide brief knowledge regarding the hydrogen absorption and desorption characteristics of magnesium hydride. Additionally, the properties of MgH_2, the fundamentals of various fabrication processes of materials and the details of various experimental techniques for assessing hydrogen storage behavior are also presented.

2.1 Characteristics of MgH_2

MgH_2 is an ionic compound and its structure under ambient conditions is tetragonal with a space group $P4_2/mnm$. A schematic diagram of the MgH_2 crystal along with its lattice parameters is illustrated in Figure 2-1 [41]. There exists a polymorph of MgH_2 at higher pressures (80 kbar) which is orthorhombic [42]. The calculated binary phase diagram for Mg-H system at 1 bar pressure of hydrogen is shown in Figure 2-2 [12]. According to the phase diagram, MgH_2 is stable up to a temperature of 288°C, which is very high for transportation application. Alloying

of magnesium hydride with various elements like Ni, Cu, Al, Ti, Fe etc. are reported to reduce the thermodynamic stability of MgH_2 and thereby lowering the dehydrogenation temperature [17, 25, 43-49]. First principles calculations of total energy and the heat of formation of the magnesium hydride alloyed with the different metals like Al, Ti, Ni, Fe and Cu have indicated that the bonding between the magnesium and hydrogen is weakened due to alloying [18, 50, 51]. Among all the alloying elements studied, addition of Al exhibited significant reduction in the heat of formation of MgH_2 (76 kJ/mol to 28 kJ/mol). In addition, Al has other beneficial properties like light weight, oxidation resistance, better heat conduction and cheaper compared to other alloying elements [26]. Therefore, the effect of Al addition on hydrogenation and dehydrogenation properties of Mg was carried out in this study. Since MgH_2 has very low solubility for many metals under equilibrium conditions, non equilibrium processing methods have been developed to produce these alloy powders [27].

2.2 Fabrication of Mg-Al Alloys

Earlier techniques of preparation of Mg based alloys include arc melting or induction melting of the alloying elements [8, 29, 52-54]. The Mg-30at%Al alloys were prepared by arc melting of the pure metals. Homogeneous alloys are prepared by using this method but it was observed that the composition of the alloy was difficult to control This was attributed to the high volatility of Mg at those temperatures [30]. In addition, milling of the final cast product was required as high surface area enhances the hydrogenation processes. Rapid solidification is another technique that was employed to produce high quality alloy powders but this technique also require a final step of ball milling to produce the powder [32].

Ball milling is a very common technique used to fabricate the magnesium based alloy powders [55-58]. Nanocrystalline phases along with enhanced solubility of alloying elements in Mg are created using this technique [19, 39]. These properties have been observed to have

significant impact on the hydrogenation of magnesium powders [19]. For example, it was observed that nanostructured pure Mg powder produced by ball milling showed significant improvement in hydrogen absorption kinetics than the microcrystalline powder as shown in Figure 2-3 [19]. Similar improvements are reported in alloy systems like Mg-Ni, Mg-Ti where supersaturated solid solutions or intermetallic compounds with nanostructure [45, 59]. These improvements in hydrogenation characteristics is attributed to the higher amount of grain boundaries and defects present in nanocrystalline materials which help in faster diffusion of hydrogen atoms [40]. Mg-Al alloy powders are also produced by ball milling. Previous studies on this system reported an increase in the solubility of Al in Mg [28, 60]. In addition, the kinetics of absorption was also observed to be faster than pure Mg powder [28]. Even though, ball milling offers significant advantages, it suffers with a few drawbacks. The powders produced by ball milling are contaminated by either oxides or milling materials. The process requires comparatively longer time, and the size of the powder is limited by the ball milling media [61]. From the above discussions it can be concluded that innovative techniques are required to produce the alloy powders with better hydrogenation characteristics.

Electrodeposition is another technique extensively used to synthesize nanomaterials [33, 62]. It offers several advantages over other methods of fabrication like production of high purity alloys, nanocrystalline powders and the composition of the alloy powders can be controlled effectively by changing the electrodeposition parameters [34, 63] . It is recently shown that Mg-Al alloy powders can be produced using electrodeposition with varied compositions [33]. This technique is applied in this research to synthesize the powders for hydrogenation studies.

2.3 Characteristics of Mg-Al Alloys

The equilibrium phase diagram of Mg-Al system is shown in Figure 2-3 [64]. Along with the terminal solid solutions of fcc-Al, hcp-Mg, intermetallic compounds of β-Al_3Mg_2, γ-

$Mg_{17}Al_{12}$, the line compound R (composition 42at%Mg) are the phases present in the Mg-Al alloy system. The solubility of Al in hcp-Mg and Mg in fcc-Al under equilibrium conditions is very less. In addition both the intermetallic compounds present in Mg-Al system exhibit a solubility range for Al. As most of the processing techniques employ non-equilibrium conditions, the characteristics of the alloys vary in each sample.

Ball milling of Mg and Al powders in the proportion of 90:10 indicated that $Mg_{17}Al_{12}$ phase forms after short time of ball milling. Further increase in milling time increased the ratio of the $Mg_{17}Al_{12}$ phase to hcp-Mg phase up to 3 hours of milling and remained constant above that time period [28]. The lattice parameter of hcp-Mg decreased with increase in milling time demonstrating increased Al solubility. This increased Al content in the initial raw materials also increased the $Mg_{17}Al_{12}$ phase content [28]. An arc melt sample with 30at% Al exhibited both the hcp-Mg and γ-$Mg_{17}Al_{12}$ intermetallic phases in the fabricated powders [65]. Bulk metallic alloying is another technique which was employed to produce the Mg-Al powders [66-68]. The hcp-Mg and the $Mg_{17}Al_{12}$ intermetallic phases were identified in the fabricated powders with low amount of Al. However, these phases were produced at a shorter processing time when compared to the other studies [68].

A detailed investigation of microstructural analysis of the hcp-Mg rich alloy powders using electron microscopy indicates that the γ-$Mg_{17}Al_{12}$ precipitate can form either continuously inside the grains or discontinuously along the defects like grain boundaries [69]. Several orientation relationships were predicted to exist between the γ-$Mg_{17}Al_{12}$ and hcp-Mg [70, 71]. However, only a few diffraction patterns of the phases showing the orientation relationship were presented [71]. In one particular study the morphology of $Mg_{17}Al_{12}$ phase was shown to be either rod or lath in shape using the HRTEM [69]. It was observed that the morphology was dependent on the

orientation of the phase. High resolution TEM studies along with micro diffraction carried out on the alloy AZ91 (composition Mg-9Al-1-Zn-0.3 Mn) illustrated that the primary orientation relationship between $Mg_{17}Al_{12}$ phase and hcp-Mg phase is $(011)_{\gamma}//(0001)_{\alpha}$, $[1\text{-}11]_{\gamma}//[2\text{-}1\text{-}10]_{\alpha}$. which corresponds to the burgers relationship [69]. These precipitates formed after 8 hours of aging treatment at 200°C were observed to be extremely fine of about 25-50 nm in width to 100-150 nm in length. Convergent Beam Electron Diffraction (CBED) or the microdiffraction was used to identify the orientation relationships due to the large lattice parameters of the γ-$Mg_{17}Al_{12}$ phase.

From the above studies it can be concluded that due to low solubility of Al in hcp-Mg, the stable γ-$Mg_{17}Al_{12}$ phase is formed during the processing of Mg-Al alloy powders. However, by employing the non-equilibrium processes the solubility of Al in hcp-Mg can be increased to an extent higher than that of predicted by the equilibrium phase diagram.

2.4 Pressure Composition Isotherms in Metal Systems

Pressure Composition Temperature (PCT) curves are important sources of fundamental information related to thermodynamic properties of metal hydrides. The thermodynamic properties, namely enthalpy and entropy of formation/dissociation, can be calculated using the PCT curves developed at different temperatures. Sufficient time is provided during the development of PCT curve to achieve near equilibrium conditions.

A schematic diagram of a general PCT curve is shown in Figure 2-4. The line AB represents the maximum solubility of hydrogen in the material. After the material is saturated with hydrogen, increase in pressure results in nucleation of hydride. In an ideal case, at a given temperature and for a pure metal-hydrogen system, the formation/dissociation of metal hydride should occur at a constant pressure according to the Gibbs phase rule [6]. This region is observed

as the plateau BC in Figure 2-4. This constant pressure of hydride formation is defined as equilibrium plateau pressure as it is denoted by a plateau region on the PCT curve. Furthermore, both the equilibrium plateau pressure of formation/dissociation of metal hydride should be same theoretically, but almost all PCT curves reported in the literature show a hysteresis, indicating that the plateau pressures are different [47, 72]. At the end of the plateau region, increasing the pressure during experiment raises the pressure of the system without any further or little absorption of hydrogen into the material, as the material is completely saturated with hydrogen. The metal hydride phase generally being ionic in nature, it exhibits very low solubility for hydrogen.

Figure 2-5 shows the effect of temperature on the PCT curves. With the increase in temperature the solubility and the equilibrium plateau pressure of hydride formation increases. After a certain temperature, defined as critical temperature, increase in temperature causes the plateau region to disappear and the α solid solution of hydrogen in metal continuously transform into MgH_2 phase.

Hysteresis in the PCT curves is not well understood. Several models have been developed previously to explain the hysteresis in the powders [73-76]. They attribute it to either the defects, in homogenities, compositional differences present in the material or to the elastic-plastic constraints that occur during the hydride formation. The large volume expansion during the hydride formation in metal-hydrogen systems cause the elastic or plastic constrains on the unreacted metal. These volume expansions frequently cause an irreversible process of plastic deformation and dislocation generation during the hydride formation. Therefore, the hydride fraction in all the particles is not the same during the absorption of hydrogen and depends on the particle size, defects and inhomogenities present in each particle. This causes pseudo equilibrium

during the experiment rather than a true equilibrium and thereby the absorption curve shows a sloping plateau. The opposite is true in desorption as the volume is contracted and hence it almost occurs at a constant pressure. Furthermore, the nucleation of metal hydride/metal during hydrogenation/dehydrogenation respectively may also cause the hysteresis in the PCT curve. As larger driving force is required during the nucleation of metal hydride, the plateau region starts at a slightly higher pressure than that of the equilibrium plateau pressure and hence this causes a hysteresis in the material. Similar is true when nucleation of metal is required during desorption.

The hysteresis was observed to be lower in the materials with nanocrystalline grains and is attributed to the significant defects and grain boundaries that are present in material that aid in the nucleation of phases [77]. However, most of the PCT curves are conducted at higher temperatures and under equilibrium conditions. Under these conditions the nanograins grow to a large extent and the effect of low hysteresis cannot be explained with respect to the interfaces. For example, PCT curves of pure Mg powder in milled and unmilled condition at 350°C are presented in Figure 2-6. It is observed that the equilibrium plateau pressure of formation is not affected significantly by milling while it is lower for unmilled powder during desorption. This signifies further the fact that the nanograins in the material does not contribute for the observed low hysteresis as the equilibrium plateau pressure of hydride formation is similar in both the materials. The other possible reason for the low hysteresis is the size of the particles rather than the grain size of the material used in this study. The higher surface area/volume ration in the milled particles when compared to the unmilled particles may be the reason for nucleation of Mg.

2.4.1 Determination of Enthalpy and Entropy from PCT Curves

The fundamental use of the PCT curve in hydrogen storage studies is to determine the enthalpy and entropy of the hydride formation/dissociation. The equilibrium plateau pressures of

hydride formation/dissociation are used to calculate these thermodynamic parameters (Figure 2-5). The pressure corresponding to the mid-plateau region is considered as the equilibrium plateau pressure. The relation between the pressure and the temperature is given by the Van't hoff equation:

$$\ln\left(P/P_0\right)=\frac{\Delta H}{RT}-\frac{\Delta S}{R} \tag{2-1}$$

where P is the plateau pressure of formation/dissociation, P_0 is the atmospheric pressure, ΔH is the enthalpy of hydriding/dehydring reaction, ΔS is the entropy of hydriding/dehydring reaction, T is the absolute temperature and R is the gas constant.

2.4.2 Effect of Addition of Alloying Elements on PCT Curve

Addition of alloying elements to pure metals increases the number components of the system. Due to this addition the PCT curve of the alloys is affected significantly as the number of phases and the components participating in the transformation change [16, 43, 78]. For example, PCT curves of Mg-35wt%$FeTi_{1.2}$ are shown in Figure 2-7. The plateau region which corresponds to the metal hydride formation was observed to show a significant slope when compared to that of pure metal [40]. This behavior of the hydride formation in metal alloys was attributed to the different phase distribution and composition of the alloys [40]. Furthermore, multiple plateaus were observed in some alloys with more than one phase as shown in Figure 2-8 [79]. These multiple plateau regions were explained in terms of hydride formation from various phases present in the initial alloy powders [25, 28, 79].

2.4.3 PCT Curves Developed for Mg-Al Alloys

A very few PCT curves of Mg-Al system are reported in the literature [21,27-29]. Most of the isotherms developed are for the compositions close to that of the intermetallic compounds $Mg_{17}Al_{12}$ and Al_3Mg_2. The isotherms developed for the Mg-Al alloys close to that of the

intermetallic compound $Mg_{17}Al_{12}$ exhibited either a sloping plateau or multiple plateaus depending on the initial composition of the material. The PCT curves developed for $Mg_{17}Al_{12}$ at high temperatures like 400°C did not illustrate a plateau region and the amount of hydrogen absorbed is also very low [28]. Although no direct Van't Hoff plot has been developed for a given Mg-Al alloy, the limited available equilibrium plateau pressures for various Mg-Al alloy compositions have been collected and plotted in reference [80]. The Van't hoff plot developed is shown in Figure 2-9 and the enthalpy calculated indicated similar values to that of the pure Mg powder.

In another study, PCT curves were developed for the intermetallic compound Al_3Mg_2 at different temperature as shown in Figure 2-10 [81]. Only one plateau region was observed in the PCT curve and the analysis after the hydrogenation indicated the presence of β-MgH_2 and fcc-Al in the alloy powders. The enthalpy of hydride formation calculated from the van't hoff plot developed from these PCT curves was about 62kJ/mol which was lower than the pure Mg [81].

Only one study reported a PCT curve for hcp-Mg alloy powder. The PCT curve developed at 400°C for Mg-10at%Al alloy powder is shown in Figure 2-11. A plateau region around 0.7 MPa pressure was observed in this alloy system and this region was followed by a slope with significant amount of hydrogen absorption. The equilibrium plateau pressure of this alloy was slightly higher than that of pure Mg powder studied under similar conditions. This alloy was not studied at different temperatures and hence no data about the enthalpy of hydride formation and dissociation were calculated.

2.5 Hydrogen (de)absorption Characteristics in Mg Based Alloys

Sorption studies of hydrogen in magnesium and its alloys were started as early as 1960 [11]. Since magnesium is light in weight, cheap in cost and posses high capacity for hydrogen,

tremendous research have been carried out to use it as a hydrogen storage material. In addition to high thermodynamic stability, the kinetics of absorption/desorption were the main concerns to employ it in fuel cell applications [82]. Several advancements and modifications to the microstructure were made to overcome these difficulties. The major breakthroughs that occurred to overcome these problems were addition of catalysts, creation of nanostructured material, and design of new alloys with Mg as primary constituent [21, 36]. Furthermore, new processing techniques were also developed to achieve one or more of these characteristics [19, 33, 83].

2.5.1 Addition of Catalyst

The sequence of steps taking place during hydrogenation is shown in Figure 2-12 [3]. Hydrogen molecule reaches the surface of the metal and breaks into two hydrogen atoms. These atoms chemisorb into the surface and diffuse into the bulk of the metal. When the metal reaches saturation at that temperature and pressure, the hydride nuclei are formed and grow. In case of Mg, the rate limiting step was observed to be the dissociation of hydrogen on the surface [21, 52]. Due to the high affinity for oxygen, Mg transforms to MgO even at low partial pressures of oxygen. The major processing techniques like ball milling, which produce the bulk Mg powders, contaminate the surface by poisoning with oxygen [61]. MgO is a stable compound and have high activation energy for breaking the hydrogen molecule into atoms [61]. Hence to enhance the dissociation of hydrogen molecule catalysts were added to Mg [20]. d-block transition metals and their compounds were considered as effective catalysts to break hydrogen molecule [21, 84, 85]. Since these metals are heavy and are added to aid the reaction, the amount of the catalysts is kept low so that the total gravimetric capacity of the material is not lowered significantly.

Some of the primary metals which are used as catalysts are Ni, Fe, Mn, Nb, V, Pd, Ti [20, 48, 86, 87]. It was observed that addition of 1at% Ni to Mg decreased the onset temperature of hydrogenation from 275 to 175°C and the hydrogenation capacity of the material was increased

by 50% in the same amount of time without catalyst [88]. Ball milling of Mg_2Ni, FeTi and $LaNi_5$ with Pd catalyst was reported to improve the kinetics of absorption even at much lower temperatures and maintain less sensitivity to air exposures [48]. A Mg-5at%V powder was observed to absorb 4.1wt% hydrogen at 200°C in 10 minutes while only 1wt% hydrogen was absorbed by pure Mg powder under the same conditions [86]. The effectiveness of the catalyst was observed to depend on its distribution on the surface, the surface area of the catalyst, amount of catalyst, and its chemical affinity towards hydrogen. These properties were optimized by changing the processing conditions of the powder. In addition, nano-catalysts of various metals were developed and the absorption kinetics of Mg powders was observed to increase ~ 2 fold by using these catalysts [40, 89]. Recently it was observed that other compounds of d-block metals are much better and effective catalysts than the pure metals [90-92]. In particular these catalysts were observed to help better during desorption of hydride. About 6 wt% of hydrogen was released from MgH_2 in 10 minutes at 300°C with the presence of Cr_2O_3 or Fe_3O_4 on the surface while conventional ball milled MgH_2 took about 50 minutes to release hydrogen [91]. DSC studies carried out on MgH_2-0.5mol% Nb_2O_5, Fe_3O_4, and ZrO_2 indicated that the dehydrogenation temperature is reduced by the addition of oxide catalysts as illustrated in Figure 2-13 [61]. In this study the onset temperature of hydrogen was observed to be the same irrespective of the catalyst, but the kinetics of desorption was highest when Nb_2O_5 was added. The advantages and disadvatages of the various alloying elements during hydrogenation/dehydrogenation processes were listed in Table 2-1.

It was shown theoretically that the d-block metals help in the dissociation of hydrogen molecule due to the interactions of d-orbital with the electrons in hydrogen molecule. This orbital interacts with the s-s electrons in the hydrogen molecule and forms an intermediate

hydride [85, 93]. For example, NiH is formed when hydrogen molecule was split and the hydrogen diffuses through Ni and interacts with Mg near the surface and gets chemisorbed. This is known as spill over mechanism [85]. Ab-initio calculations have shown that effectiveness of a catalyst on the MgH_2 surface was dependent on the d-orbital occupancy of the d-block metal added. If the d-orbital is unoccupied or highly occupied, the electrons are either donated from the bonding orbitals of Mg-H or received from the d-block metal and thereby weakening the Mg-H bond strength [22, 94]. In case of oxide catalysts a different theory is proposed regarding their catalytic effect. Since Mg has higher affinity towards oxygen, the catalytic oxides are partially reduced to lower stoichiometry oxides and a complex oxide of d-block metal, magnesium and oxygen is formed near the interface. The participation of Mg in forming the oxide creates a decrease in concentration of MgH_2 and several defects are formed making the hydride non stoichiometric. This reduces the bond-strength of Mg-H and improves the kinetics of desorption [61].

2.5.2 Microstructure

Increasing the surface area to volume ratio of the material, refining the grain structure into nanoscale and presence of second phase particles are some of the microstructural changes that lead to faster kinetics of hydrogen absorption [19, 40, 95]. Ball milling is generally employed to reduce the particle size [17, 49]. It is observed that milling the Mg particles with catalyst helps in better dispersion of the catalyst and lowers the particle size [49]. As illustrated in Figure 2-14, the kinetics of Mg were improved by reducing the grain size from micron size to 50 nm and further down to 30 nm [19]. In another study it was illustrated that the full capacity of 7.6wt% hydrogen can be achieved at 1 MPa pressure in ball milled powders hydrogenated at 300°C while unmilled powders absorb only about 6.1 wt% even at high temperatures like 400°C [2]. The faster kinetics was attributed to the easier diffusion of hydrogen atoms through the grain

boundaries and the interfaces produced during the milling. It was also shown that the strain created in the material may accommodate the volume expansion that was associated with the hydride formation and thereby increase the rate of hydrogen absorption in the material.

The diffusion of hydrogen through MgH_2 is very slow and hence the presence of precipitates inside the material may help in providing the interfaces that may act as path for diffusion of hydrogen [95]. For example, the kinetics of hydrogen absorption in Mg-Cu alloy was observed to be higher than that of the ball milled pure Mg. The particles in the Mg-Cu alloy consist of the intermetallic phase Mg_2Cu and are predicted to provide the required interfaces for hydrogen diffusion [95]. In addition, the intermetallic particles may also act as nucleation sites and can improve the rate of hydride formation.

2.5.3 Composition and Alloying

Alloying of magnesium with various metals like Ni, Fe, Al, Cu, Ti etc have been observed to modify the kinetics of hydrogen absorption and desorption [43, 72]. Several non-equilibrium processes have been developed to prepare the alloys of Mg as it has very little solubility for the most of the alloying elements under equilibrium conditions [27]. Another aspect that was studied during alloying is the hydrogenation behavior of intermetallic compounds that are formed between Mg and the other metals. Among the various intermetallic compounds of Mg alloy systems, Mg_2Ni is the most studied due to its better hydrogenation properties. It was also shown that alloying of Mg with small amounts Al, In and Ga can decrease the activation energy of hydrogenation and improve the sorption kinetics. Theoretical studies carried out on MgH_2 with different alloying systems have shown that the enthalpy of formation and dissociation was reduced [18]. This reduction in enthalpy was attributed to the interaction of alloying element with the Mg-H bond strength. Due to the different chemical affinity of the alloying element the interaction between the alloying element and hydrogen changes and hence the stability of the

crystal is changed. In addition, it is predicted that the difference in valency of the alloying element and Mg creates defects in the material which will help in the diffusion of the hydrogen and thereby the kinetics of hydrogen absorption and desorption of the material.

Al is one of the alloying elements that are predicted to reduce the enthalpy of hydride dissociation and improve the kinetics of hydrogen absorption and desorption. It is also proposed that Al can act as heat transfer medium during desorption due to its high thermal conductivity. In addition, the higher affinity towards oxygen renders the formation of MgO which hampers the kinetics of hydrogen absorption and desorption significantly.

2.5.4 Hydrogen Absorption/desorption Behavior of Mg-Al Alloys

The hydrogenation of Mg-Al powders was conducted in both bulk alloys and in thin films [31, 96]. Most of the experiments of hydrogenation in alloy powders of Mg-Al alloys were primarily conducted at high temperatures in the range of 300-400°C. The initial studies carried out on Mg-1at%Al and 4at%Al have suggested that the activation energy of the hydride formation was lowered at lower concentrations of Al while at higher concentrations they approached to that of pure Mg. The kinetics of hydrogen absorption in Mg-X at%Al (where, X= 10,75,42) at 400°C are shown in Figure 2-15 [28]. It can be noticed that the kinetics did not change significantly with addition of Al in these alloy powders at 400ºC. However, the activated samples of Mg-8mol%Al have shown significant improvement in the desorption kinetics as presented in Figure 2-16 [97]. At 300°C, the total hydrogen of about 5 wt% present in the Mg-8mol%Al was completely released within 300 seconds, while the hydrogen from pure MgH_2 released only about 2.5 wt% in 1500 seconds. Air exposed samples of pure MgH_2 and MgH_2 alloyed with Al (42at%Al) were studied for their dehydrogenation kinetics using insitu-XRD. The kinetics measured from the calculations of area under the XRD curves indicated that the

activation energy for the release of hydrogen is lowered in case of MgH_2-Al powders. This was attributed to the higher affinity of aluminum towards oxygen.

Hydrogenation studies of Mg-Al thin films indicated the formation of $Mg(AlH_4)_2$ a complex magnesium aluminum hydride when the composition of the film was about 33at%Mg. In this study the thin films in the whole range of compositions present in the phase diagram of Mg-Al system were deposited and capped with Pd. The hydrogenation results at 110°C under 1 bar pressure of hydrogen signified that MgH_2 was formed in the alloys with rich Mg contents and $Mg(AlH_4)_2$ was observed when the Al content was about 33at%.

Table 2-1. Advantages and disadvantages of alloying elements on stability of MgH_2.

Alloying element	Advantages	Disadvantages
Al	• Light weight • Good conductor of heat • Less oxide formation • Theoretical calculations predicted low enthalpy of hydride formation	• Low solubility • Forms intermetallic compounds $Mg_{17}Al_{12}$ and Al_3Mg_2 • Disproportionate reaction takes place.
Cu	• Can act as catalyst • Good conductor of heat • Forms intermetallic that enhances diffusion • Theoretical calculations predicted low enthalpy of hydride formation	• Heavy metal and reduces the capacity • Forms intermetallic in the 1st cycle and hence loses the catalyst activity
Ti	• Excellent catalyst • Destabilizes the Mg-H bond if present in the MgH_2 crystal lattice.	• Forms TiH_2 which requires higher temperature for hydrogen release • Low solubility in Mg • Forms intermetallic compounds.
Fe	• Good catalyst • Forms complex hydrides • Reduces the dehydrogenation temperature	• Heavy metal and reduces the capacity • Forms Mg_2FeH_6
Ni	• Excellent catalyst • Helps in hydride nucleation. • Forms Mg_2NiH_4 • Reduces dehydrogenation temperature	• Heavy in weight • Los solubility • Forms intermetallic compounds of Mg_2Ni and $MgNi_2$
V	• Excellent catalyst • Helps in hydride nucleation • Reduces dehydrogenation temperature	• Heavy in weight and reduces capacity • Low solubility • Forms VH_2 which is very stable
Nb	• Excellent catalyst • Helps in hydride nucleation • Changes the electronic structure in Mg-H bonding	• Heavy in weight and reduces capacity • Forms $NbH_{1.5}$ and reduces the catalytic activity

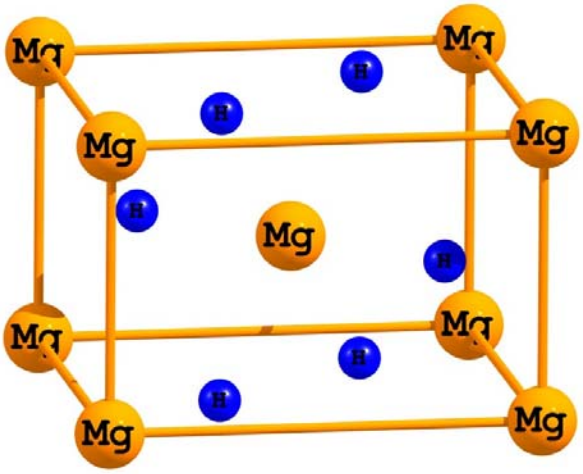

Figure 2-1. Schematic diagram of crystal structure of MgH_2.

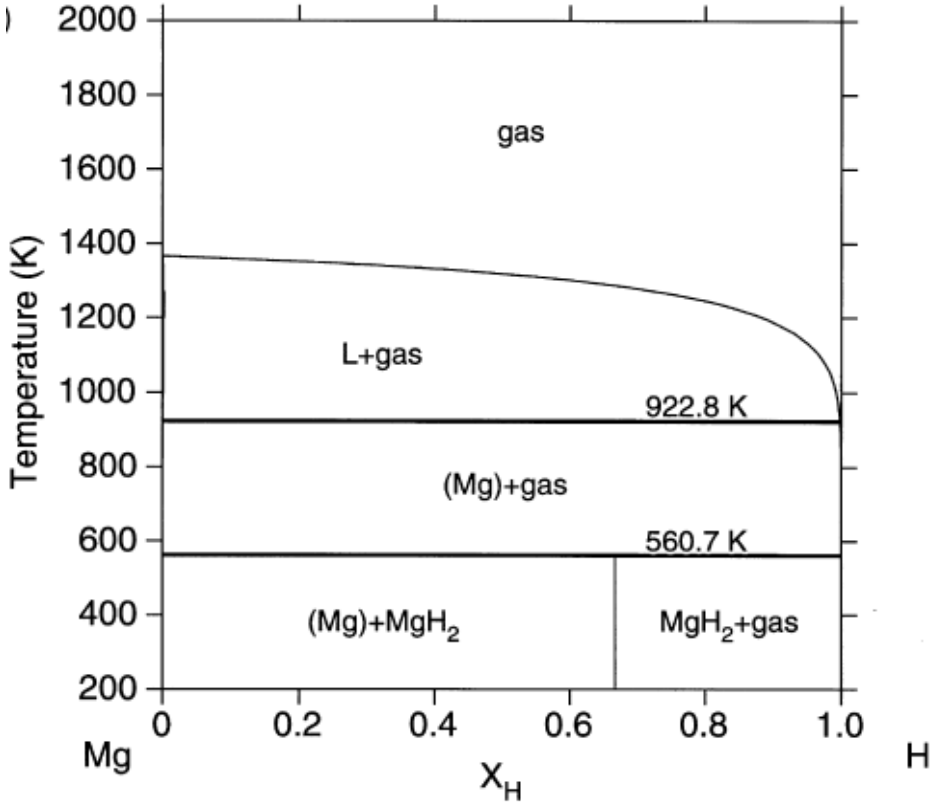

Figure 2-2. Binary Phase diagram of Mg-H system calculated at 1 bar pressure of hydrogen [reproduced from [12]].

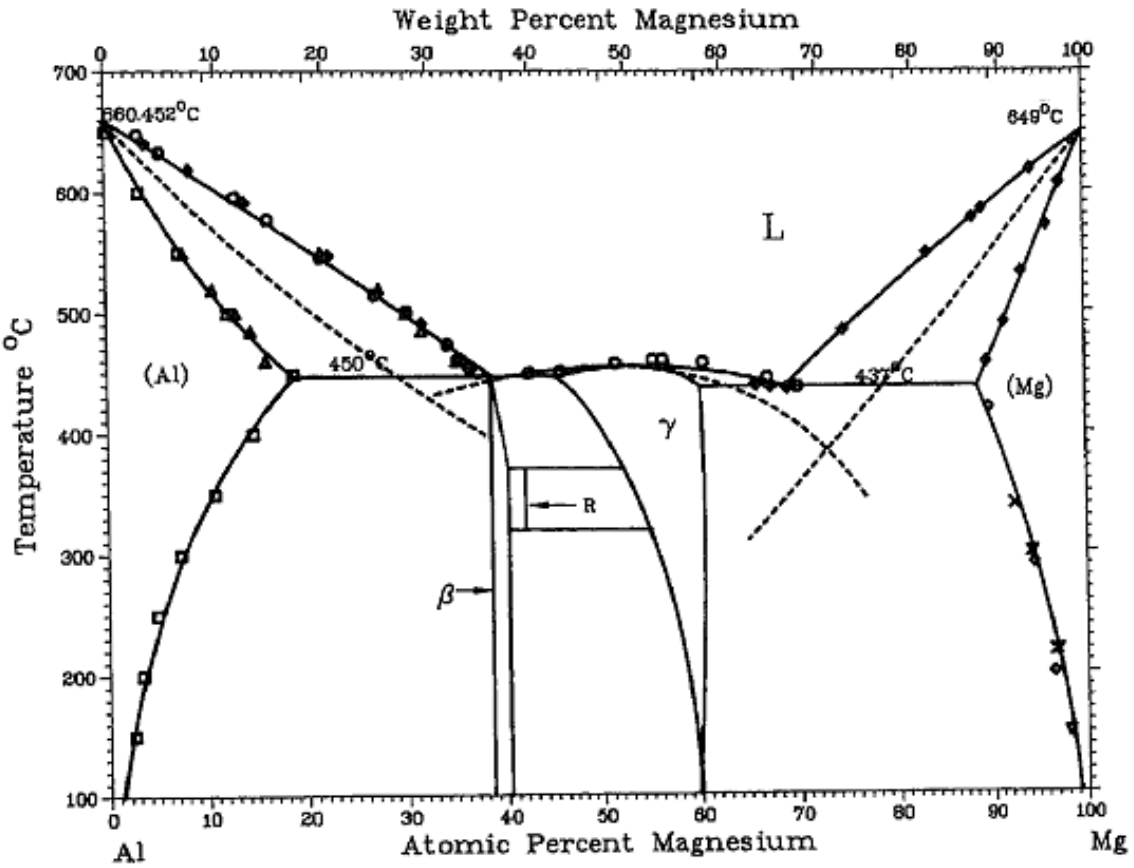

Figure 2-3. Binary phase diagram of Mg-Al system indicating the carious phases present in the system [reproduced from [64]].

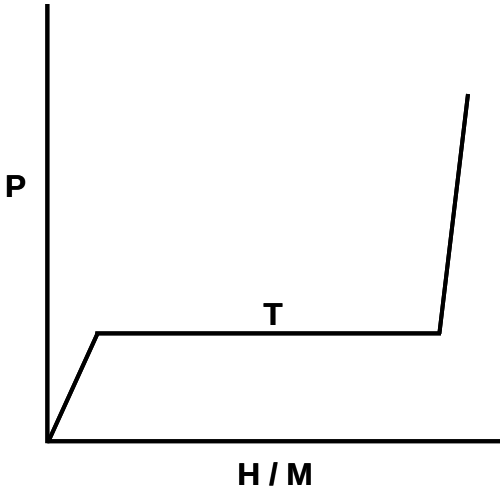

Figure 2-4. Schematic representation of a Pressure-Composition- Temeprature (PCT) curve.

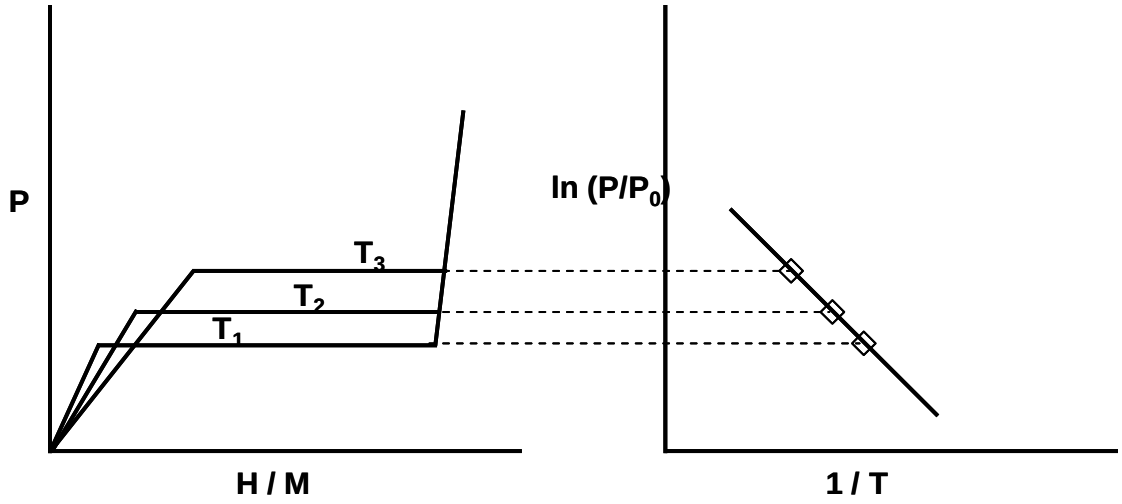

Figure 2-5. Schematic representation of PCT curve at different temperatures showing the effect of temperature on equilibrium plateau pressure and the development of van't hoff plot from different plateau pressures.

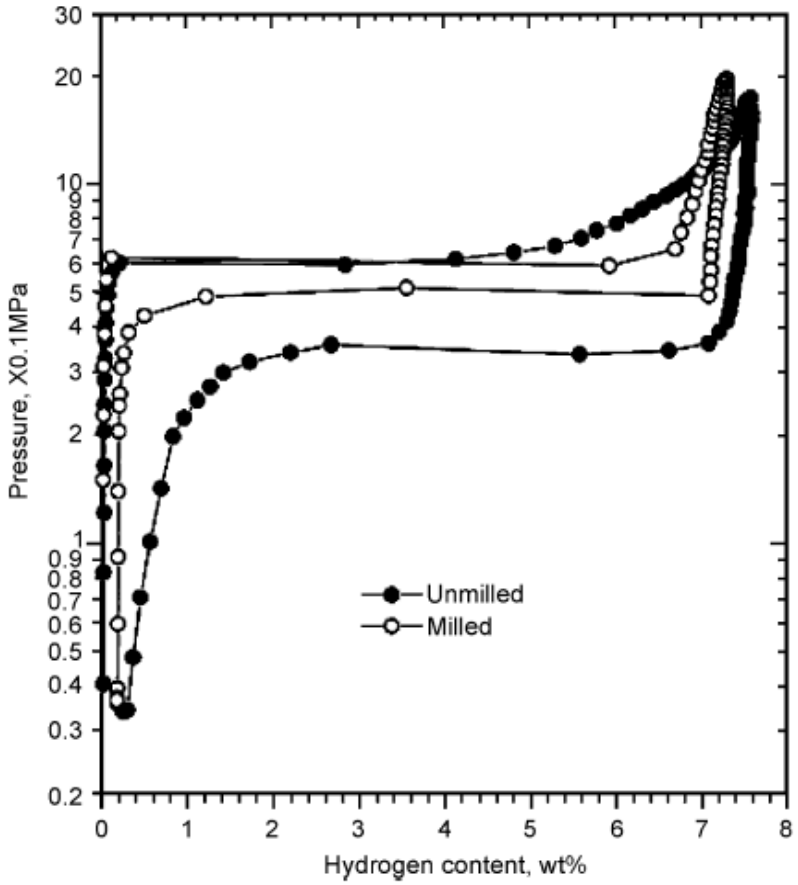

Figure 2-6. PCT curves of milled and unmilled Mg powders developed at 350°C demonstrating the differences in hysteresis observed in the material [reproduced from [98]].

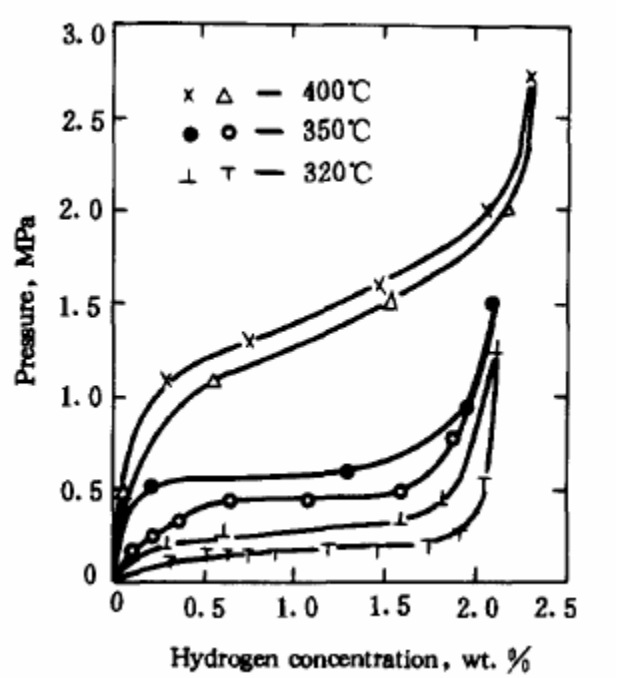

Figure 2-7. PCT curves of Mg-Fe alloy powders elucidating the effect of temperature on the shape of the PCT curve [reproduced from [16]].

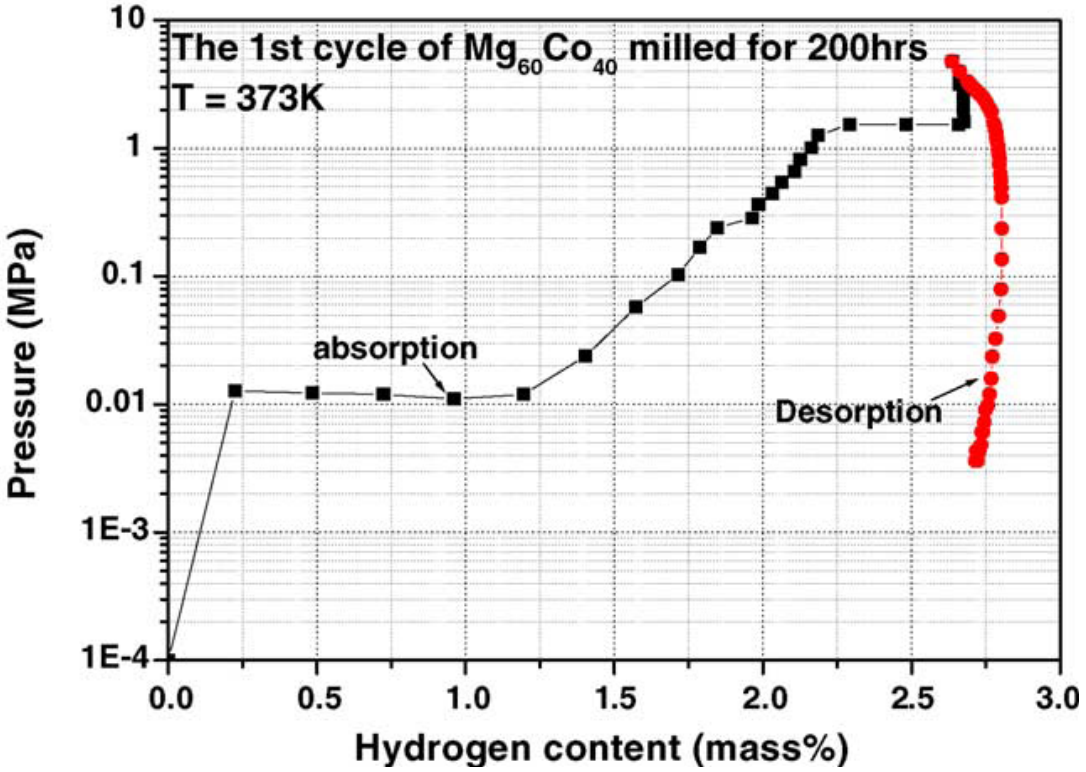

Figure 2-8. PCT curve of Mg-Co alloy powder at 100°C, indicating the multiple plateaus corresponding to the various phases present in the powder [reproduced from [79]].

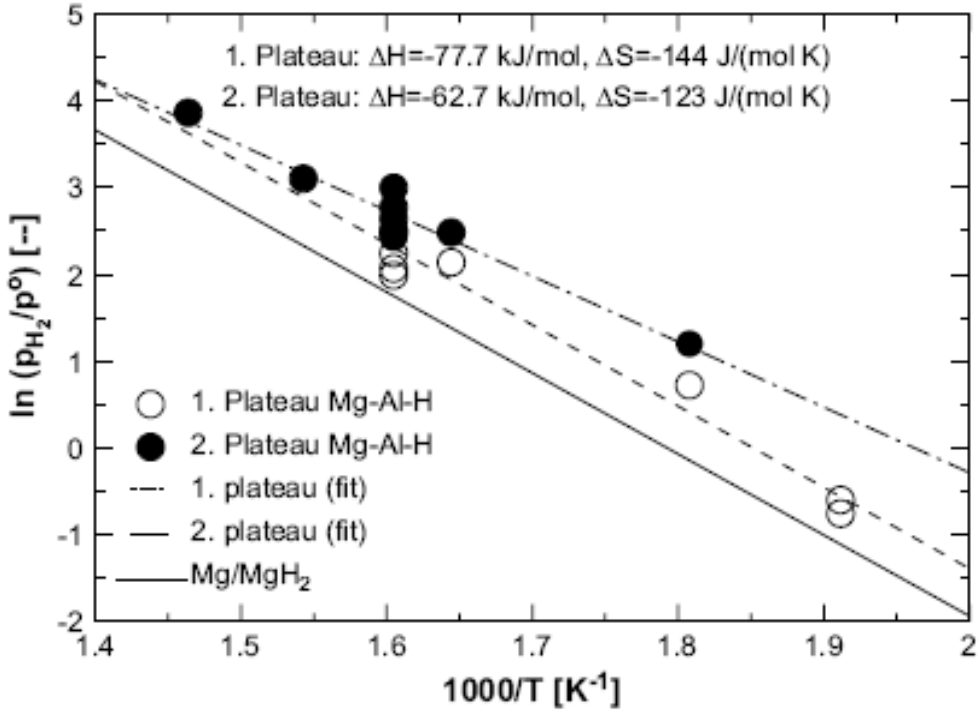

Figure 2-9. Van't hoff plot developed for Mg-Al alloys from various experiments [reproduced from [80]].

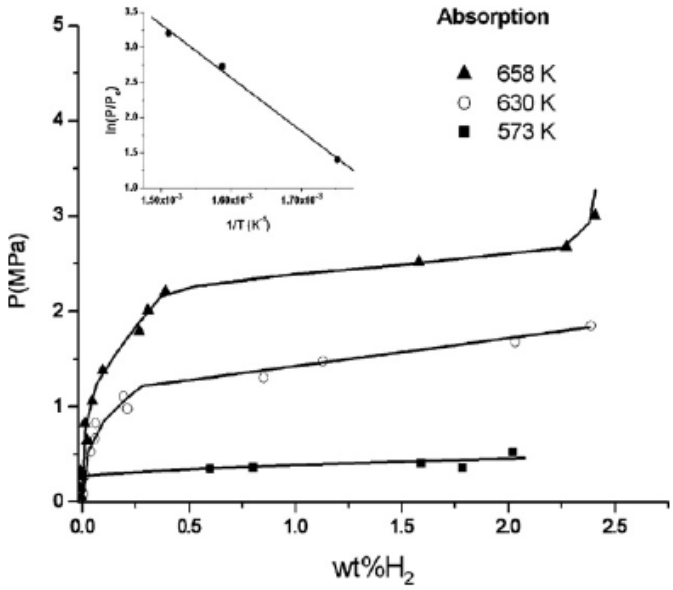

Figure 2-10. PCT curves of Al_3Mg_2 powder developed at different temperatures illustrating the change in enthalpy of MgH_2. The corresponding Van't Hoff plot can be seen in the inset [reproduced from [81]]

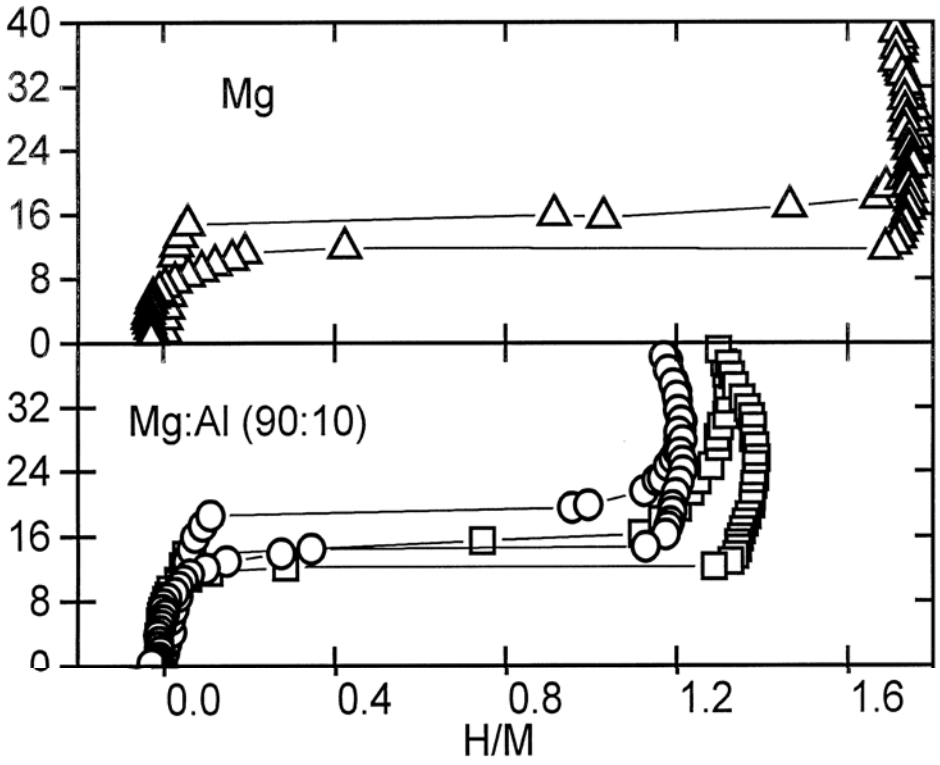

Figure 2-11. PCT curves of pure Mg and Mg-10at%Al (%Al= 50%, 42%) developed at 400°C revealing the rise in plateau pressure of Mg with the addition of Al [reproduced from [28]].

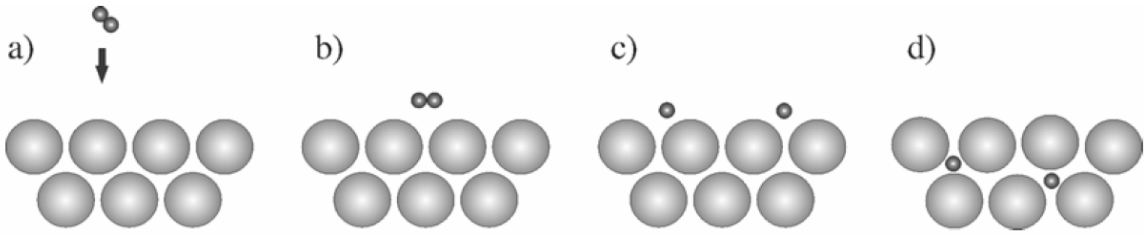

Figure 2-12. Schematic diagram of various stages that occur during the absorption of hydrogen in the metal and hydride formation [reproduced from [6]].

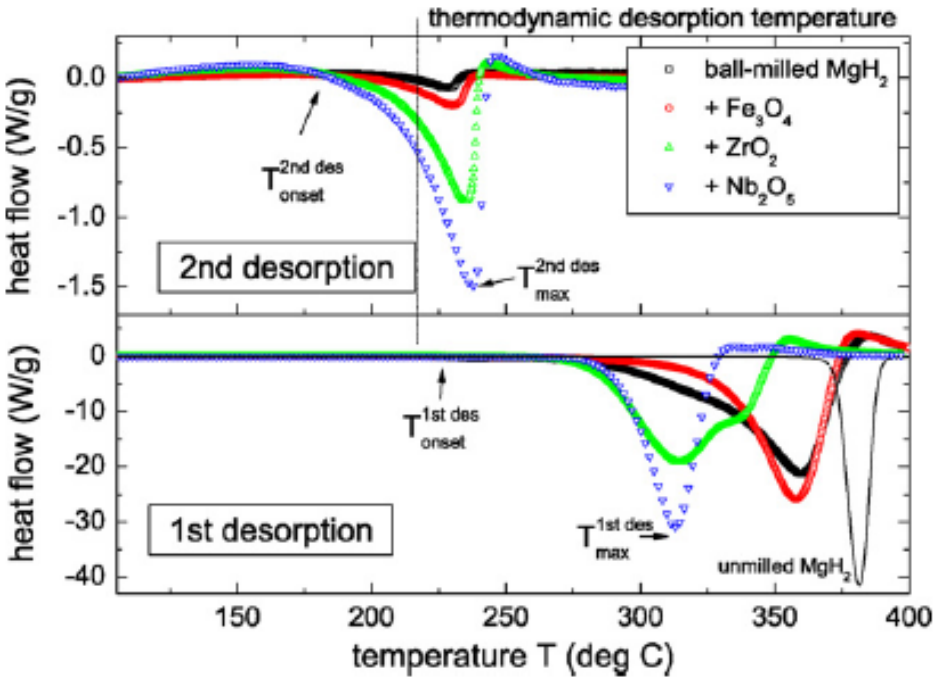

Figure 2-13. DSC curves of Mg-5 mol% X (X= Nb_2O_5, Fe_3O_4,ZrO_2) illustrating the reduction in hydrogen release temperature with the addition of oxide catalysts [reproduced from [61]].

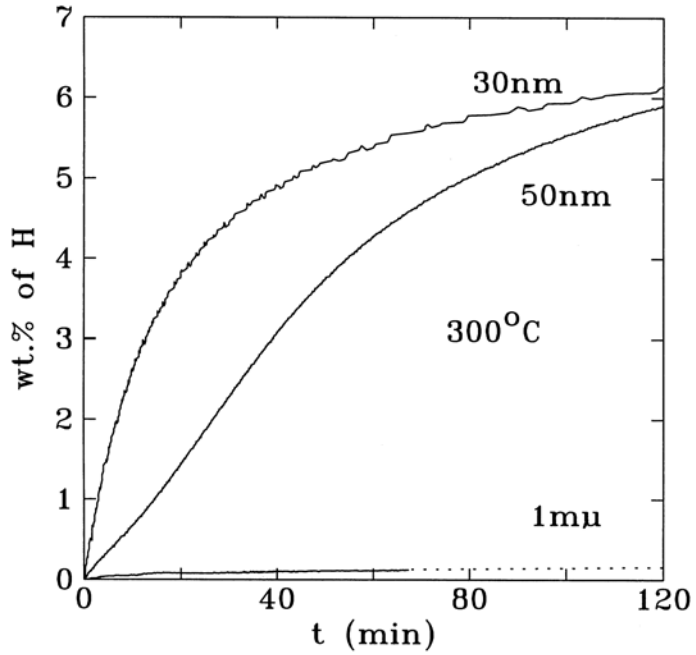

Figure 2-14. Hydrogen absorption curves of pure Mg with different grain size created by ball milling showing the faster absorption in nanograined Mg [reproduced from [19]].

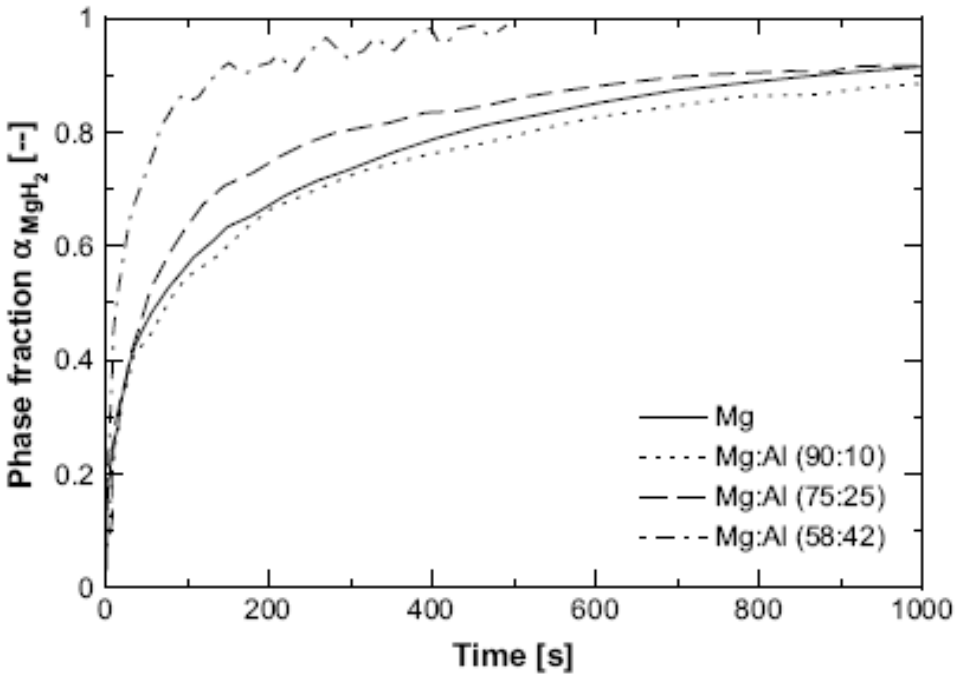

Figure 2-15. Hydrogen absorption curves of Mg-Al alloy powders at 400°C demonstrating the effect of Al addition on the kinetics of hydride formation [reproduced from [28]].

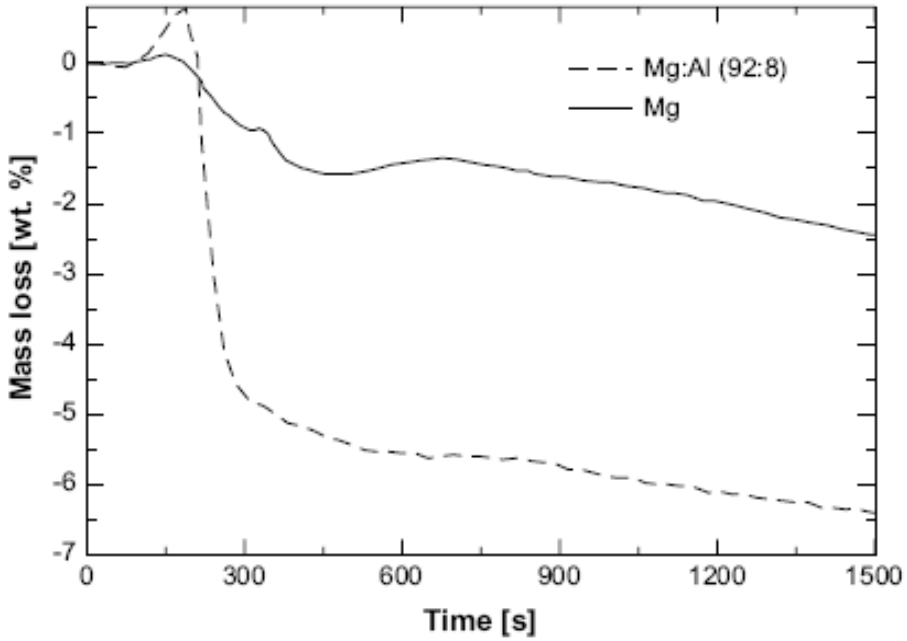

Figure 2-16. Hydrogen desorption curves of pure Mg and Mg-8 mol%Al alloy powders in TGA at 300°C. Hydrogen is released in a short time when compared to pure Mg powder [reproduced from [97]].

CHAPTER 3
EXPERIMENTAL PROCEDURES

Mg-Al alloy powders being developed in this study are anticipated to be used as hydrogen storage materials. In the past, researchers have demonstrated that specific characteristics of materials like nanocrystalline grains, higher surface area/volume ratio, oxide free surfaces have improved the kinetics of hydrogen absorption and desorption of hydrogen [19, 87, 92]. Furthermore, it was shown that alloying of pure Mg affect the thermodynamic properties of hydride formation and dissociation [43, 47, 99]. Different processing techniques like ball milling, mechanochemical synthesis, induction melting, rapid solidification, electrodeposition have been developed to achieve the required characteristics in Mg-Al alloys [28, 30, 31, 33]. Among those techniques electrodeposition has several advantages for fabricating alloy powders. It was elucidated that nanocrystalline metal alloy powders with high purity along with a good control on morphologies and composition can be synthesized using electrodeposition [34]. Hence this technique is employed for processing the Mg-Al alloy powders in this study.

The raw materials employed in the synthesis of Mg-Al alloy powders via electrodeposition were extremely sensitive to moisture and oxygen, therefore all the handling and fabrication was conducted in an argon filled glove box. The glove box employed was maintained at a very low O_2 (< 1 ppm) and H_2O (<5 ppm) levels to avoid any contamination during the production and handling of powders. Nickel was added as catalyst to enhance the kinetics of hydrogen absorption and desorption. The Ni coated electrodeposited Mg-Al alloy powders were hydrogenated using a house built absorption unit. Additionally, the Mg-Al alloys were also tested for their thermodynamic properties at Florida Solar Energy Center (Dr. Slattery's laboratory) located in Cocoa, Fl. Desorption of hydrogenated powders was conducted using a Differential Scanning Calorimetry/ Thermogravimetric Analyzer (DSC/TGA). The Mg-Al

powders at various stages of hydrogenation/dehydrogenation processes and PCT experiments were analyzed using various analytical characterization techniques like SEM, XRD, EPMA, TEM. The material processing procedures, analytical testing and the sample preparation for various characterization techniques applied in this research are explained in this chapter. Moreover, the procedure applied during the development of Pressure Composition Temperature (PCT) curves is also described in detail.

3.1 Materials Fabrication

3.1.1 Electrodes Preparation

The electrodes used during the electrodeposition were prepared outside the glove box. Pure copper (99.99%) and graphite rods (99.9%) in cylindrical shape were employed as cathodes (working electrodes). The dimensions and shapes of the cathodes are shown in Figure 3-1(a). The electrodeposition was conducted on graphite electrode because the powders deposited can be scraped of easily from the graphite surface and if any graphite particles are included it is beneficial during hydrogenation. It was shown in earlier studies that the graphite particles can act as catalyst during the hydrogenation [100, 101]. The Cu electrode was electrolytically polished using a solution composed of 82.5 vol% orthophosphoric acid in deionized water [102]. A potential of 1.1V was applied between the working electrode and the reference electrode made of aqueous KCl solution using a Princeton Applied Research (PAR) potentiostat. The Cu cathode was polished for 5 minutes and it was rotated at a speed of 200 RPM to polish the surface uniformly. A steel sheet was employed as the second electrode during the electropolishing of copper. The graphite electrodes were machined using the lathe mill to remove the previously electrodeposited layer and were ultrasonically cleaned in toluene. A set of 2 copper electrodes and 5 graphite electrodes were used in each experiment. The diameters and the weights of all the electrodes (copper and graphite) were measured and taken into the glove box.

A pure Mg sheet (Fine Metals Inc, 99.999%) or a combination of pure Mg and pure Al (Fine Metals Inc, 99.993%) sheet were used as anodes during the electrodeposition processes. The metal sheets were 1mm in thickness. The anodes used for the deposition processes are presented in Figure 3-1(b) and (c). These metal sheets were polished using the 800 grit metallographic paper on the surface and were ultrasonicated in toluene for 15 minutes before taking them into the glove box for electrodeposition.

3.1.2 Electrodeposition of Mg-Al Alloy Powders

The aim of the present study was to prepare Mg-Al alloy powders using the electrodeposition process. The reduction potentials of Mg and Al (-1.706V for Al and -2.375V for Mg) being lower than the hydrolysis of water, electrolytes based on aqueous solutions will release hydrogen at the cathode instead of metal deposition. Hence, from the previous studies conducted in our laboratory, an electrolyte based on organometallics was used for the synthesis of Mg-Al alloy powders [34].

The electrolyte employed during the electrodeposition processes was prepared using the similar principles that were developed earlier for fabrication of Al-Mg alloy powders [33]. It should be noted that the previous study was conducted using a 30 mL electrolytic setup while in this study a 100 mL electrolytic setup was employed. The amount of electrolyte was increased by 3.3 times and bigger electrodes were used to produce sufficient amount of alloy powders for hydrogenation studies. A rotating cylinder electrode cell setup was employed in this study. A schematic representation of the experimental setup is shown in Figure 3-2. The anodes employed in these experiments were annular in shape as shown in Figure 3-1(b) & (c). A 250 mL glass beaker was used as the electrolytic cell. A PAR 263/273 potentiostat/galvanostat system with a maximum output of 2 amps was employed to apply the required current for electrodeposition. The PAR system was controlled via a computer written program while the rotator of cathode was

controlled externally. The final electrolyte composition after mixing the various chemicals in the proportions described in earlier studies was as follows [33].

1 mol Na[AlEt4] + 2 mol Na[Et3Al-H-AlEt3] + 2.5 mol AlEt3 + 6 mol toluene.

The electrodeposition process of Mg-Al alloy powders developed comprised of two steps.

i) Pre-electrodeposition process.
ii) Electrodeposition process.

The first step was termed as pre-electrodeposition process in which a copper electrode (working electrode or cathode) was used along with the pure Mg sheet as anode. From the initial composition of the electrolyte mentioned above, it can be noticed that it does not contain any magnesium components. Hence to produce Mg-Al alloy powders, Mg was introduced into the electrolyte using the pre-electrodeposition process [34]. The aim of this process was to incorporate significant amount of Mg into the electrolyte which can be subsequently used to produce the alloy powders that will be employed in the hydrogenation studies. Depending on the required composition of the Mg-Al powders after electrodeposition, a galvanostatic electrodeposition was conducted for a specific amount of time at a particular temperature as the pre-electrodeposition process. From the knowledge of previous studies conducted in our laboratory on electrodeposition of Mg-Al alloy powders, a current density of 60mA/cm^2 and a temperature of 90°C or 60°C were employed during pre-electrodeposition process in this study [34]. Toluene was added during the electrodeposition to keep the electrolyte level at 100 mL as it evaporates during the experiment. For production of alloy powder with high Mg content, longer pre-electrodeposition times were employed. In these experiments, the total pre-electrodeposition time was divided into 2 equal parts and conducted on different copper electrodes while the anode remained the same. The change of cathode enhances the Al deposition from electrolyte as it was shown that the initial layers on the cathode during the electrodeposition of Mg-Al powders on

copper substrate comprises of fcc-Al rich solid solution [33]. This preferential deposition of Al enriches the electrolyte with Mg ions which help in producing hcp-Mg rich powders during the electrodeposition. After the pre-electrodeposition process, the copper cathodes were cleaned in toluene which was maintained at 60°C for 10 minutes. The cleaning process was repeated 3 times in new toluene to completely eliminate the organometallics from the powder.

After the pre-electrodeposition process, the copper cathodes were replaced by the graphite cathodes and the Mg anode with either a pure Mg sheet (new) or a combination of Mg and Al sheets. The type of anode is decided depending on the composition of the powder to be produced. In order to produce powders by electrodeposition, higher deposition rates are required during the electrodeposition processes [103]. So, a current density of 150mA/cm^2 was employed during this process. Furthermore, all the electrodeposition processes were conducted at 60°C, and 200 RPM. The graphite electrodes were immersed into the electrolytic solution up to a length of 2 cm from the bottom. The area of the electrode inside the electrolyte was calculated using the initial diameter and the total current obtained was incorporated into the program. One of the problems encountered during the electrodeposition process was the evaporation of the solution due to the rise in temperature during the deposition. It was shown that if a Mg anode is employed during the electrodeposition of Mg-Al alloy powders, an exothermic reaction occurs near the surface of the anode which causes the temperature of the electrolyte solution to increase. The temperature of the electrolyte during the experiment increased from 60-85°C and got stabilized around 85°C. To maintain the electrolyte level and the temperature, toluene is added at regular intervals. The other issue faced during the initial experiments was to retain the produced powders on the surface of the electrode instead of falling into the electrolyte due to their weight. Hence, to overcome these problems the time of the electrodeposition was optimized for the

maximum production of powders without losing the electrolyte (due to evaporation) and the powders by falling into the electrolyte. The electrodeposition was carried for 45 minutes and toluene was added during the experiment to keep the level of the electrolyte at 100 mL and also to improve the conductivity. Similar to pre-electrodeposition the powders after electrodeposition, on the graphite electrode were also cleaned using toluene at 60°C for 10 minutes (3 times). Finally, the powder on the electrode was scraped using a scalpel into a clean beaker with toluene and preserved. During the cleaning process the electrolyte was placed on a second heater that was maintained at 60°C to avoid the crystallization and thereby preserving the same electrolytic chemistry for further depositions.

The electrodeposition process was repeated 5 times on different graphite electrodes to produce sufficient amount of alloy powders for hydrogenation studies. To produce the powders of similar compositions in all the electrodeposition the anodes were cleaned inside the glove box using a spatula and a pair of tweezers. The subsequent electrodeposition was conducted on a new graphite rod along with the cleaned anodes. The powders from all the electrodeposits were collected in a beaker with clean toluene.

The pre-electrodeposition and electrodeposition conditions used to fabricate the Mg-Al alloys in the present study are shown in Table 3-1. The ratio of anode is changed during the electrodeposition to produce different composition powders. A pure Mg sheet and a 80%Mg + 20%Al sheets were used in this study.

3.1.3 Addition of Catalyst

The powders collected from the electrodeposition were filtered and weighed using a balance with an accuracy of 0.005 g. To enhance the kinetics of hydrogen absorption and desorption they were coated with a catalyst. Many d-block based transition elements are used as catalyst during hydrogenation/dehydrogenation of Mg powders [20, 49, 87, 104]. Ni is one of the

effective catalysts that were shown to improve these processes and hence it is used as catalyst in this study [21]. The Ni coating procedure was conducted inside the glove box to avoid the exposure of powders to oxygen and moisture. An organometalic based Ni compound was used and the procedure described in the Patent: 4,554,152 was used to coat the powders [105]. Bis-(1,5) cyclooctadiene Ni (Strem Chemicals, 98.3% pure) was used as the source of Ni. A schematic representation of the Ni-coating setup is shown in Figure 3-3 The organometallic Ni and the Mg-Al powders were taken in 0.12:1 proportion and were refluxed in toluene at 110°C for 6 hours. During refluxing, it was difficult to circulate cooling solvent inside the glove box and hence a long jacket was used as shown in the Figure 3-3**,** so that the toluene vapors are condensed on the walls and drop back into the flask. After 6 hours, the powders were filtered and finally rinsed with anhydrous hexane (Fisher brand, 99.99999%).

3.2 Hydrogen Absorption

3.2.1 Hydrogenation Setup

The schematic of the hydrogenation setup used in this study is shown and labeled in Figure 3-4. This setup was built to conduct hydrogenation experiments based on volumetric method (sieverts type) [106, 107]. The hydrogenation setup can be divided into two parts viz. reaction chamber and reservoir chamber. As the names indicate the reaction chamber was used for the reaction of hydrogen with the powders and the reservoir chamber was used for constant supply of hydrogen into the reaction chamber. The two chambers were separated using a regulator that controls the flow of hydrogen from reservoir chamber to the hydrogenation chamber. A pressure sensor was located such that the pressure in either of the chambers can be measured at a given point of time. Two J-type thermocouples (Omega- TJ36-ICSS-180-6) were used in the setup to measure the temperatures in the reaction chamber and the reservoir chamber. The thermocouple in the reaction chamber was inserted such that it was located close to the sample surface to

indicate the temperature of the sample while the thermocouple on the reservoir chamber was attached on the surface of the reservoir and this was maintained at room temperature. The whole setup was connected to high purity Ar (Airgas, 99.99999 %) gas, high purity hydrogen (Airgas, 99.99999%) gas cylinders and the vent-hood via a roughing pump. The temperatures, pressure and the duration of the experiments were controlled using the computer controlled program developed in the Lab-view software from national instruments. The data was recorded using the DAQ system (Omega –DAQ 55) and simultaneously a real time pressure was also monitored using the pressure indicator (Omega –DP25B-E; volts: 115). A pressure sensor from omega (PX880-1KGi) that can operate between 1-1000 psi was employed in this study and has the capability of recording the pressure changes of 0.01 psi. All the tubing used in building the system was from Swagelok and were fixed using the corresponding pressure fittings to avoid any leakages.

3.2.2 Hydrogenation Procedure

The Ni coated powders after filtration were weighed precisely using the balance and loaded into the hydrogenation chamber inside the glove box. After loading the sample the hydrogenation chamber was sealed using wrenches and the valve on the other end was also closed. The sealed hydrogenation chamber was brought out of the glove box and connected to the hydrogenation setup. The air present in the tubing was evacuated using the vacuum pump and then back filed with high purity argon. The whole system including the tubing was flushed with Ar gas 3 times and finally with high pressure of hydrogen. After flushing, the valve near to the hydrogenation chamber was closed and a heating tape was wound around the chamber. The chamber was heated using the resistance heater which was connected and controlled by the DAQ system through a relay. The regulator that was connecting the reservoir chamber and the reaction chamber was set to a pre decided pressure value. The hydrogenation chamber was heated to the

temperature of the experiment and then the valve near the chamber was opened. Immediately, after opening the valve, the valve near the pressure sensor was rotated to read the pressure on the reservoir chamber side and the valve between the reservoir and the hydrogen gas cylinder was closed. The reservoir was always maintained at a higher pressure (approx. 2 times) than the experimental pressure, so that the gas flow was always from reservoir to the reaction chamber. As the pressure in the reaction chamber drops due to the absorption of gas into the material, enough gas enters through the regulator to compensate the pressure loss and a drop in pressure on the reservoir side was measured. The pressure in the reservoir was recorded as a function of time and this drop represents the amount of gas that was absorbed into the material.

Using the Ideal gas equation, the drop in pressure in the reservoir was converted into the number of moles of hydrogen absorbed.

$$n = \Delta PV / RT \tag{3-1}$$

where ΔP is the drop in pressure

n is the no of moles of hydrogen absorbed

T is the reservoir temperature

R is the universal gas constant

V is the volume of the reservoir chamber along with the tubing

The number of moles of hydrogen calculated was converted into the weight of hydrogen as

$$W_H = n * 2 \text{ gms} \tag{3-2}$$

and the weight percent of hydrogen was calculated by using the initial weight of the powder used in the experiment. Approximately 0.3-0.5 gms of powder was used in each experiment to obtain reasonable amount of pressure drop. The compressibility of the gas is ignored in the calculation.

To identify if the system was leaking, before conducting the hydrogenation experiments the whole hydrogen setup was checked for leaks. Different types of leak tests were performed on the hydrogenation setup. In each test different sections (reaction chamber and reservoir chamber) were isolated and then pressurized separately. The drop in pressure is recorded as a function of time and temperature in that section was also recorded to understand the pressure differences due to fluctuations in temperature. For example, the curve in Figure 3-5 was generated by running the test by following similar procedure as that of hydrogenation at 250°C. The straight line in the curve represents that the pressure was not changed with time which denotes no leak in the chamber. Leak tests were conducted at all the temperatures and pressures of hydrogenation studied in this research. The pressure sensor and the thermocouples were calibrated at regular intervals.

3.3 Hydrogen Release Experiments

The hydrogen release experiments were conducted in a Setaram setsys evolution TGA/DSC. During the thermogravimetric analysis the changes in the weight of the sample were observed as a function of time and temperature. The weight loss or gain by the sample during the experiment is representative of the reaction taking place in the material. For example, in the present study the weight loss observed during the heating of a sample is indicative of the amount of hydrogen released. The powders after hydrogenation were unloaded from the hydrogen reaction chamber in the glove box without exposing to atmosphere and stored. To conduct the desorption experiments the powders were brought out of the glove box using a vacuum container. Partial vacuum was created in the chamber inside the glove box so that the powders were not exposed to air. Just before running the hydrogen release experiment in TGA, the powder was removed from the vacuum chamber and was weighed precisely using a balance that

has an accuracy of 0.0005 g. After recording the initial weight, the sample was loaded into the furnace of TGA.

The TGA along with the furnace is flushed with He and enough time was provided to equilibrate the balance under the He flow. Then the sample was heated from room temperature to 400°C at the rate of 5°C/min. The weight loss along with the heat absorbed by the sample (because release of hydrogen is endothermic reaction) during the heating of the sample was recorded as a function of time and temperature. The weight loss during the experiment corresponds to the amount of hydrogen release from the material. The wt% of hydrogen was calculated by considering the initial weight of the sample. To remove the instrumental error from the observed weight loss, same crucible was run in the similar conditions with out the hydrogenated powder and the weight loss observed during this experiment was subtracted from the weight loss in the previous experiment. The final weight loss observed after the empty crucible run denotes the actual amount of hydrogen present in the powder.

To evaluate the microstructure and phases present at different stages of dehydrogenation, the samples were heated to the temperatures of interest at the rate of 5°C/min in TGA and were cooled rapidly to room temperature at the rate of 50°C/min to freeze the microstructure present at that temperature. The corresponding structural analysis was conducted on the powders obtained from these experiments.

The TGA was calibrated for the temperature and the weight loss using the standard copper sulphate penta hydrate ($CuSO_4.5H_2O$). One of the curve generated using the standard material is shown in Figure 3-6(a) and the weight losses and transformation temperatures at different stages were compared to the standards provided by the company (Figure 3-6(b))and it was observed that they correspond to each other within the experimental error.

3.4 Annealing of Mg-Al Powders

It has been shown that the Mg-Al alloy powders produced by electrodeposition comprise of supersaturated solid solutions of hcp-Mg and fcc-Al [33]. In addition, it was also demonstrated that very fine nanocrystalline structure of alloy powders can be produced by electrodeposition. The microstructure produced in these experiments is metastable in nature. The rigorous conditions (high current density, high speed of rotation and low temperature) employed to fabricate the alloy powders during electrodeposition produces powders with the metastable phases. Hydrogen absorption being a high temperature and time taking process, the microstructure of electrodeposited Mg-Al powders will be affected due to annealing in those conditions. Hence to understand the differences in microstructural and phase changes between hydrogen absorption and the experimental conditions like temperature and time, annealing experiments were conducted on the Mg-Al powders at the hydrogenation temperatures and times. To obtain the same conditions during that of hydrogenation, the annealing experiments were conducted in the hydrogenation chamber itself but with out pressurizing with hydrogen. Powders were loaded into the hydrogenation chamber as described in the previous section, and the chamber was connected to the hydrogenation system. After flushing the system with Ar, the reaction chamber was heated to the temperature of the experiment and held at that temperature for specific period of time. Annealing experiments were conducted for two different periods of time at each hydrogenation temperature. The shorter time experiment was designed to understand the phase changes that take place in Mg-Al powders before the reaction chamber was pressurized with hydrogen in the hydrogenation experiment. In this experiment, the powder was heated to the hydrogenation temperature in the same heating rate as that of hydrogenation experiment and once the temperature was reached, the powders were quenched immediately to preserve the phases. In, the second experiment the powder was heated to the temperature of

interest and was held for 5 hours at that temperature and then quenched to room temperature. The annealed powders were characterized for the phases, microstructure and compositions using XRD, and SEM.

3.5 Procedure for Conducting a PCT Experiment

The PCT experiments can be conducted on both volumetric and gravimetric absorption units. A system which works on the volumetric principle (sievert's principle) was used in this study [106]. The Pressure Composition Temperature (PCT) experiments were carried out on a Hiden Isochema (HTP1) instrument located in Dr. Slattery's facility at Florida Solar Energy Center (FSEC), Cocoa, Fl. This unit is shown in Figure 7-2(a) along with the schematic (Figure 7-2b) of the various chambers present inside the equipment. The Ni-coated electrodeposited powders were thoroughly rinsed in ultra high purity hexane (99.99999%) and were stored in small bottles. These bottles were filled with ultra high pure hexane before enclosing in a vacuum jar. The vacuum jar was sealed inside the glove box and then shipped to the facility in Cocoa. The sealed vacuum jar was taken into a glove box and the powders were filtered from the hexane and weighed precisely before loading them into the reaction chamber. Approximately 0.3-0.4 gm of powder was used in each experiment.

The reaction chamber shown in the schematic was detached from the system and taken into the glove box along with a transfer cylinder. The reaction chamber has a provision to insert a thermocouple from the bottom of the chamber to measure the temperature of the sample during the experiment and another hole on the top for pressurizing the chamber. The powders were loaded into the reaction chamber and it was sealed in a bigger transfer cylinder. A piece of glass wool was used to cover the hole before loading the sample. The loaded transfer chamber was placed on the top of the absorption unit. A removable glove compartment was then attached to the absorption unit and was evacuated. The glove compartment has a provision to back fill with

argon. The evacuated glove compartment was backfilled with argon and the procedure was repeated. Finally, after backfilling the glove compartment with argon, the reaction chamber from the transfer cylinder was taken out and loaded into the furnace of the absorption unit using the gloves of the compartment. After loading the chamber successfully the glove compartment was detached from the absorption unit before running the experiment. By using the detachable glove compartment the samples were loaded into the absorption unit without exposing them to air and also the temperature of the sample was also measured accurately by placing a thermocouple very close to the sample surface.

After loading the sample, a calibration of volume of the reaction chamber and the piping involved was carried out using a high purity helium gas. This calibration was conducted at room temperature and at different pressures of helium. Finally the reaction chamber was evacuated and the sample was heated to the temperature of the experiment. After attaining the reaction temperature the sample was exposed to a measured volume of hydrogen pressure. To achieve this, the piping between the valve FCV1 and the valve PCV4 (Figure 7-2(b)) was pressurized to a known value and then the valve PCV4 was opened to expose the sample to hydrogen. The software then waits till the pressure in the chamber reaches an equilibrium value before shutting the PCV4 valve. Based on the volume calibration and the observed pressure the amount of absorbed hydrogen is calculated using the ideal gas equation. In the next step the piping between the FCV1 and the PCV4 was pressurized to a higher pressure and the PCV4 was opened again and allows the pressure in the chamber to reach equilibrium. The same procedure was repeated in incremental steps of pressure till the maximum limit of the equipment. The absorbed hydrogen gas is calculated at each step and a PCT curve is developed from the data.

After reaching the maximum pressure during the desorption part of the PCT curve, the piping between the FCV1 and PCV4 was evacuated and backfilled with hydrogen to a lower pressure than the reaction chamber. Then the opening of the PCV4 valve results in flow of hydrogen gas from the reaction chamber and the system was allowed to reach equilibrium. The difference in pressure during the step was calculated as the amount of hydrogen gas released. The compressibility of the gas at various pressures was considered during the calculation of the amount of hydrogen absorbed into the material. An upper time limit is provided in the software to move onto the next step if equilibrium is not reached in that specified time.

3.6 Analysis Methods and Characterization Techniques

3.6.1 Compositional Analysis

The compositional analysis was carried out using a JEOL 733 micro probe (EPMA) and a JEOL JSM 6400 (EDS) Scanning Electron Microscope (SEM). The error in compositional analysis using EPMA being very low (0.5%), it was used to evaluate the precise composition of components in particular phases while SEM-EDS was used to identify the compositions in bulk regions of the samples. The samples for the compositional analysis were prepared by mounting the powders in a cold mount made of epoxy (Buehler). After the epoxy was hardened the samples were polished using the metallographic paper (Buehler 400 grit paper) until the powders in the epoxy were exposed. Sequentially, after the 400 grit paper the block was polished using a 800 and 1200 grit papers in that order for about 10-15 minutes. After each stage of polishing the surface of the block was cleaned using a cotton ball dipped in ethyl alcohol and finally ultrasonicating the block in ethyl alcohol for 10 minutes. The cotton ball was used to remove the particles which are firmly stuck on the surface. Following the polishing on the grit papers, the sample was polished using 9,6, and 1 micron diamond pastes and the Leco microid diamond compound extender from Leco was used as lubricant. About 15-20 minutes was spent on each

polishing stage to remove the scratches and the sample is cleaned with the cotton balls dipped in ethyl alcohol after each stage. In addition ultrasonication in ethyl alcohol was also carried out to remove the particles effectively. After the final stage of polishing and ultrasonication the samples were coated with carbon to improve the conductivity during the SEM. Additional carbon paint was also applied in case of EPMA samples for better focus of the beam.

3.6.2 X-ray Diffraction

A Phillips APD 3720 powder X-ray diffractometer with Cu-K_α raditation was primarily employed in this study to identify the phases and their lattice parameters. The alloy powders at various stages of experiments were analyzed using the X-ray diffractometer. The sample was prepared by sticking a double stick tape on the standard glass slide and spreading the powder on the surface of the tape. The height of the edge of the slide was adjusted to the powder level by applying more tape. To correct the x-ray diffraction patterns for the instrumental error, tungsten (W) powder was mixed in the samples during the analysis. The experimental peak positions (2theta value) of the phases were identified by fitting the peaks using the software "Profile Fit" and the final 2 theta positions were identified by adjusting them using the tungsten peaks in the pattern. All the scans were performed between the 2 theta ranges of 20-90 degrees.

The lattice parameters of the hydride phase from different samples were identified using the (110) and the (101) peaks of magnesium hydride. After correcting the X-ray diffraction patterns for the instrumental error the 2 theta positions were used in the following equations to identify the lattice parameter. Bragg's law which is described in the equation was used to calculate the d-spacing of the particular peak

$$n\lambda = 2\ d\ Sin\theta \tag{3-3}$$

where λ is the wavelength of the radiation used (1.54056)

d is the d-spacing of the corresponding plane

θ is the half of the angle measured from the x-ray diffraction pattern

The (110) peak was used for identifying the "a" lattice parameter and using this value and d-spacing of the (101) peak the "c" lattice parameter was calculated. The equations used for the calculations of lattice parameters were shown.

$$\frac{1}{d_{110}{}^2} = \left(\frac{h^2 + k^2}{a^2} \right) \tag{3-4}$$

and

$$\frac{1}{d_{101}{}^2} = \left(\frac{h^2}{a^2} + \frac{l^2}{c^2} \right) \tag{3-5}$$

It should be noted in some of the samples the amount of the powder and the standard material was kept constant to identify the proportion of different phases at various stages of the experiments [108].

3.6.3 Scanning Electron Microscopy

A JEOL JSM 6400 SEM was employed to observe the morphology of the alloy powders. The initial powders were analyzed by mounting the scraped powders on an aluminum stub using the carbon paint. The distribution of different phases in the powders was also analyzed using the SEM. The average atomic numbers of different phases were exploited in the backscattered electron imaging (BSE) mode to identify the phases. The different phase fractions of the powders were also analyzed by using the BSE images in the software Image J. Multiple images of each sample was taken and the volume fraction of the different phases in the microstructures was calculated.

3.6.4 Transmission Electron Microscopy

A JEOL 200CX Transmission electron microscope (TEM) was used to identify the microstructure of the Ni-coated electrodeposited powders. The TEM samples were prepared using the Leica Ultracut UCT ultramicrotome. The powders were embedded in a mixture of resins made up of SPI-PON 812, NMA and DMP 30 from SPI supplies in the proportions described in the reference. The resins were cured at 50°C for 24 hours and these capsules were used to cut the TEM samples using the ultramicrotome. The face of the capsules was trimmed using the razor blade before loading them into the ultramicrotome. The samples were loaded with the cutting face parallel to the edge of the knife. A diamond knife was employed to cut the sample and the capsule was oscilated with different speeds to obtain the samples. A boat attached to the diamond knife was filled with a mixture of deionized water and ethyl alcohol. The TEM slices that were cut float on the surface of the boat and they were separated using an eyebrow before fishing onto the carbon coated copper grid of 3 mm size.

These grids were used in the TEM to identify the grain size, microstructure and different phases of the powders. The TEM was operated both in bright field and dark field mode along with the selected area diffraction to identify the different phases in the material.

3.6.5 Insitu X-ray Diffraction

The insitu X-ray diffraction technique was employed to identify the phases that were evolved during the release of hydrogen. The Inel insitu XRD present in Dr. Jacob Jones laboratory at university of Florida is employed to identify the phases during the desorption. The hydrogenated powders were transferred to the furnace of the XRD instrument and were heated from room temperature to 450°C in air at the rate of 5°C/min. During the heating of the sample the copper K_α radiation was used to obtain the X-Ray diffraction patterns from the powder as a function of temperature and time. To understand the evolution of different phases and to interpret

the hydrogen release temperature, the collected diffraction profiles were plotted in 3-dimensions using Matlab. The differences in the intensity of the peaks as the sample is heated were identified and were interpreted for the evolution of phases.

3.6.6 Phase Fraction Analysis

The microstructure of the Mg-Al powders consisted of various phases before and after hydrogenation experiments. The quantification of these phases was necessary to compare various effects like temperature and amount of hydrogen absorption in different samples. The phase fraction analysis on Mg-Al powders was carried out using the Image J software. Backscattered electron mode was employed to identify the different phases as the average atomic number of all the phases was different. Multiple images of each sample were taken from different particles randomly and these images were used in the Image J software to identify the fractions of different phases. The brightness in the image mode was adjusted such that the contrast corresponding to one phase was highlighted and the area under the distribution curve was calculated. By normalizing this area with the total area of the particle will give us the phase fraction. This method was employed on both the hydrogenated and annealed powders to interpret the evolution of phases at different temperatures and pressures.

Table 3-1. Experimental conditions for during electrodeposition of Mg-Al alloy powders

Parameter	Pre-electrodeposition	Electrodeposition
Current Density (mA/cm^2)	60	150
Cathode rotation speed (RPM)	200	200
Cathode	Copper	Graphite
Anode	100% Mg	-
Temperature (°C)	60	60
Time (mins)	180	45

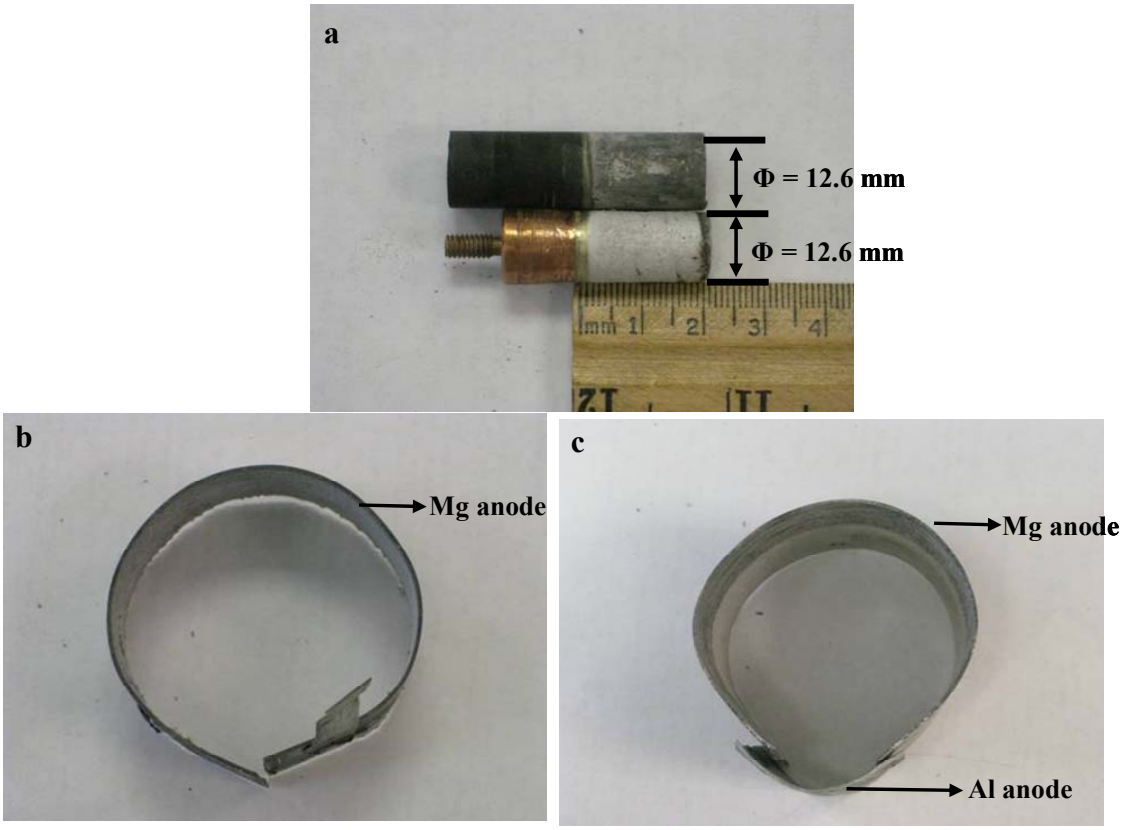

Figure 3-1. Photographs showing the shapes and sizes of the electrodes used in electrodeposition. (a) side view of the Copper and graphite cathodes. Top view of the (b) Pure Mg anode (c) Mg + Al anode.

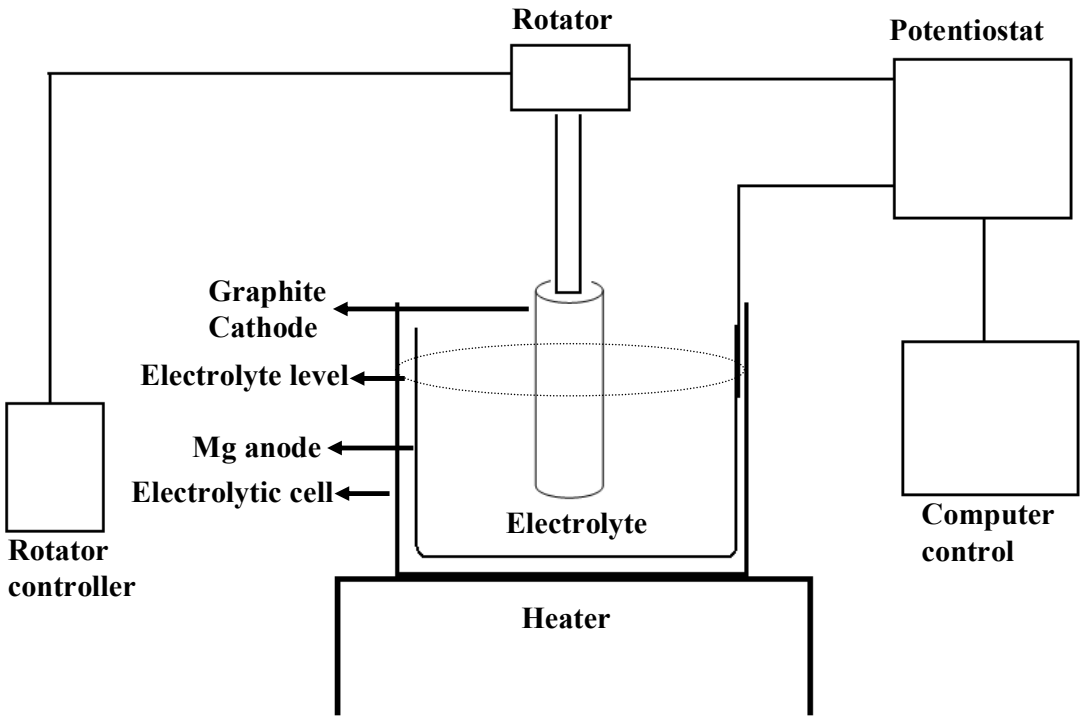

Figure 3-2. Schematic representation of rotating cylinder electrodeposition setup

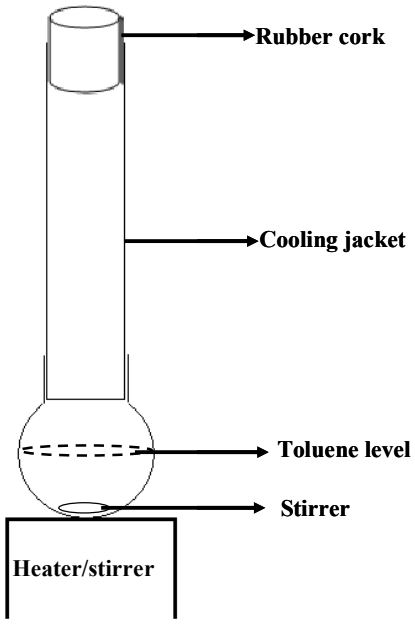

Figure 3-3. Schematic of the modified setup used for Ni-coating inside the glove box.

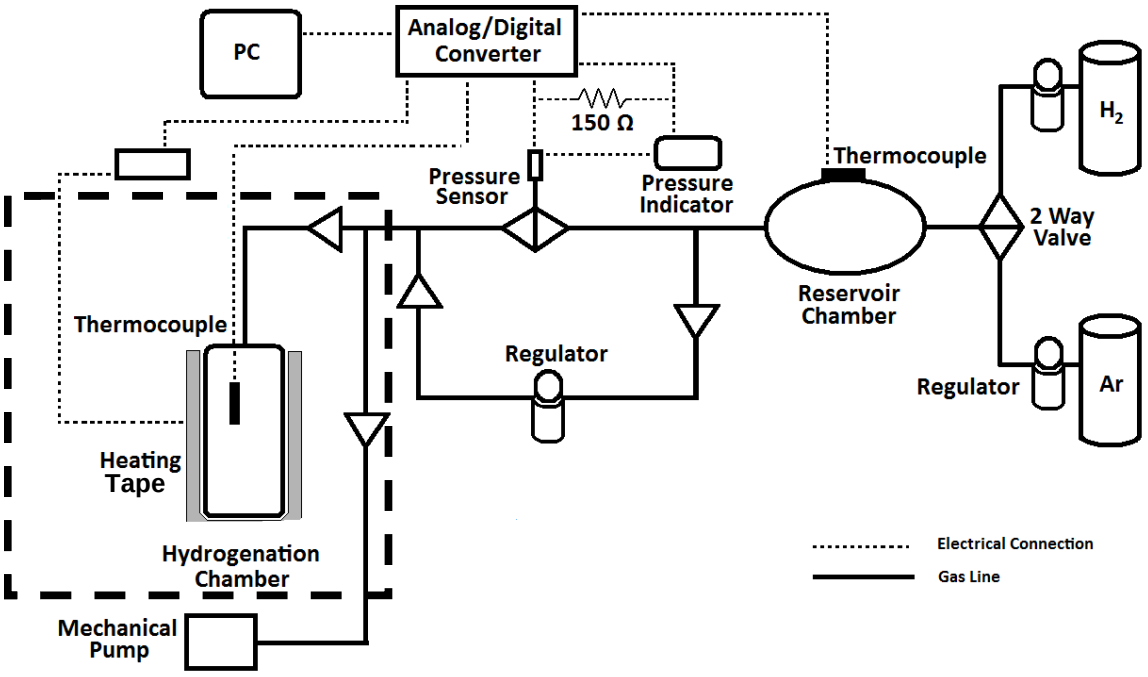

Figure 3-4. Schematic representation of the hydrogenation setup used in this study.

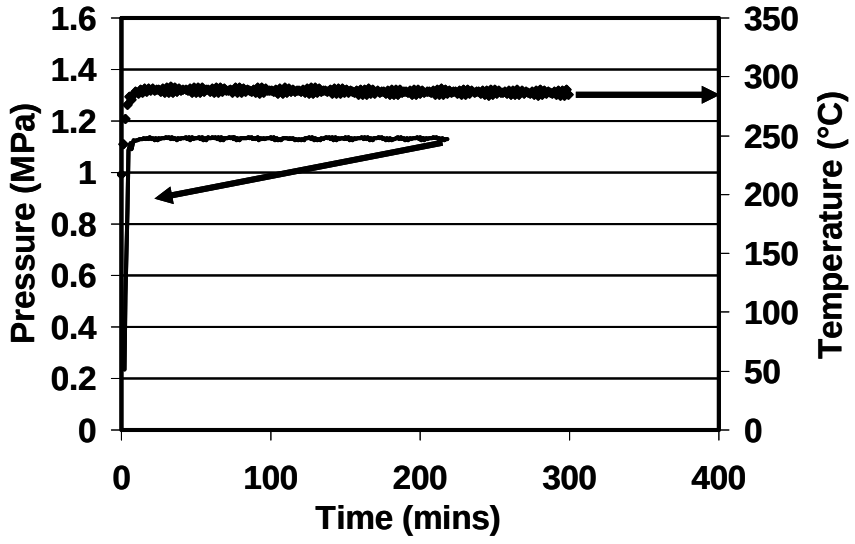

Figure 3-5. Pressure and temperature vs. time plot obtained by a leak test indicating that there is no leak during the test.

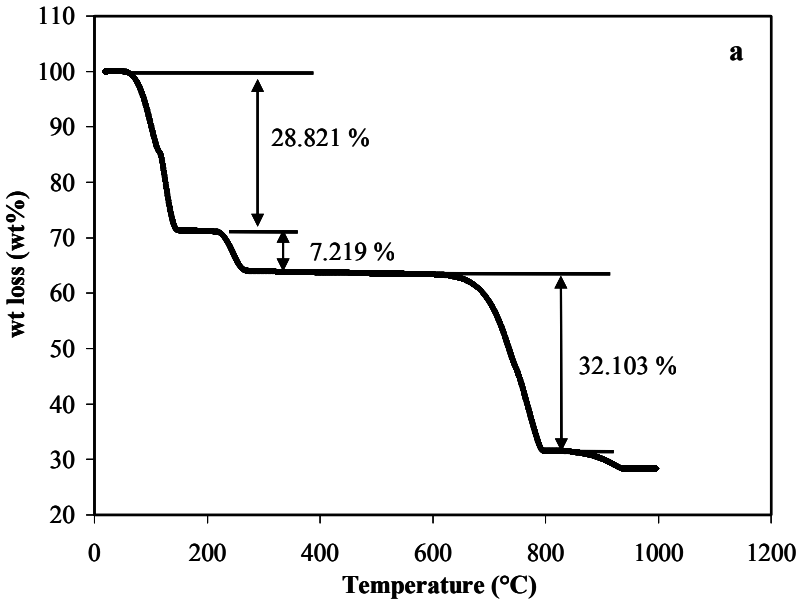

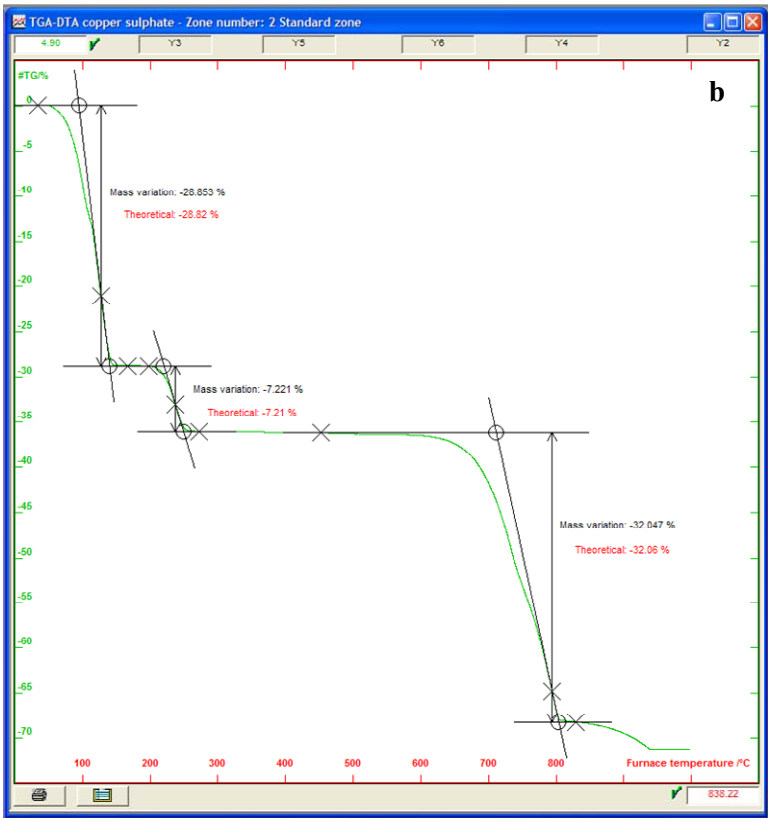

Figure 3-6. (a) Wt loss vs. Temperature (TGA plot) curve obtained during the calibration of TGA/DSC using $CuSO_4.5H_2O$. (b) Standard Wt loss vs. Temperature (TGA plot) curve provided by the Setaram Company for TGA/DSC calibration.

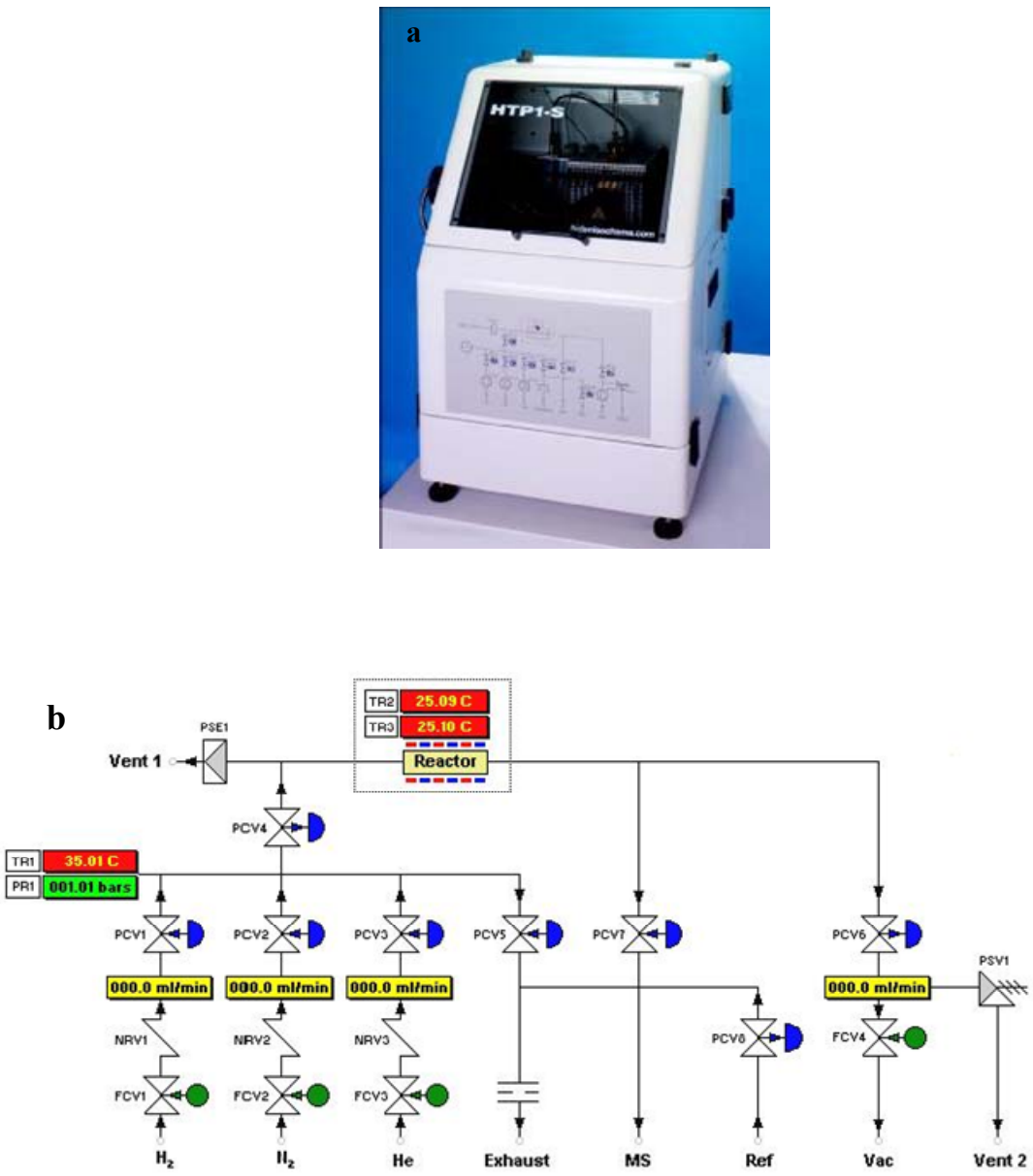

Figure 3-7. (a) Photograph of the HTP1 volumetric absorption unit used for PCT development. (b) Schematic diagram of the reaction chamber and the piping involved for the development of PCT curve.

Figure 3-8. Photograph of the Inel insitu X-ray diffractometer used for studying the phase evolution during desorption of hydrogenated powders.

CHAPTER 4
CHARACTERIZATION OF POWDERS

This chapter details about the initial characteristics of the electrodeposited Mg-Al alloy powders before the hydrogenation processes. The alloy powders were characterized for their morphology, phases, composition and microstructure. The Mg-Al alloy powders were coated with the catalyst Ni and its distribution on the surface was established using the EDS mapping technique in SEM. Also a pure Mg powder was employed in the hydrogenation studies and its initial characteristics were also studied and described in this chapter.

4.1. Characterization of Electrodeposited Mg-Al Powders

4.1.1 Morphology and Size of Powders

The morphology of the majority of Mg-Al powders fabricated using electrodeposition is shown in Figure 4-1. While the high Al content electrodeposited powders have been shown to exhibit different morphologies [33],only a single morphology (globular morphology), was observed in the high Mg (>88 at%) powders fabricated in this study. As shown in Figure 4-1(a) the particles, due to the high current density employed in this study, are observed to be 0.5 mm to 1 mm long. The particles were dendritic in nature as is evident from Figure 4-1(b). These dendrites have many branches that grow in multiple directions. Figure 4-1(c) demonstrates that they exhibit a hierarchical structure consisting of aggregates of approximately 20 μm in size. These aggregates were composed of individual 2-0.5 μm size units, which were somewhat flat and faceted (see Figure 4-1(d)). The globular morphology observed in the electrodeposited Mg-Al powder was reported previously, except the roughness of the morphology was different [33]. The morphology of Mg-Al powder in this study was characterized with lower roughness than the previously observed morphologies in electrodeposited Al-Mg powders.

The root of the dendrites showed a smooth globular morphology as shown in Figure 4-2(a). This morphology was observed exclusively at the beginning of the dendrites (the root) and counted for a small fraction of the total weight of the powders fabricated (Figure 4-2(b)).

In addition to the morphology shown in Figure 4-1(c), occasionally, a less rough globular morphology was also observed as illustrated in Figure 4-3(a). At higher magnifications as shown in Figure 4-3(b), it is observed that this morphology also exhibited a hierarchical structure with much finer units which were round (globular) in shape. It is to be noted that this type of morphology was observed in very less number of particles and the reasons for its formation could be due to the localized differences in the composition of the electrolyte [4].

4.1.2 Addition of Catalyst

The methodology and materials used to coat the powders with Ni are discussed in Chapter 3. After Ni coating, it was observed that the branches of the dendrites fell apart during the coating procedure and the particles became smaller as shown in Figure 4-4 (compare to Figure 4-1(a)).The distribution of Ni on the surface of the powders was characterized using the EDS mapping in SEM. A secondary electron micrograph along with the corresponding EDS-map of Ni is shown in Figure 4-5. It can be seen from Figure 4-5(b) that Ni is distributed finely on the surface. Further analysis on different powders indicated that the Ni content was not similar on all the particles. The EDS spectra of different particles taken for the same amount of time are shown in Figure 4-6. The EDS peak corresponding to that of the Ni was shown in the spectra. The intensity of the peak varied from one particle to the other as shown in Figure 4-6(a) and (b), which demonstrates that the total amount of Ni on each particle was different. It is anticipated that the particles with variation of Ni content on the surface may cause different hydrogenation behavior in the particle under the same conditions.

4.1.3 Phases Present in the Alloy Powders

The XRD profiles of all the powders fabricated in this study are shown in Figure 4-7. The Mg-Al powders primarily consisted of the hcp-Mg phase, $Mg_{17}Al_{12}$ intermetallic compound and a small quantity of fcc-Al phase. The amount of the intermetallic phase increased with the Al content of the electrodeposited powders. The addition of 4at%Al shifted the peak positions of the hcp-Mg to higher values (e.g. (101) peak shifted from 36.582° for pure Mg (from std to 36.693° for the Mg-4at%Al alloy). This observation indicates a decrease in the lattice parameter of the hcp-Mg phase with Al addition, which is in accordance with the previously reported results [43]. No significant change in the 2 theta positions of the peaks for hcp-Mg was found with increasing the Al content of the alloy from 4at% to 8at%, suggesting that the amount of Al dissolved in Mg was similar in these two powders but the additional Al in the latter powder was precipitated as the intermetallic phase. However, the hcp-Mg peak in the powder with 10at%Al shifted to a higher 2 theta position when compared to 4 and 8at%al alloy powders. Furthermore, the Mg-Al alloy powders showed wider Mg peaks, elucidating their finer grain size.

Previous studies on electrodeposition of the Mg-Al powders using similar electrodeposition conditions indicated that the formation of intermetallic was suppressed during the synthesis and only supersaturated solid solutions of fcc-Al and hcp-Mg rich phases were observed [33]. In contrast to those studies it was noticed that the intermetallic compound was also present in the electrodeposits fabricated in this study. This intermetallic content increased after the Ni coating. To identify the reasons behind the formation of the intermetallic phase, electrodeposition was conducted for different time intervals and the XRD analysis was carried out. The XRD profiles from these powders along with the powders after Ni coating are shown in Figure 4-8. This Figure indicates that for shorter time intervals of electrodeposition, only supersaturated solid solutions of Mg in fcc-Al and Al in hcp-Mg were observed while for

depositions conducted for longer time periods, the intermetallic compound of $Mg_{17}Al_{12}$ was also present in the powders. It was noticed during the experiments that the temperature during the electrodeposition was increased from 60°C to 85°C. From the XRD analysis it can be concluded that the longer time periods at high temperatures involved during the processing of the alloy powders by electrodeposition causes the in-situ annealing and leads to the precipitation of the intermetallic compound in hcp phase. Furthermore, coating of Ni was conducted at 110°C for 6 hours which precipitated more intermetallic compound.

4.1.4 Composition of the Alloy Powders

The composition of the alloy powders was evaluated on mechanically polished samples after electrodeposition. An illustration of a polished particle is presented in Figure 4-9(a). The corresponding EDS map of Al in the particles is illustrated in Figure 4-9(b). It can be noticed from the EDS map that the root of the particle was rich in Al when compared to the remainder of the particle.

The precise at% of Al in the powder was analyzed using the EPMA technique. At least 6 particles and 10-15 points on each particle were considered for EPMA composition analysis. Amount of Al at multiple points on the particle was measured and the average value along with standard deviation is calculated. The Mg-Al alloy powders fabricated in this study can be divided into 2 categories depending on the type of anode used during the electrodeposition process.

A 100% Mg sheet is used for the production of Mg-Al powders with low contents of Al in hcp-Mg phase. The compositional analysis of the electrodeposited powder on hcp-Mg phase from these particles indicated the presence of 4 ± 0.4 at%Al. A particle used for EPMA compositional analysis is shown in Figure 4-10. The numbers indicated on the powder represent the %Al at that particular location.

For fabricating a powder with relatively higher amount of Al in hcp-Mg, an anode with 80%area of Mg and 20%area of Al was employed during the electrodeposition process. The EPMA compositional analysis of the powder fabricated from this alloy indicated that 8 ± 0.1 at%Al was observed in hcp-Mg phase. A SEM/BSE image of a dendritic particle illustrating the different amounts of Al from this experiment is shown in Figure 4-11.

The different phases in the alloy powders were identified by using the backscattered imaging. The SEM/BSE images from an Mg-8at%Al powder are presented in Figure 4-12. The root of the dendrite appears bright (higher average atomic number) and its compositional analysis indicated the presence of 18at%Mg. The grey contrast encompassed the whole dendrite. A relatively uniform distribution of Al was found in most dendrites. The formation of the fcc-Al phase at the root of the Mg-rich dendrites has been observed previously and shown to be associated with the high nucleation barrier required for the formation of hcp-Mg on the graphite substrate [34]. The XRD results of both the powders have indicated the presence of the intermetallic compound $Mg_{17}Al_{12}$ inside the hcp-Mg phase. The contrast or the composition corresponding to the intermetallic phase is not observed during the SEM analysis. The SEM analysis suggest that this intermetallic compound is present as very fine phase inside the hcp-Mg phase and could not be observed in the powder particles even at high magnifications due to low resolution of BSE imaging.

Because of the low volume fraction of the fcc-Al phase, the Al content of the hcp-phase was found to be similar to the bulk composition of the alloy powders as confirmed by the ICP technique. For example, the apparent average Al content of 8.1± 0.2 at% of the hcp-Mg phase as evaluated by EPMA for deposit 2 was very close to the bulk composition of 8.7 at% Al as measured by the ICP technique. The composition of the powders fabricated using the

electrodeposition is very sensitive to the initial conditions of the electrodes and raw materials. It was observed that in one of electrodeposited Mg-Al powder fabricated using the 80% Mg and 20%Al anodes, the composition of the powder as analyzed by EPMA was about to 10at% Al in hcp-Mg phase. This deviation in the composition can be attributed to the conditions of the electrode during the deposition.

4.1.5 Microstructural Characterization of Mg-Al Alloy Powders

The microstructure of the powder after coating with Ni was evaluated using the transmission electron microscopy technique. The TEM samples were prepared by embedding the powders in the polymer and cutting thin slices using the ultramicrotome. The bright field and dark field TEM micrographs of the Mg-8at%Al alloy powder are presented in Figure 4-13(a) & (b) respectively. The corresponding diffraction pattern of the TEM micrographs is presented in Figure 4-13(c). The diffraction spot corresponding to the plane (002) was used to image the micrograph in dark field mode. In the diffraction pattern other than the hcp-Mg phase, diffused rings corresponding to the MgO were identified and indexed (Figure 4-13(c)). It is believed that the MgO was formed during the sample preparation of TEM as it involved cutting the slices using ultramicrotome and fishing the 50 nm slices from the water in the boat of microtome. The average grain size of the Mg-8at%Al alloy powder calculated from multiple images was measured to be 44 ± 5 nm. Since the electrodeposition conditions were same in all the powders fabricated, similar grain sizes were anticipated in all the electrodeposited powders. The non-uniformity of the diffraction spots in the ring patterns and their clustering suggested a strong microtexture in the Mg(Al) alloy powders. This behavior is believed to be associated with the sub-micrometer size faceted units shown in Figure 4-1(d). The intermetallic phase could not be detected by the conventional TEM techniques probably owing to their small size. Several slices from different samples were cut using the ultramicrotome and were analyzed in the TEM. Figure

4-14(a) shows the TEM micrograph imaged from a different sample. The microstructure indicated that the grains were slightly elongated which also represented that these materials were highly textured. The corresponding dark field micrograph is shown in the Figure 4-14(b). Figure 4-15 shows the microstructural analysis carried out in the HRTEM on Mg-8at%Al alloy powder. The d-spacing measured from the micrograph shown in Figure 4-15 was close to that of $(0001)_{Mg}$ basal plane and no phases corresponding to intermetallic were identified in the sample. One of the problems aroused during the TEM analysis was the samples used to peel off from the polymer when the beam was focused on the sample.

The structure of the intermetallic compound is complex and the lattice parameter is very high (about 10.56Å). Therefore, the diffraction spots from this crystal form very close to the transmitted beam due to large d-spacing involved and were unable to get resolved during the TEM analysis. Furthermore, previous studies on bulk Mg-9at%Al alloys illustrated that the $Mg_{17}Al_{12}$ phase was formed as fine precipitates in the order of 100 nm size laths after carrying out annealing treatment for 8 hours at 200ºC [69]. However, the Mg-Al alloys employed in this study were in powder form with nano size grains and were processed at much lower temperatures. Therefore, the intermetallic phase formed in the Mg-Al powder fabricated using electrodeposition was expected to be very fine and was unable to get detected even at high magnifications.

4.2 Characteristics of Pure Mg Powder

To compare the effect of Al addition to Mg on hydrogenation properties, pure Mg powder from Alfa aesar was bought and tested under the same hydrogenation conditions. The pure magnesium powder exhibited a wide range of particle sizes and shapes as seen in Figure 4-16. The mean particle size of the pure magnesium powder based on the volume fraction was measured to be 43 μm. These powders were also coated with Ni using the same procedure

mentioned in Chapter 3. The XRD profile after the coating of Mg with Ni is shown in Figure 4-17. Other than the peaks corresponding to hcp-Mg phase, the peaks corresponding to the internal standard tungsten and the catalyst Ni phases were observed in the powder. The evaluation of the microstructure in TEM indicated that the grain size of this powder was in micrometer regime. The TEM samples were prepared using the ultramicrotomy, similar to that of Mg-Al alloy powder. The bright field and dark field TEM micrographs of the pure Mg powder after coating with Ni are shown in Figure 4-18 (a) & (b) respectively. The average grain size of the particles was about 1.5±0.3 μm. The diffraction pattern from the grains presented in Figure 4-18(c) shown a spot pattern with the spots corresponding to the hcp Mg.

4.3 Summary and Conclusions

Hcp-rich Mg-Al alloy powders were fabricated with 4, 8 and 10 at%Al using the electrodeposition technique. The electrodeposition parameters were chosen such that there was extensive growth of dendrites and the grain size of the powders fabricated was in the nanoregime. Ni was added as catalyst to promote the hydrogen absorption and desorption. The Ni coating procedure rendered particles with different amounts of Ni on the surface. The primary phases present in these powders were hcp-Mg, the intermetallic compound $Mg_{17}Al_{12}$ and small amounts of fcc-Al. The compositional analysis indicated that the fcc-Al was found at the root of the dendrite while the hcp-Mg was formed on top of fcc-Al. The intermetallic compound observed in the powders was formed due to the insitu annealing of the powder during the electrodeposition and its content increased after the Ni coating. The microstructure of the electrodeposited powders after Ni coating revealed the presence of nanocrystalline grains in the hcp-Mg phase. However, the presence and distribution of the intermetallic compound in hcp-Mg was not observed in the microstructural analysis due to their fine size.

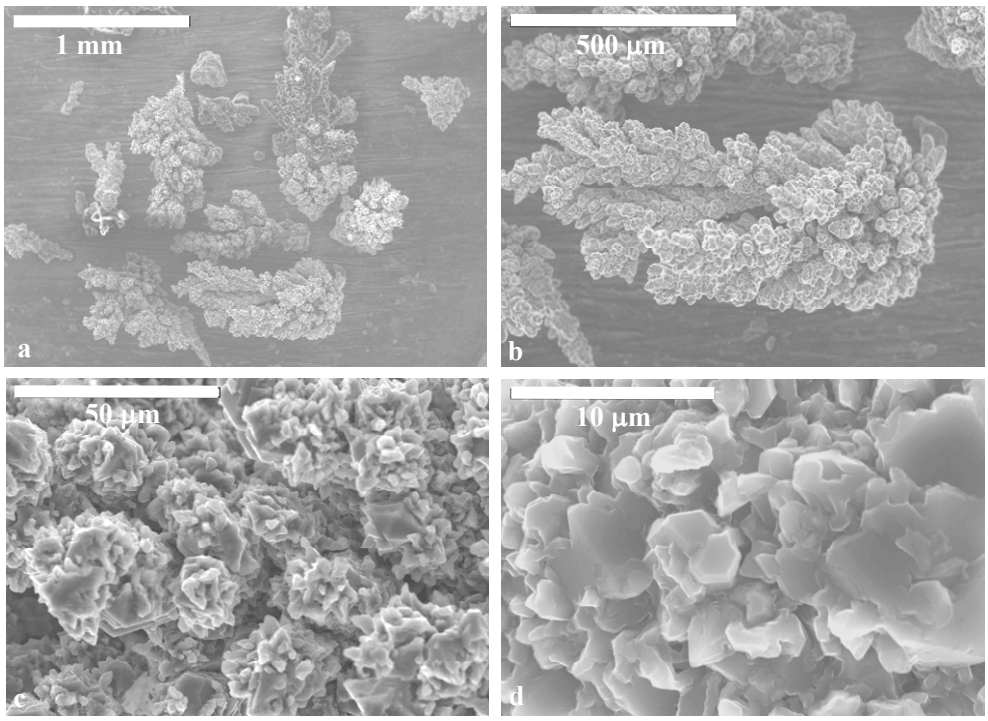

Figure 4-1. SEM micrographs revealing the dominant morphology of powders present in electrodeposited hcp-rich Mg particles, (a) low magnification micrograph illustrating the particle size, (b) the dendritic nature of the electrodeposited Mg-Al particles, (c) higher magnification micrograph showing the branches of the dendrite, (d) finer structural units present in the branches of the powders.

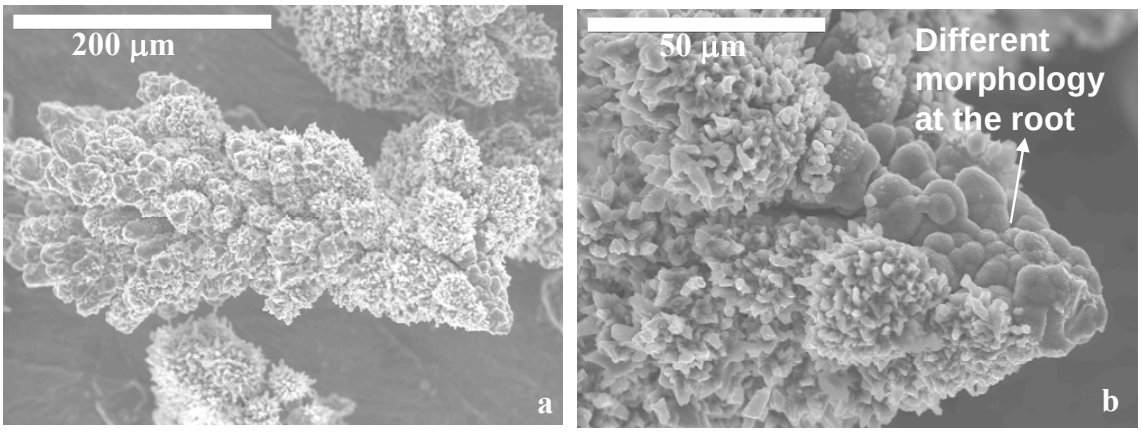

Figure 4-2. (a) SEM micrographs of the Mg-Al particles showing different morphology at the root of the dendrite. (b) Higher magnification image showing the different globular morphology at the root of dendrite.

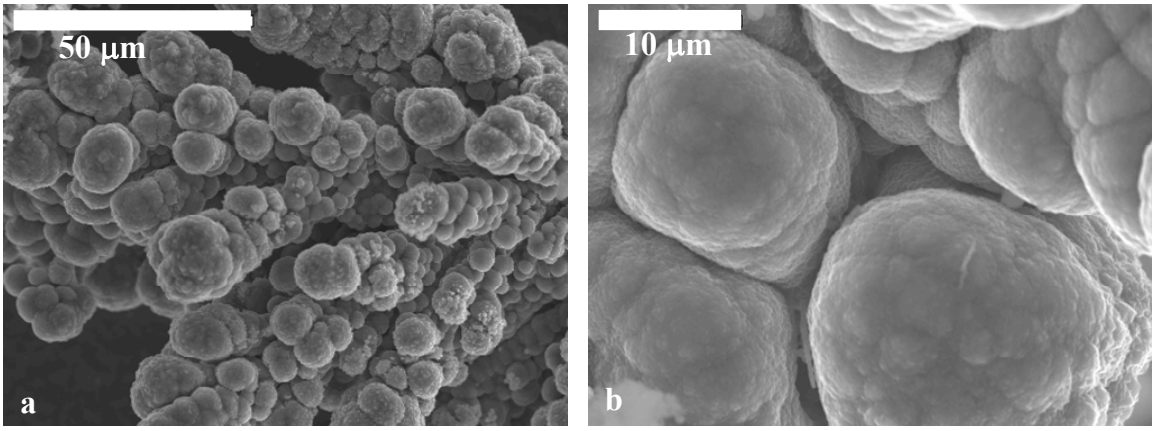

Figure 4-3. (a) SEM micrograph of the morphology present in lower amounts. (b) Higher magnification image showing the globular shape of the branches.

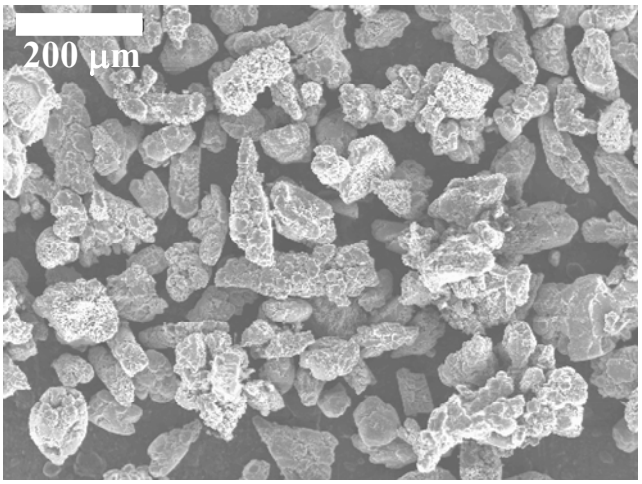

Figure 4-4. SEM micrographs illustrating the breakage of electrodeposited Mg-Al particles after coating with Ni.

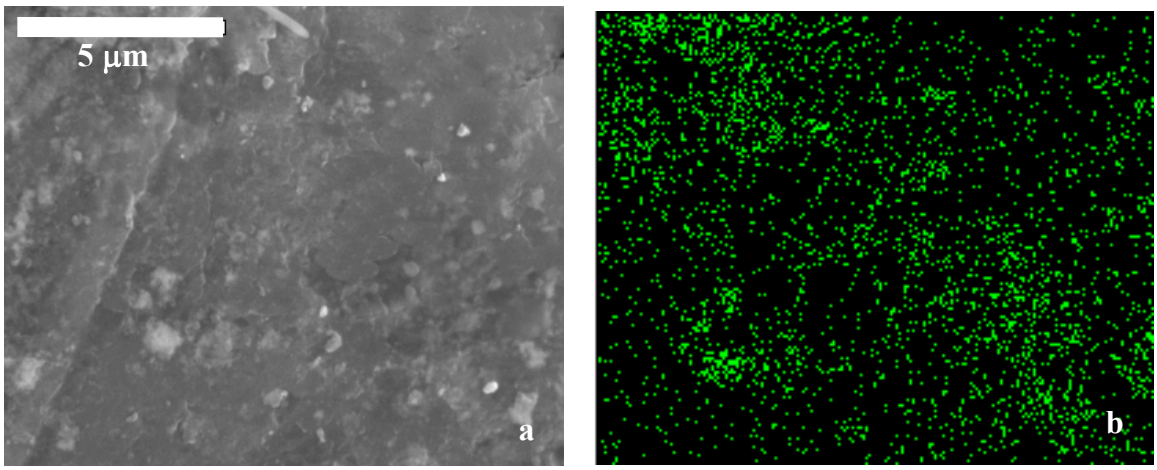

Figure 4-5. (a) Higher magnification SEM image of a Ni-coated Mg-Al particle, (b) the EDS Map of Ni for the micrograph shown in (a).

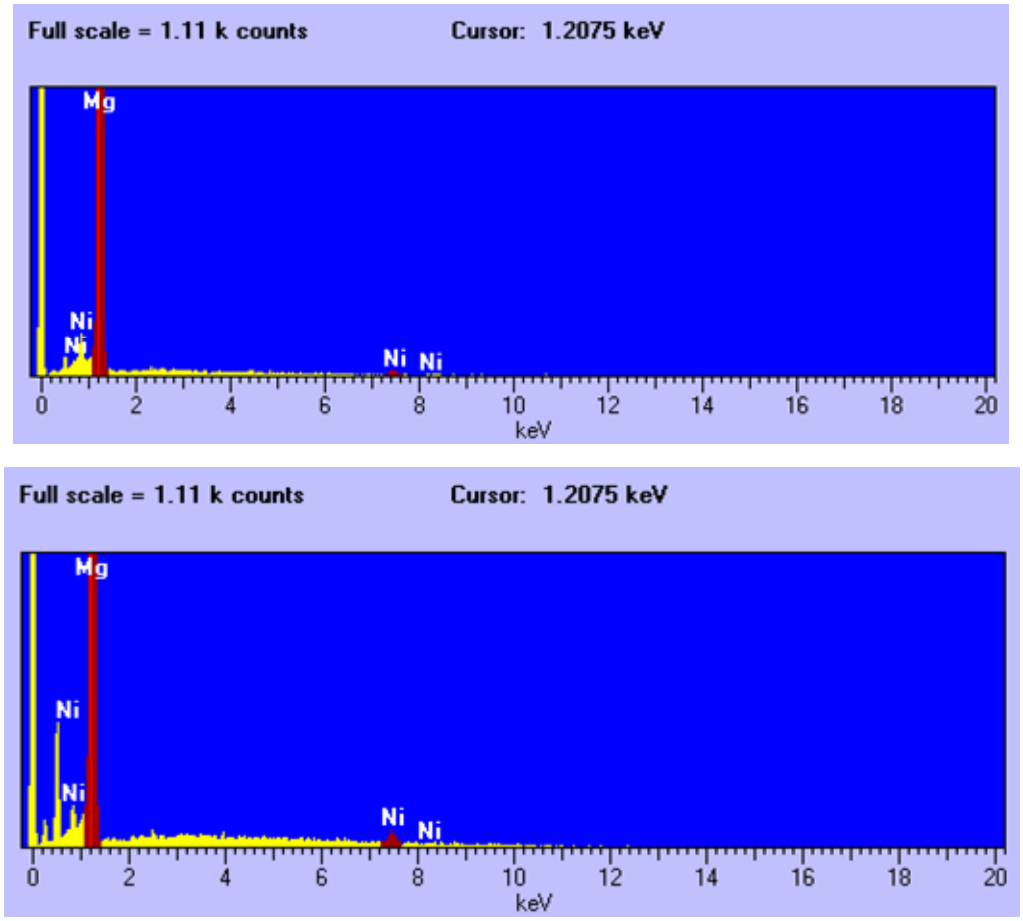

Figure 4-6. Energy Dispersove Spectra of Ni in two Mg-Al particles demonstrating the differences in Ni content.

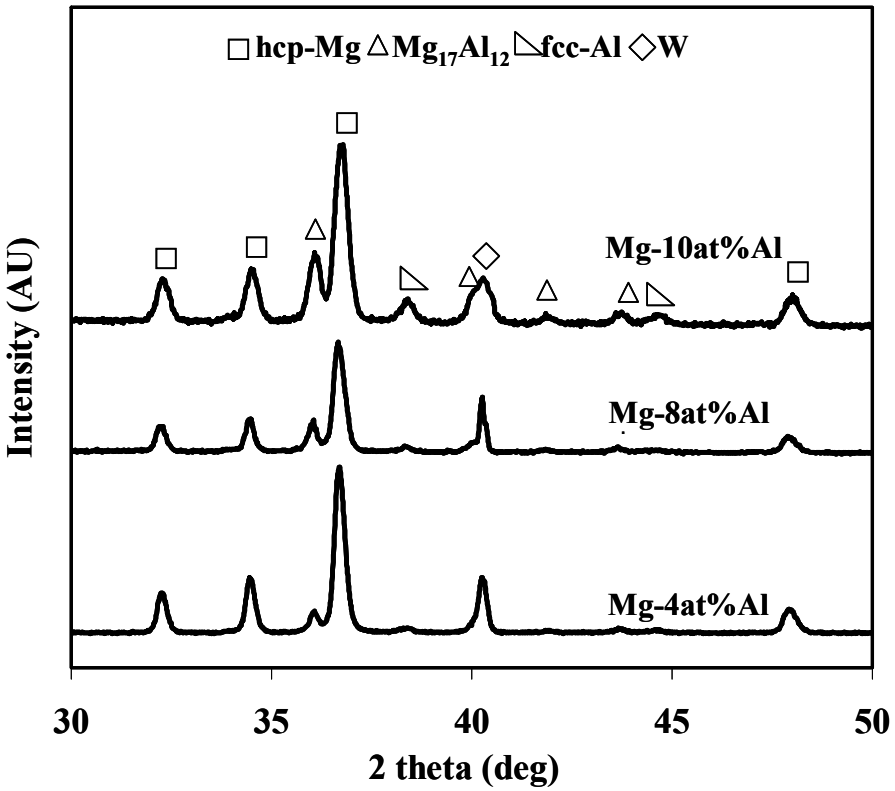

Figure 4-7. XRD profiles of electrodeposited Mg-4at%Al, Mg-8at%Al and Mg-10at%Al powders after Ni coating illustrating the various phases present in the material before hydrogenation.

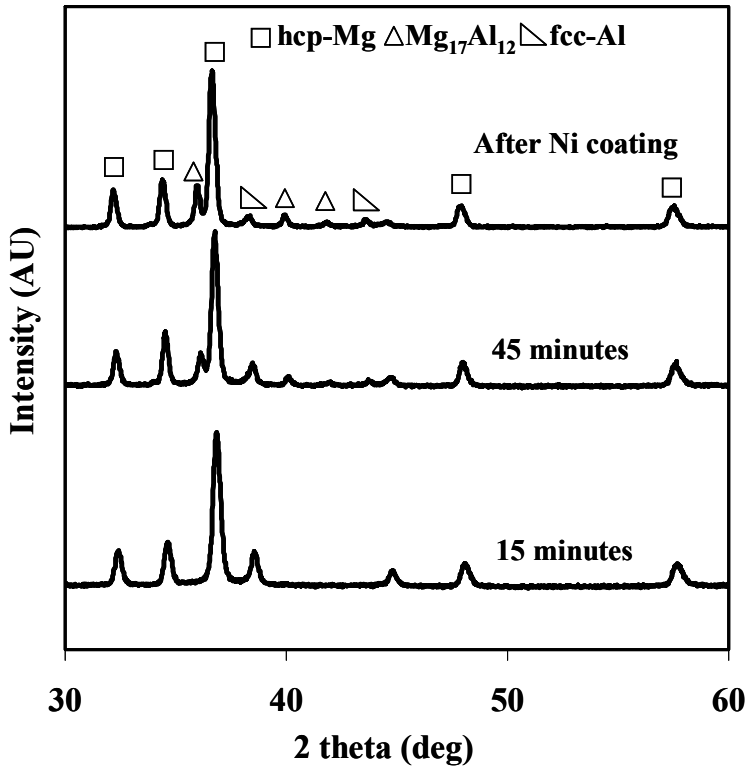

Figure 4-8. XRD profiles of Mg-8at%Al alloy powders deposited for different time intervals and after Ni-coating procedure showing the variation of intermetallic content at each stage

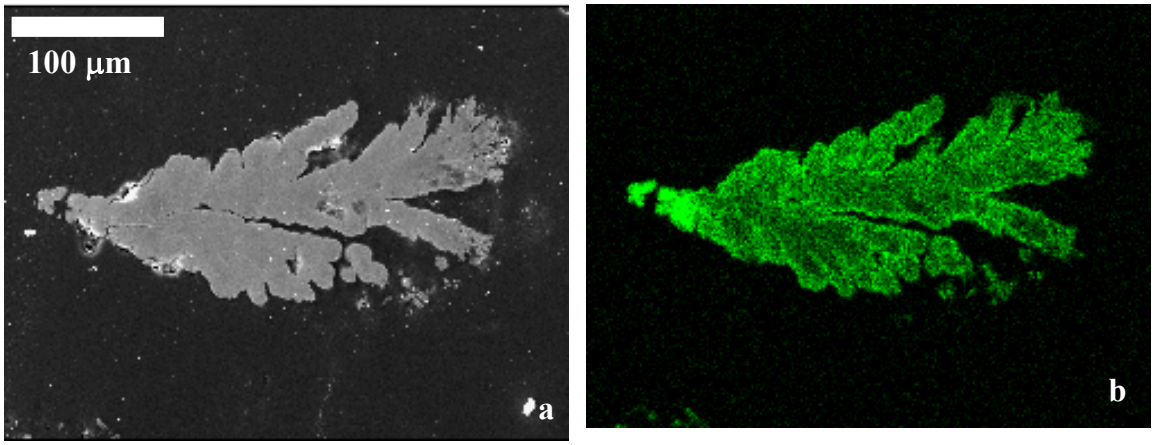

Figure 4-9. (a) SEM Micrograph of a Mg-8at%Al particle and (b) the corresponding EDS map of Al depicting its distribution in the particle.

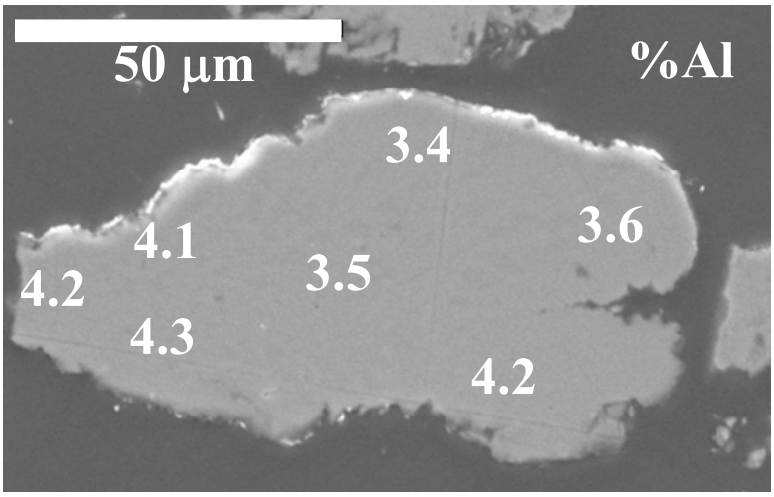

Figure 4-10. EPMA composition analysis of a Mg-Al powder fabricated using the 100%Mg sheet as anode demonstrating the Al distribution in the powder.

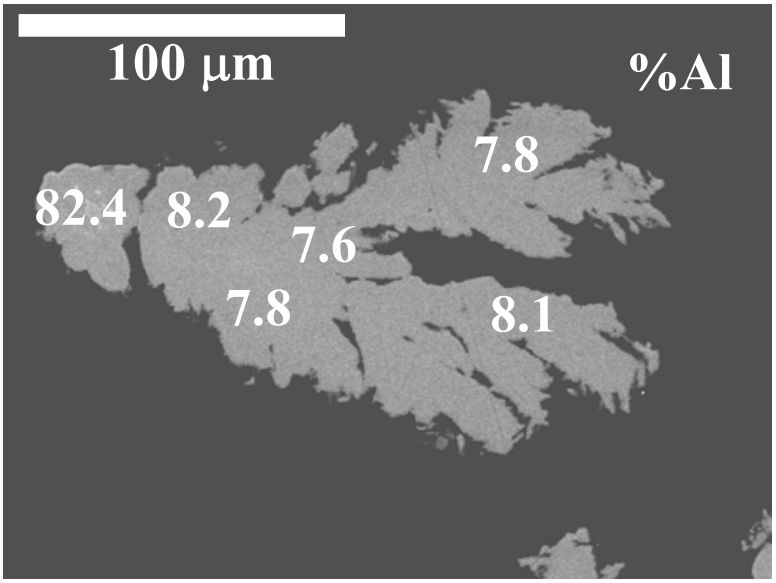

Figure 4-11. EPMA composition analysis of a Mg-Al powder fabricated using the 80%Mg + 20%Mg sheet as anode along with the measured Al content at various points on the powder.

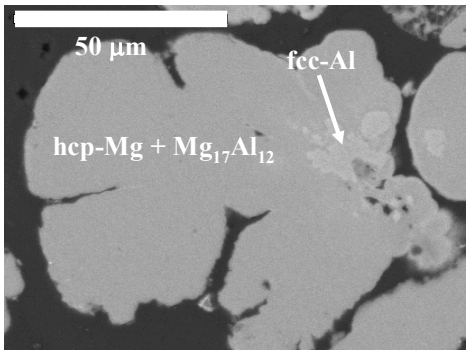

Figure 4-12. A SEM/BSE micrograph of Mg-Al particle illustrating the distribution of different phases in the Mg-8 at%Al powder.

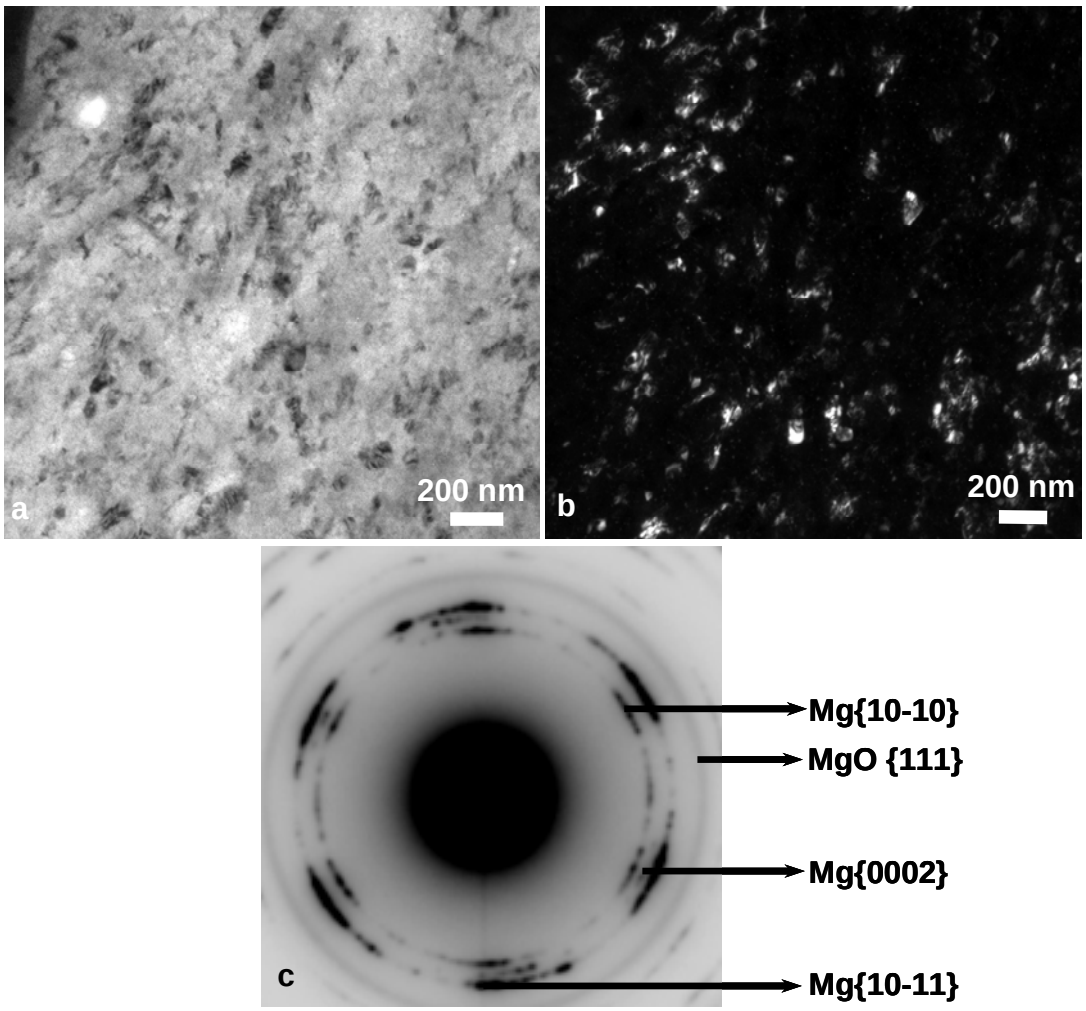

Figure 4-13. (a) Bright field and (b) dark field TEM micrographs of the Mg-8at%Al powder revealing the grain size of the material. (c) The selected area diffraction pattern from the region shown in (a).

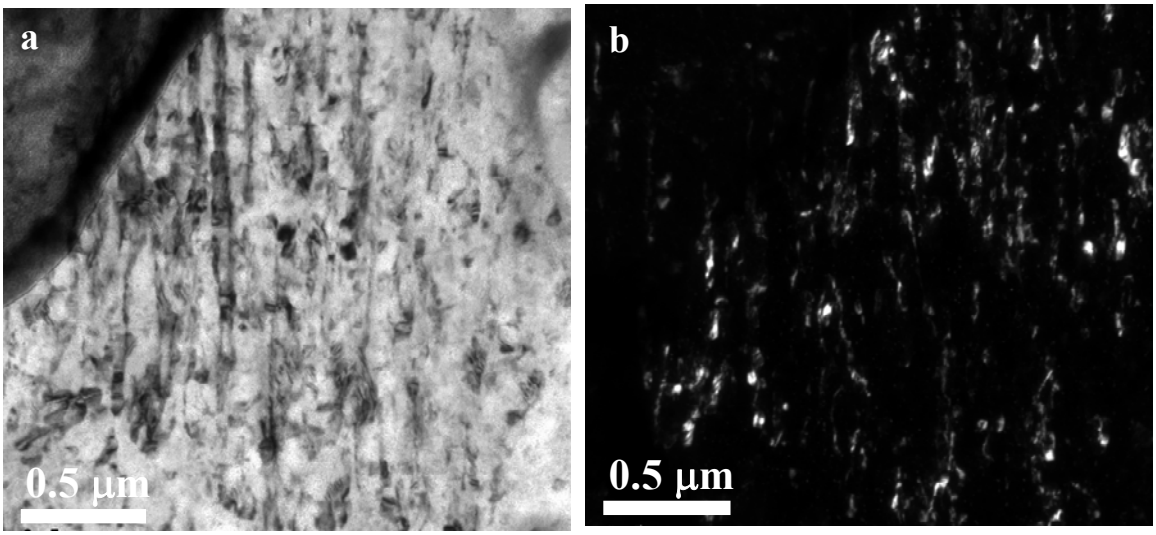

Figure 4-14. TEM Micrographs of Mg-8at%Al alloy powder revealing grain size in (a) Bright field, and (b) Dark field after the coating with Ni.

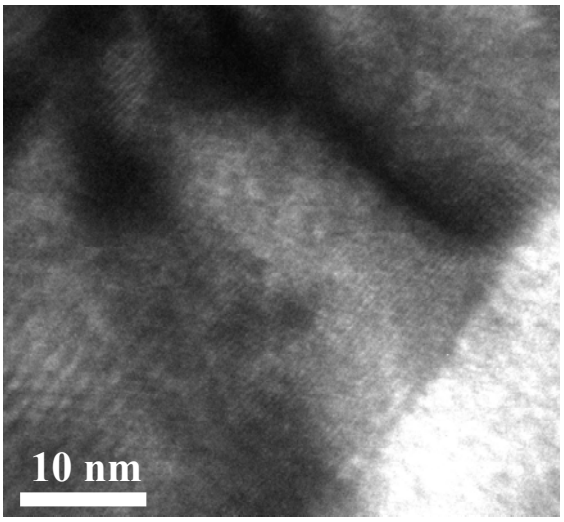

Figure 4-15. Bright-field micrograph of an Mg-8at%Al alloy powder at high magnifications using HRTEM.

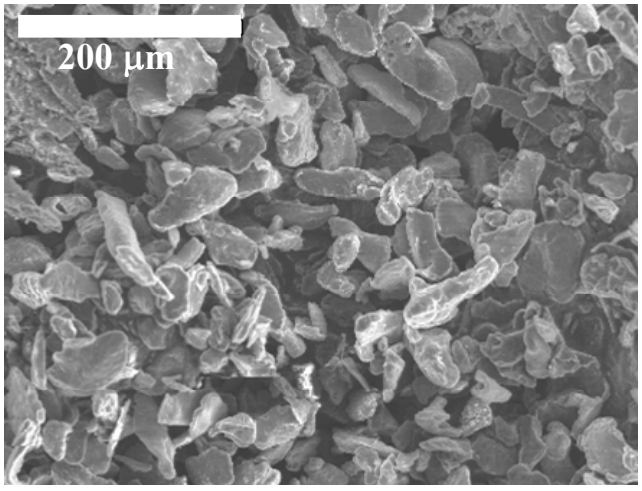

Figure 4-16. SEM micrograph of Pure Mg powder illustrating the morphologies and particle sizes.

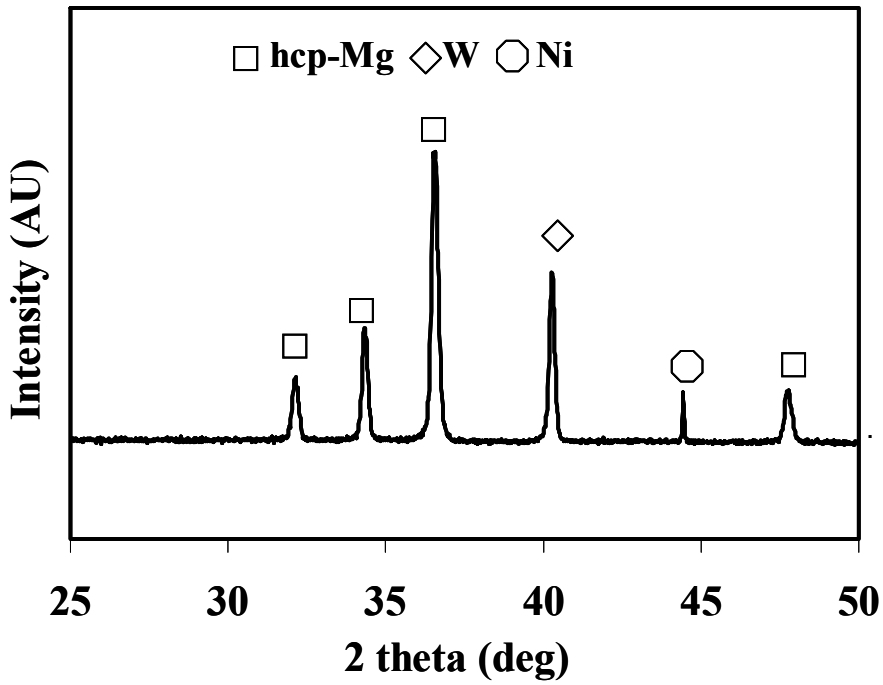

Figure 4-17. XRD profile of pure Mg powder after Ni-coating.

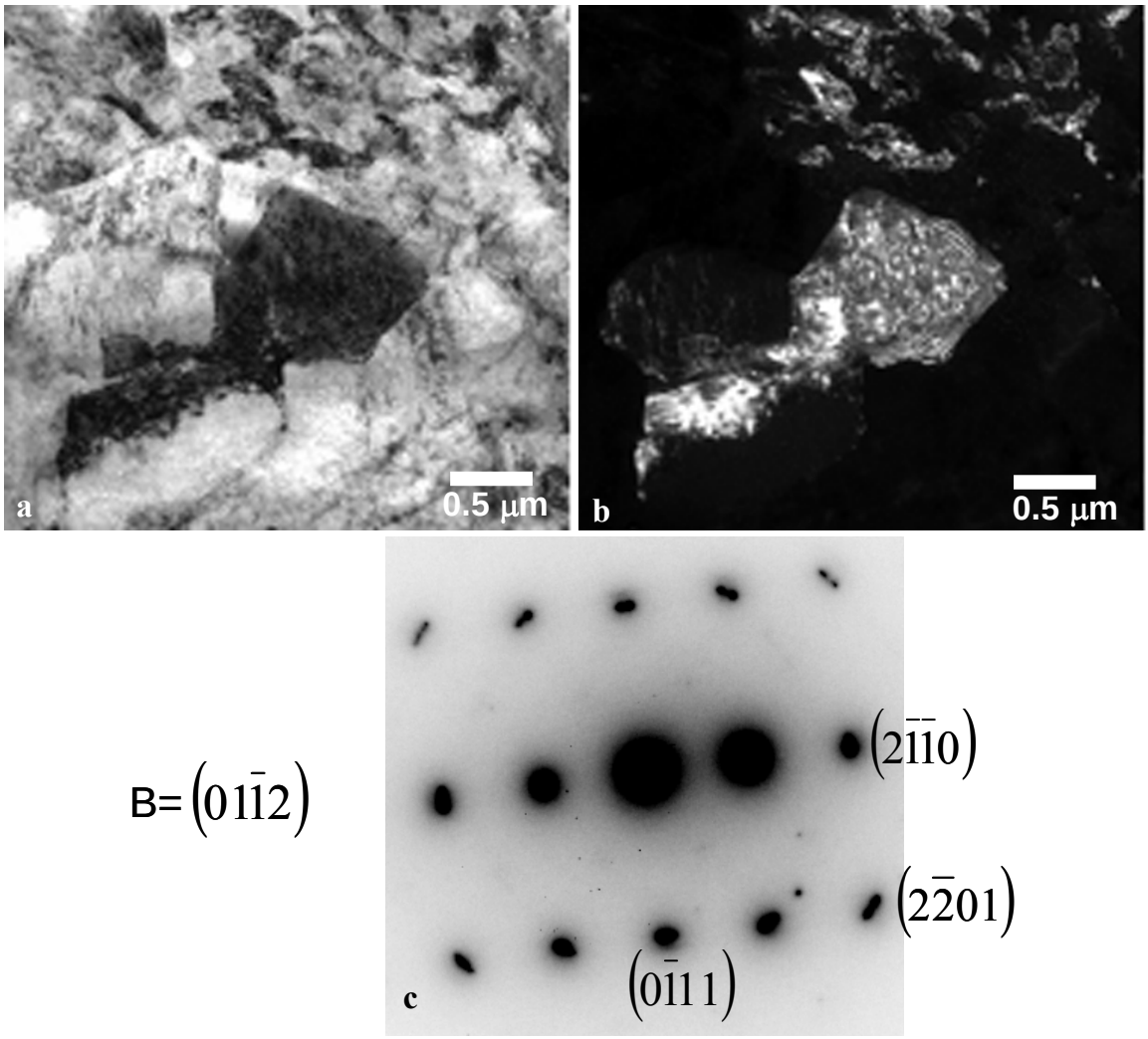

Figure 4-18. (a) Bright field and (b) dark field TEM micrographs illustrating the microstructure of the pure Mg powder. (c) The selected area diffraction pattern from the region shown in (a).

CHAPTER 5
MICROSTRUCTURAL EVOLUTION DURING PRESSURE COMPOSITION ISOTHERMS

One of the methods to evaluate hydrogenation and dehydrogenation processes is to establish the pressure-composition isotherms. These isotherms are developed under equilibrium conditions. As explained in Section 2.4, PCT tests are conducted at relatively high temperatures and sufficient time is given at each step to obtain equilibrium conditions. These isotherms are usually carried out to identify the thermodynamic properties of enthalpy and entropy of hydride formation and decomposition.

The major limitation in using magnesium hydride as a hydrogen storage system is its high enthalpy of formation [8]. Theoretical calculations have reported that the enthalpy of formation was reduced from 76 to 28 kJ/mol with Al incorporation in magnesium hydride [18]. Therefore, there has been significant interest to investigate the effect of Al on the stability of magnesium hydride. Depending on the composition of the alloy several phases may exist in the starting microstructure, namely hcp-Mg, $Mg_{17}Al_{12}$, and Al_3Mg_2 and the equilibrium plateau pressure of hydride formation from these phases is different. For example, the magnesium hydride formation from $Mg_{17}Al_{12}$ phase was observed to take place around 0.8-0.9 MPa pressure of hydrogen at 350°C [28]. In case of the Al_3Mg_2 phase, at the same temperature, the equilibrium plateau pressure of hydride formation was reported to be significantly higher (1.4 MPa) [28]. An equilibrium plateau pressure of hydride formation of about 1.6 MPa had been observed for an Mg-10at%Al at 400°C [28].

Most of the PCT studies reported for Mg based alloy powders focused on measuring the enthalpy and entropy of formation/dissociation of metal hydride [43, 49, 109]. However, no direct Van't Hoff plot had been developed for a given Mg-Al alloy. But the sparsely available equilibrium plateau pressures for various Mg-Al alloy compositions have been collected and the

Vn't Hoff plot was developed as was shown in Chapter 2 (See Figure 2-10) [80]. This curve indicates that the enthalpy of formation/dissociation of MgH_2 does not change significantly by the addition of aluminum. It should be noted that the equilibrium plateau pressure data were compiled from different experiments and a consistent set of data for a particular Mg-Al alloy powder has not been developed so far. Since the PCT curves in Mg-Al alloy powders with more than one phase are complex, it is necessary to investigate the evolution of different phases to measure the thermodynamic properties precisely.

One of the aims of this study has been to evaluate the enthalpy and entropy of magnesium hydride formation in Al-rich hcp-Mg solid solutions. A systematic approach was considered to evaluate the phase transformations during the development of the PCT curves for Mg-Al alloy powders. In addition, PCT curves for a commercially available pure Mg powder were also developed to understand the effect of Al addition to hcp-Mg. An Mg-10at%Al alloy powder was employed to investigate the phase transformations that occur during the development of a PCT curve at 350°C. Using the knowledge about the phase transformations in Mg-10at%Al powder, the effect of temperature, and Al content in hcp-Mg are demonstrated by establishing PCT curves for Mg-8at%Al and Mg-4at%Al alloy powders. Finally, the effect of Al addition on enthalpy and entropy of formation/dissociation of magnesium hydride are evaluated using the Van't hoff plots developed from these PCT curves.

5.1 PCT Curves for Pure Mg Powders

The pressure-composition isotherms for the commercial pure Mg powder, obtained within 275-350°C temperature range, are illustrated in Figure 5-1(a). Figure 5-1(b) represents the plot with a logarithmic scale for the pressure axis for additional clarity. The pressure of hydrogen during the initial stages of the experiment was increased by 0.025 MPa at each step and the step size was increased to 0.05, 0.1, 0.25 MPa at higher pressures. The small step size used during the

initial stages was to provide enough data points to observe the solubility of hydrogen in the hcp-Mg phase. To achieve equilibrium conditions during the experiment, a time period of 30 minutes was provided at each step. The total time to develop each PCT curve was approximately 46 hours.

The maximum solubility of hydrogen in the Mg powder at different temperatures tested is provided in Table 5-1, which elucidates an increase in the solubility limit with an increase in temperature. Furthermore, at a constant pressure the solubility of hydrogen at higher temperature is observed to increase with temperature.

It has to be recognized that two methods have been used in the literature to identify the solubility of hydrogen in magnesium. One method (method-1) involves the volumetric measurements of hydrogen absorption in Mg-H system at a constant pressure and temperature. The experiments using this method were generally conducted at low pressures ($P<1.013$ bar) to avoid hydride formation [12]. The other method (method-2) evaluates the pressure composition isotherms at high pressures and high temperatures [11]. The solubility calculated in the present study is based on method-2. The solubility data reported varied significantly based on the method of determination. The results obtained using method-2 for hydrogen solubility are always one order higher than that of method-1. For example, the solubility of hydrogen was calculated to be 0.001 wt% at 450°C at 0.4 MPa using method-1 while about 0.02 wt% of hydrogen was reported to be soluble in Mg at 440°C and 0.45MPa when measured with method-2 [11, 12, 110].

From Table 5-1 it can be noticed that the solubility of hydrogen in pure Mg from this study were a lot higher (0.02wt% at 440°C to 0.09wt% at 350°C) than the reported data using both the methods. The higher solubility values in this study can be attributed to the experimental

approach of the PCT curve, as the solubility of hydrogen in this method was determined near the three-phase equilibria of hcp-Mg, H_2 gas and MgH_2. The solubility values represent the maximum hydrogen (saturated) solubility in hcp-Mg at that temperature and pressure. Furthermore, the solubility data reported in the literature was for bulk Mg, while the Mg considered in this study is in powder form. The higher surface area of the powder also contributes to the higher solubility value as the solubility of hydrogen in magnesium involves a gas-solid reaction which increases with increase in surface area.

When maximum solubility of hydrogen is reached, a plateau region follows, which represents the formation of MgH_2 (Figure 5-1). The equilibrium plateau pressures of hydride formation and dissociation at different temperatures are presented in Table 5-1. Decreasing temperature resulted in a reduction of the equilibrium plateau pressure from 0.48 MPa at 350°C to 0.08 MPa at 275°C. The plateau pressure of 0.67 MPa during absorption was reported for unmilled Mg powder at 350ºC which is close to the value observed in this study [98]. However, MgH_2 powders fabricated by reactive mechanical milling showed higher plateau pressures than the pure Mg powders [2]. Consistent with previously reported data [2], the PCT curves exhibited hysteresis, i.e., the plateau pressures of absorption and desorption at a given temperature are different. The difference in the equilibrium plateau pressure between absorption and desorption at 350°C for the unmilled Mg powder was reported as 0.25 MPa which is slightly higher (0.22 MPa) than for pure Mg powder used in this study [98]. The hysteresis observed in this study is due to the difficulty in nucleation of hcp-Mg during desorption of hydrogen from β-MgH_2. As the temperature of the PCT is reduced the hysteresis in pure Mg powder also reduced and the total amount of hydride is also lower. This observation suggests that the particles were hydrogenated completely to the theoretical capacity during absorption and upon desorption the

nucleation of hcp-Mg is hindered at equilibrium plateau pressure. However, further decrease in pressure helps in breaking the Mg-H bond and nucleates hcp-Mg.

At the end of plateau region the pressure increases steeply as a function of the absorbed hydrogen. The length of the plateau region was found to decrease with decreasing the test temperature. At 350ºC the total amount of hydrogen absorbed was close to the theoretical capacity of 7.6 wt% and it decreased to as low as 6.4 wt% at 275ºC. These results are consistent with the reported values in the literature, where a complete transformation of hcp-Mg into MgH_2 was observed in the unmilled and milled Mg powders at 350°C and 10MPa pressure [98]. Furthermore, the hydrogen content previously reported was ~ 6.8wt% at 300°C for mechanically milled hcp-Mg under high pressure [2].

Several factors may contribute to the apparent loss of capacity with reducing temperature. The transformation of hcp-Mg to β-MgH_2 involves a significant change in volume (approximately 32%). At lower temperatures the strain created due to hydride formation is not relieved and further transformation of hcp-Mg into magnesium hydride is inhibited[75]. In addition, the nucleation of magnesium hydride is fast while the growth is slow at relatively low temperatures like 275ºC. These conditions of hydride transformation forms a layer of MgH_2 around the surface and further hydrogenation of hcp-Mg is restricted as hydrogen has to diffuse through the hydride layer which is very slow. Therefore, the total amount of hydrogen stored is less at low temperatures.

From Figure 5-1(b), it can be noticed that the dehydrogenation part of the curve is not complete. i.e., not all hydrogen is released. This is due to the lack of enough assigned data points towards the end of the experiment. Due to the slow kinetics at low temperatures the total number of steps required to complete the dehydrogenation process is high. However, when the PCT

system moves to the next experiment, the reaction chamber is evacuated till the pressure in the system reaches a minimum value as mentioned in Chapter 3. Even though the data is not acquired during this step, the sample is allowed to dehydrogenate completely before the start of next experiment.

5.2 PCT Curves for Electrodeposited Mg-Al Alloy Powders

Three electrodeposited Mg-Al alloy powders with 4at%, 8at% and 10at% Al content were characterized in this study. The Mg-10at%Al alloy powder was used to identify the phase evolution during the development of PCT curve at 350°C. This goal was achieved by partially hydrogenating or dehydrogenating along the path of the PCT curve at 350°C. Initially a complete absorption part of the PCT was carried out on a sample and based on the obtained curve new tests were designed, where the test was stopped at various points along the curve. The absorption part of the Mg-Al powder during PCT was conducted to design further experiments for identifying the phase transformations. The samples from each experiment were evaluated for phases and microstructures. The details of the experiments are described in the following sections.

5.2.1 Microstructural Evolution during PCT Test at 350°C

The PCT curve for Mg-10at%Al alloy powder at 350ºC is shown in Figure 5-2. A comparison of PCT curves for pure Mg powder and Mg-10at%Al powder (Figure 5-3) depicts that the PCT curve of Mg-Al powder exhibits a continuous increase in slope during hydrogen absorption in contrast to relatively flat region for pure Mg powder. The solubility limit of hydrogen near the saturation point of the PCT curve in Mg-10at%Al was noticed to be lower than that of pure Mg powder. For the Mg-Al powder the hydride formation demonstrated a short plateau followed by a sloping curve rather than a flat region as was observed for the pure Mg powder. Furthermore, the PCT curve indicates a second plateau region at a higher pressure. To

understand the reasons behind the differences, the PCT curve for the electrodeposited Mg-10at% Al alloy powder was divided into several stages as shown in Figure 5-2 and separate experiments were carried out to evaluate the phase transformations in these stages. This division was based on the change in the transformation reaction, which was predicted by plotting the slope of the PCT curve versus the hydrogen wt% for both the hydrogenation and dehydrogenation parts of the PCT experiment as shown in Figures 5-4(a) and (b). A significant change in the slope of PCT curve indicates a change in phase transformation or a combination of phase transformations.

From the Figure 5-4(a) it can be noticed that during the hydrogenation process the first significant change in slope occurs at 0.01 wt% of hydrogen. The absorption up to solubility limit is defined as stage 1. Immediately after stage 1, the slope of the PCT curve drops to almost zero (flat region), which indicates the formation of a hydride phase. This region is defined as stage 2 and the slope of the curve in Figure 5-4(a) remained same till the hydrogen concentration in Mg-Al alloy powders reaches approximately 2.5 wt%. After this stage the slope increases till the hydrogen content of ~ 4.0 wt% (stage 3). Further increase of the pressure resulted in a drop of the slope of the PCT but does not reach zero. This region corresponds to the stage 4 of the PCT curve. Beyond this stage, with increase in pressure, no significant absorption of hydrogen was observed (stage 5).

The change in slope during desorption part of the PCT curve is shown in Figure 5-4(b). The slope of the desorption part of the curve is very high initially till the hydrogen wt% in the powder reached 4.6wt% where its value drops close to zero. The region till the hydrogen wt% in the powder is 4.6wt% is defined as stage 6 while the region where the slope is almost equal to zero is defined as stage 7 as indicated on the Figure 5-4(b).

Several experiments were conducted, where the powders were pressurized to various points along the PCT curve for the Mg-10at%Al powder and were analyzed for their phases and microstructure. These samples are identified in Table 5-2. Quantitative metallography was employed to calculate the phase fractions in the alloy powder at the end of each experiment. After each experiment the samples were cooled under hydrogen pressure. It should be noted that the cooling of the sample takes time and during this time period it is anticipated that slightly more amount of hydrogen is absorbed into the material. Hence, the phases that are analyzed do not correspond exactly to the points on the PCT curve, but they will be close enough for evaluating the transformations occurring during the PCT curve. Similar to that of pure Mg the pressure of hydrogen during these experiments was increased by 0.025 MPa at each step initially and then increased to 0.05, 0.1, 0.25 MPa at higher pressures. However, the time provided for reaching equilibrium at each step was selected to be longer (60 minutes) than the experiments conducted for pure Mg in-order to achieve true equilibrium as our previous experience on similar powders indicated that complete equilibrium could not be achieved in 30 minutes.

As described in Chapter 4 the phases present in the initial powder (sample S1) before the PCT experiment were hcp-Mg solid solution with small amounts of the intermetallic compound $Mg_{17}Al_{12}$ and fcc-Al phases (Figure 4-7). Figure 5-5 presents the results of characterization of the Mg-10%Al powder after 4.2wt% hydrogen absorption (sample S2), which correspond to the middle of stage 4 (see Figure 5-2). The resulting PCT curve from this experiment is shown Figure 5-5(a). The XRD profile of sample S2 is presented in Figure 5-5(b). A comparison of this profile with that of sample S1 reveals that significant amount of β-MgH_2 has formed in sample S2. In addition, the relative intensities of the peaks corresponding to the intermetallic compound $Mg_{17}Al_{12}$, and fcc-Al were reduced. A new peak corresponding to the Al_3Mg_2 intermetallic

compound was also observed in the XRD profile of sample S2. It has to be noted that the peak corresponding to the hcp-Mg was not present, indicating its complete transformation into magnesium hydride and incorporation in other phase. A comparison of the relative intensities of $Mg_{17}Al_{12}$ reveal that part of the intermetallic compound $Mg_{17}Al_{12}$ was transformed into MgH_2 as the relative intensity was decreased. In addition, the peak corresponding to the fcc-Al phase present in the sample S1 (See Figure 4-7) was not observed in sample S2. This observation suggest that fcc-Al phase absorbs more Mg at 350°C (solubility is higher) and upon cooling it is precipitated as part of Al_3Mg_2 at room temperature.

Representative SEM/BSE micrographs of sample S2 are shown in Figure 5-5(c) and (d). The phases were identified by their composition analysis (Table 5-3) and are labeled on the micrographs. Consistent with the XRD results, the grey contrast corresponding to hcp-Mg phase, which was observed in sample S1, was not found in these particles. In general, two types of particles were observed in sample S2 based on the amount of hydride. Some particles were hydrogenated to a significant extent while the others were partially hydrogenated. The dark phase, which corresponds to the MgH_2 phase, formed like a network inside the powder in some particles (Figure 5-5(c)) while it was restricted only near the surface in other particles as shown in Figure 5-5(d). The fcc-Al phase observed in these particles was disconnected as shown in Figure 5-5(c). From the microstructural analysis it can be concluded that Al was rejected from hcp-Mg phase during the hydride formation and precipitated as fcc-Al phase. Similar theories have been proposed in the literature that during the hydrogenation of Mg-Al alloys [28, 80], the Mg-Al alloy powder dis-proportionates during hydrogen absorption into fcc-Al and hcp-Mg phases. The hcp-Mg phase formed during this reaction absorbed more hydrogen to form the β-

MgH_2 while the fcc-Al does not transform [26, 28, 80, 97, 111]. This observation is attributed to the low solubility of Al in MgH_2 [112].

Figure 5-6 presents high magnification SEM/BSE micrographs of sample S2. It appears that MgH_2 nucleates at specific locations on the surface and grows into particle as indicated by the white dashed lines on the micrograph. The various nucleation points on the surface can be the triple junction of catalyst, hcp-Mg and hydrogen or any defects on the surface. In addition, cracks were observed in MgH_2 grains due to the stress in hydride because of the excessive volume expansion during the hydride formation. Higher magnification image of a particle from sample S2 (Figure 5-7), which is hydrogenated to a significant extent, illustrated that the MgH_2 was under significant stress and hence extensive cracking was observed in the hydride grains.

The fractions of different phases for sample S2 are presented in Table 5-4. As was mentioned previously two types of particles were found in this sample (See Figure 5-5). In Table 5-4, the values in the first row correspond to the particles that were hydrogenated to a significant extent (Figure 5-5(c)) while the second row represents for particles that were partially hydrogenated (Figure 5-5(d)). The phase fraction analysis illustrated that during hydrogenation all the particles did not absorb hydrogen equally. The differences in the absorption behavior of the particles can be attributed to the catalyst distribution, and the thermal and elastic stresses created during the transformations. Analytical model developed for hydrogenation of metal particles also predicts that at any given instance, the fraction of metal transformed into hydride in the particles is not same for all the particles but it follows a log-normal distribution [2, 76]. The origin of the two kinds of particles can be attributed to the different sizes of the particles or the distribution of catalyst on the surface of the particle. As noticed from the results in the present study, stress was developed in the particles during the hydrogenation and inhibited the hydride

growth. The amount of stress in the particle was dependent on the size of the particle and hence the total hydride formed in each particle was affected.

Sample S3 was hydrogenated to the maximum pressure (9MPa) that was possible in the PCT system to understand the phase transformations after the stage 4 and to characterize the powders after the completion of hydrogen absorption part in the PCT experiment. The slope of the PCT curve rose significantly as is evident in Figure 5-4(a) after the stage 4. The PCT curve and the XRD profile of the sample S3 are presented in Figure 5-8(a) and (b). The β-MgH_2 phase along with the fcc-Al phases were observed in this sample. Very small peak corresponding to the intermetallic compound Al_3Mg_2 was also present in the XRD profile. By comparing the XRD profile of sample S3 with S1 and S2, it can be concluded that the intermetallic compound $Mg_{17}Al_{12}$ was hydrogenated completely to form the Al_3Mg_2 and this intermetallic further hydrogenated to form MgH_2 and fcc-Al.

The microstructure of sample S3 as observed in SEM/BSE mode is shown in Figure 5-8(c) and (d). Other than the β-MgH_2 phase, the only other contrast (bright) that was observed correspond to fcc-Al as indicated by the compositional evaluation (Table 5-3). The microstructure of the particles in this sample was noticed to be similar to that of the particles that are completely hydrogenated in sample S2. The MgH_2 in sample S3 formed as a network all around and inside the particle. As demonstrated in Figure 5-8(c), fcc-Al phase was present inside the particle and a significant amount in chunks near the root. The amount of Al in the hydride was about 0.8at% owing to its low solubility and confirming that Al was being rejected during the hydrogenation of the hcp-Mg. A higher magnification image of the hydrogenated powder is shown in Figure 5-8(d). Similar to that of sample S2 extensive cracking was also observed in this sample.

The phase fractions found in sample S3 indicated that the hydride content was increased and the amount of fcc-Al phase was present similar to that of the particles that were completely hydrogenated in sample S2. Even though a small peak corresponding to the intermetallic compound Al_3Mg_2 was seen in the XRD profiles of sample S3, the contrast corresponding to that phase was not detected in the SEM/BSE images because of its very low volume fraction. From the above results it can be concluded that the intermetallic compounds of $Mg_{17}Al_{12}$ and Al_3Mg_2 hydrogenate at higher pressures and form the β-MgH_2 and fcc-Al.

Stage 6 corresponds to the initial change in slope during the start of desorption as shown in Figure 5-4(b). With the drop in pressure, the concentration of hydrogen was not reduced significantly until the pressure of the system reached 2 MPa. Hence no samples were analyzed in this stage as the phases would be similar to that of the hydrogenated powder.

Stage 7, which was defined as the release of hydrogen from the magnesium hydride, was studied to understand the evolution of different phases during the desorption process. Sample S4 was produced by dehydrogenating the powder partially till the hydrogen content in the powder was about 3 wt%. The PCT curve for this sample is shown in Figure 5-9(a). After cooling the sample S4 to room temperature, the XRD profile (Figure 5-9(b)) indicated the presence of the hcp-Mg, $Al_{12}Mg_{17}$ phases in the powder. Other than these phases, peaks of remaining β-MgH_2 were also observed in the XRD profile. Furthermore, the fcc-Al phase present in sample S3 was not observed in this sample. These results suggest that upon desorption of hydrogen from the β-MgH_2 phase, hcp-Mg was formed and it reacted with the fcc-Al present in the powder to form the intermetallic compound $Mg_{17}Al_{12}$.

Representative SEM/BSE micrographs of sample S4 are presented in Figures 5-9(c) and (d). Similar to sample S2, two different particles were observed in sample S4, namely, particles

with low amount of hydrogen released (Figure 5-9(c)) and particles with significant amount of hydrogen released (Figure 5-9(d)). In addition, two other contrasts were observed in the SEM/BSE micrographs. The compositional analysis on these contrasts revealed that the grey contrast corresponds to the hcp-Mg phase while the bright contrast corresponds to that of the intermetallic compound $Mg_{17}Al_{12}$. These phases are labeled on the micrographs presented in Figure 5-9. SEM/BSE micrographs of sample S4 at higher magnifications is presented in Figure 5-10. Detailed analysis of the microstructural features revealed that desorption of hydrogen started at the surface of the particle. As hydrogen was released from the powder, the hcp-Mg nucleated and reacted with the fcc-Al to form the $Mg_{17}Al_{12}$ as shown in Figure 5-10(a) near the surface. Furthermore, it can be seen in Figure 5-9(d) that the bright and grey phases are always connected to the surface with no disconnected bright phase inside the dark phase, as was seen in sample S3, were identified. Therefore, it can be concluded that desorption of hydrogen started on the surface by the nucleation of the hcp-Mg, which grew into the particle. During this process the nucleated hcp-Mg phase dissolved Al until it was saturated and formed the intermetallic compound $Mg_{17}Al_{12}$. It is to be noted that during the cooling of the sample S4, hydrogen absorption took place as the sample was cooled under high pressure. This pressure was sufficient enough to form the MgH_2 at lower temperatures as the equilibrium pressure of hydrogenation was lower at these temperatures. The newly formed hydride during cooling rejected the Al back into Mg and contributed to the formation of $Mg_{17}Al_{12}$.

The volume fractions of different phases in sample S4 is presented in Table 5-4. These values suggest that the volume fractions of the hcp-Mg and the intermetallic compound $Mg_{17}Al_{12}$ are higher in some particles (Figure 5-9(d)) when compared to the other particles. Based on the microstructures and the volume fraction calculations it can be suggested that the

dehydrogenation takes place to a different extent in various particles of the powder which is similar to the observation made for hydrogenation.

Sample S5 represents the powder that has undergone a complete hydrogenation and dehydrogenation cycle. The XRD profile (Figure 5-11(a)) of this powder illustrates the presence of hcp-Mg and the intermetallic $Mg_{17}Al_{12}$ phases which were similar to that of initial powders. It is to be noted that the peak corresponding to the fcc-Al phase was absent. The distribution of the phases present in the sample was analyzed by SEM and the corresponding micrographs are presented in Figure 5-11(b). The compositional analysis of the powders (Table 5-3) indicated that the bright phase in the microstructure corresponds to the intermetallic compound $Mg_{17}Al_{12}$ phase, while the grey phase was hcp-Mg phase. A comparison of this sample with the sample S1 represented that the intermetallic compound $Mg_{17}Al_{12}$ had grown after 1 complete cycle of hydrogen absorption/desorption at 350°C while the XRD analysis suggested that the volume fraction of the intermetallic increased slightly. In sample S1, as shown in Figure 4-6, the intermetallic compound was present as fine precipitates in the hcp-Mg, while in sample S5 the size of the intermetallic precipitates was as large as 10 μm. In addition, the fcc-Al phase, which was present in the initial powder, was not observed in sample S5. This shows that that the high temperature and longer times involved during the desorption stage of the PCT curve, dissolves the Al in hcp-Mg and forms the intermetallic compound $Mg_{17}Al_{12}$ upon cooling. The phase fractions calculated revealed that about 80% of the microstructure consisted of the hcp-Mg phase, which is lower than the initial content. The lower content of hcp-Mg in sample S5 could be due to the transformation of the hcp-Mg into $Mg_{17}Al_{12}$ by absorbing the Al which was present at the root of the initial powder.

5.2.2 PCT Curves for Mg-8at%Al Powders at Different Temperatures

Figure 5-12 illustrates the pressure-composition isotherms developed for the Mg-8at%Al alloy powders. The first PCT curves ware developed sequentially at 350°C, 365°C, 380°C and 395°C. The solubility of hydrogen in hcp-Mg is presented in Table 5-5. Addition of Al to Mg reduced the solubility of hydrogen in the hcp-Mg phase significantly. By comparing the data in Tables 5-1 and 5-5, it can be noticed that the solubility of hydrogen is much higher in pure Mg even at lower temperatures. This phenomenon was also observed previously and is attributed to the reduction in unit cell volume of hcp-Mg with addition of Al [113].

The equilibrium plateau pressures of magnesium hydride formation and decomposition at various temperatures are listed in Table 5-5. The plateau pressures indicated in the table are for the formation/dissociation of hydride from hcp-Mg. These values are obtained from the mid plateau regions of the most flat part of PCT curve. Increasing temperature rendered a higher equilibrium pressure of hydride formation. Furthermore, the extent of the plateau region, which corresponds to the hydride formation, also increased with temperature, but at a given temperature the extent was reduced significantly when compared to the results for pure Mg due to the addition of Al. Similar to the Mg-10at%Al alloy powders, rather than a sharp bend in the isotherm, the slope of the pressure-composition curves varied gradually with composition. This behavior was found to be temperature dependent such that the steepest change in slope was found at the highest temperature. In addition, at all temperatures it was observed that during the dehydrogenation part of the PCT curve the hydrogen content was initially increased and then decreased with a reduction in pressure. This observation suggests that the time limit and the pressure step size chosen during hydrogenation are not sufficient to reach equilibrium, hence instead of an equilibrium condition a pseudo equilibrium condition existed during the test and further hydrogenation took place upon the dehydrogenation part at higher pressures. From Figure

5-12 it can be noticed that the hydrogen content after the hydrogenation cycle at all temperatures did not reach zero, similar to that of pure Mg powders. However, an examination of the powder after a cycle, revealed that the final microstructure do not have any magnesium hydride, hence it is assumed that the all of the hydrogen was released from the powder even though the PCT curves indicated the presence of hydrogen in the powder.

5.2.3 PCT Curves for Mg-4at%Al Powders at Different Temperatures

The PCT curves of the Mg-4at%Al alloy powder at different temperatures are presented in Figure 5-13. Similar to that of Mg-8at%Al powder, the PCT curves were developed at 350°C, 365°C, 380°C and 395°C in that order. As indicated in Table 5-6 the solubility of hydrogen did not change significantly with a decrease in Al content Mg-4at% Al powder.

The equilibrium plateau pressures for hydride formation and decomposition along with the extent of hydride formation are presented in Table 5-6. With the rise in temperature of the PCT experiment, the equilibrium plateau pressure of the hydride formation also increased while the extent of plateau region (MgH_2 formation) remained almost constant in all the PCT curves developed at higher temperatures after the 1st experiment at 350°C. This behavior was also observed in pure Mg powders.

5.3 Enthalpy Determination

The plateau pressures given in Tables 5-1, 5-5 and 5-6 for pure Mg, Mg-8at%Al and Mg-4at%Al were used to determine the enthalpy of formation/dissociation of magnesium hydride. The enthalpy and entropy of hydrogenation or dehydrogenation can be calculated according to the Van't Hoff equation:

$$\ln\left(P/P_0\right)=\frac{\Delta H}{RT}-\frac{\Delta S}{R} \qquad (5\text{-}1)$$

where P_0 is the atmospheric pressure, ΔH is the enthalpy of hydriding/dehydring reaction, ΔS is the entropy of hydriding/dehydring reaction, T is the absolute temperature and R is the gas constant. The resulting Van't Hoff plots for magnesium hydride formation and dissociation are shown in Figure 5-14. The enthalpy and entropy values calculated from the slopes and intercepts of the linear fits to the Van't Hoff plots are represented in Table 5-7. The enthalpy of formation was reduced from 79 KJ/mol for pure Mg to 72.6 KJ/mol for Mg-Al powder, however, the enthalpy of dissociation almost remained the same for both the powders. The calculated enthalpy of hydride formation for both Mg-8at%Al and Mg-4at%Al powder were slightly lower than the enthalpy of formation of hydride reported for $Mg_{17}Al_{12}$ but higher than the enthalpy value reported for Al_3Mg_2 [80]. Even though, the enthalpy values of hydride formation/dissociation were not changed significantly from that of pure Mg powder, the plateau pressures of formation/dissociation were increased for Mg-Al alloy powder.

5.4 Discussion

5.4.1 Phase Transformations in PCT Curve of Mg-10at%Al Powders

As indicated in Figure 5-2, a hydrogenation/dehydrogenation cycle of Mg-Al alloy powder can be divided into 7 stages. The division of various stages was based on the significant change in slope of the PCT curve as it indicated a change in transformation reaction. These changes in slopes are presented in the Figures 5-4 (a) and (b) for hydrogenation and dehydrogenation parts of the PCT curve respectively. The different stages are marked on these curves to show the difference in the slope, which are related to a change in transformation reaction.

Stage 1 indicated on Figure 5-4 corresponds to the formation of α-solid solution of hydrogen in Mg-Al alloy powder. A comparison of solubility values for pure Mg and Mg-10at%Al alloy powder revealed that the solubility of hydrogen decreased with the addition of Al to hcp-Mg. These results are consistent with the calculated Al-Mg-H phase diagrams based on

the available experimental data, which suggest that the hydrogen solubility is very low in the hcp-Mg phase, and the addition of Al results in a decrease in solubility of hydrogen [12].

After stage 1, the slope of the PCT curve decreased significantly to almost zero (stage 2) and continues to be zero till the hydrogen concentration in the powder reached about 2.5 wt%. This stage indicated the formation of magnesium hydride from the hcp-Mg phase. During this transformation, Al was not dissolved in the magnesium hydride phase and the rejected Al reacted with the hcp-Mg to form the intermetallic compound $Mg_{17}Al_{12}$. In previous studies, it has been shown that under the conditions of P= 0.6 MPa, and T= 350°C during stage 2, the intermetallic compound $Mg_{17}Al_{12}$ is stable and does not form the magnesium hydride [53]. The phase transformations taking place during the stage 2 can be written as follows:

$$Mg(Al) + H_2 \Rightarrow MgH_2 + Al(Mg) \tag{5-2}$$

$$Al(Mg) + Mg(Al) \Rightarrow Mg_{17}Al_{12} \tag{5-3}$$

The rise in the slope of PCT curve and absorption of hydrogen after stage 2 indicated that the hydride formation was occurring from different phases. According to the Gibbs Phase rule, the formation of MgH_2 occurs at constant pressure in a PCT curve when 3 phases and 2 components are present in the system. However, in a multi component system with more phases participating in the transformation, it allows more degrees of freedom and hence the pressure of the system also changes with composition during the transformation. Therefore a sloping curve rather than a flat plateau region was observed during the hydride formation in Mg-Al alloy powders.

A comparison of XRD curves of sample S1 and S2 it can be concluded that the magnesium hydride was being formed from both the hcp-Mg and the intermetallic compound $Mg_{17}Al_{12}$ as relative intensities of their peaks was reduced (compare Figure 4-9 and Figure 5-5(b)). Stage 3 was observed to continue till the concentration in the powder reaches 4.1 wt% of hydrogen. The drop in the slope at the end of stage 3 illustrated that all the hcp-Mg phase present in the powder was converted into MgH_2.

The slope of the PCT curve after stage 3 was observed to drop continuously till the hydrogen concentration in the powder reaches 4.3 wt%. This region was defined as stage 4 of the PCT curve. The drop of the slope indicated that the hydride formation was occurring from a single phase. Based on the XRD analysis of sample S1 and sample S2 it can be concluded that the $Mg_{17}Al_{12}$ content decreased while the Al_3Mg_2 phase content increased. This observation suggested that the MgH_2 was being formed from the intermetallic compound $Mg_{17}Al_{12}$. The amount of hydrogen absorbed during the stage 4 was very low due to the low amount of total intermetallic present in the powder. The transformation reaction occurring during the stages 3 and 4 is given as

$$Mg_{17}Al_{12} + H_2 \Rightarrow MgH_2 + Al_3Mg_2 \qquad (5\text{-}4)$$

During stage 5 the slope of the PCT curve increased continuously till the maximum pressure available in the system was reached. By comparing the microstructural and phase analyses of the sample S2 and S3 it can be concluded that the intermetallic compound Al_3Mg_2 was hydrogenating to form MgH_2 and fcc-Al phases in stage 5. The transformation reaction taking place during the stage 5 can be represented as follows:

$$Al_3Mg_2 + H_2 \Rightarrow MgH_2 + Al(Mg) \qquad (5\text{-}5)$$

Sample S4 indicated that the phases present in the powder after partial desorption of MgH_2 were the hcp-Mg phase, the intermetallic $Mg_{17}Al_{12}$ phase along with the remaining MgH_2. The absence of fcc-Al phase in sample S4 indicated that the hcp-Mg phase dissolved the Al and transformed into the intermetallic phase of $Mg_{17}Al_{12}$. The transformation reactions involved during stage 6 can be written as follows:

$$MgH_2 + Al(Mg) \Rightarrow Mg(Al) + Mg_{17}Al_{12} + H_2 \quad (5\text{-}6)$$

Comparison of XRD profiles of sample S1 and S6 indicated that the primary phases present in the initial powder and final powder were hcp-Mg and $Mg_{17}Al_{12}$. The small amount of fcc-Al present in the initial powder was not present. This proved that the electrodeposited Mg-Al powders can be recycled for further hydrogenations as Al did not absorb hydrogen.

5.4.2 The Effect of Al Content on Different Stages of the PCT Curve

The PCT curves of Mg-10at%Al, Mg-8at%Al and Mg-4at%Al developed at 350°C are compared together in Figure 5-15 to understand the effect of Al content on the different stages of PCT curves. It is clear that increasing the Al content affected the PCT curve. Figure 5-15 illustrates that, in the case of the Mg-10at%Al powder, stages 2 and 3 are well distinguished when compared to PCT curve developed for Mg-8at%Al powder. In case of Mg-4at%Al alloy powder the slopes corresponding to the stage 2 and 3 were not distinguishable.

The shape of the PCT curve depends on the composition and the time allowed at each step to reach equilibrium. Based on the results in this study, more intermetallics ($Mg_{17}Al_{12}$) are formed with higher amount of Al in Mg. When the intermetallic phase hydrogenates along with the hcp-Mg, a slope was observed on the PCT curve (stage 3 in Figure 5-3). However, after the

hcp-Mg was completely consumed, a plateau region corresponding to the formation of MgH_2 from $Mg_{17}Al_{12}$ was observed (stage 4 of Figure 5-3).

Another variable during the experiment, the time given to reach equilibrium, also affected the shape of the curve. If the kinetics of transformation is slow and sufficient time is not given to reach equilibrium, then the points on the PCT curve represents pseudo equilibrium rather than a true equilibrium. In the present study this can be observed in the PCT curves developed for Mg-8at%Al alloy powders. The continuous increase in slope of the PCT curve at 350°C (Figure 5-15) when compared to Mg-10at%Al powder was due to lower time applied to reach equilibrium (30 minutes for Mg-8at%Al and 60 minutes for Mg-10at%Al).

The sloping nature of the PCT curve during the absorption cycle was also observed to be less during the PCT curves of Mg-4at%Al alloy powders. This suggested that decreasing the Al content the PCT curve tends to reach the shape of the PCT curve of pure Mg (Figure 5-1).

A comparison of the PCT curves for pure Mg and Mg-8at%Al powders revealed that the addition of Al decreased the plateau region (Figure 5-16). The shorter plateau region is attributed to the formation of the $Mg_{17}Al_{12}$ intermetallic phase upon hydrogenation, which consumes the hcp-Mg. The higher plateau pressure observed in the Mg-8at%Al system can be explained by the presence of Al in the hcp-Mg, which changes the equilibrium conditions for hydride formation as well as the solubility of hydrogen in Mg.

Hysteresis in PCT curves was observed for both pure Mg and Mg-Al alloy powders. In a pure metal-hydrogen system the hysteresis is defined as difference between the equilibrium plateau pressures of hydride formation to that of hydride dissociation. This difference was observed to be smaller in Mg-Al alloy powders when compared to that of pure Mg powders at 350°C. As discussed in chapter 2, previous studies have suggested that the hysteresis in metal

hydrogen systems is due to the elasto-plastic constraints in the material [76]. Similar to the model predicted in the literature, the particles in Mg-Al alloy powders also showed a variation in hydride fraction and hence exhibited the hysteresis. The smaller difference between the equilibrium plateau pressures of hydride formation and dissociation in case of Mg-Al alloy powders can be explained by considering the driving force required for nucleation of Mg from the Mg hydride. From the PCT curves shown in Figure 5-16 it can be noticed that the desorption of hydrogen started at a relatively higher pressure in the case of Mg-Al alloy powder when compared to that of pure Mg powder. The nucleation of hcp-Mg was assisted by the presence of fcc-Al in case of Mg-Al powder. However, the pure Mg powder was completely hydrogenated close to its capacity (7.6wt%) and hence the nucleation of hcp-Mg required higher driving force and this was achieved when the pressure in the system was significantly lower than the equilibrium plateau pressure. This causes a higher hysteresis in case of pure Mg powders.

5.4.3 Effect of Temperature on the Different Stages during the PCT Curve

From Figure 5-12 it can be seen that increasing the temperature of the PCT curve increases the extent of the plateau region in stage 2. Furthermore, the slope of the PCT curve also increases with temperature after stage 2. These phenomena are attributed to the solubility of Al in the hcp-Mg phase. As illustrated in Section 5.2.1, Al was rejected out of the hydride and into the hcp-Mg phase during the formation of magnesium hydride in Mg-Al powders. The rejected Al dissolved in the remaining hcp-Mg and precipitated as the intermetallic compound $Mg_{17}Al_{12}$ when the maximum solubility of Al in the hcp-Mg phase at the temperature of the experiment was reached. The solubility of Al in the hcp-Mg phase increased with temperature in the range of 350-395°C (solubility increases from 8.5at% to 12at%) [27] and hence less amount of intermetallic compound formed at higher temperatures. The higher amount of the hcp-Mg phase

available at higher temperatures caused the increase in the extent of the plateau during the stage 2 as well as the rise in the slope at higher temperatures.

5.4.4 Effect of Al Content on the Enthalpy and Entropy of Hydride

The Van't Hoff plots indicated that the addition of Al to Mg did not change the enthalpy of magnesium hydride formation/dissociation (Table 5-7) significantly while theoretical studies have suggested that the incorporation of 8 at% of Al in the magnesium hydride reduces the enthalpy to as low as 28.36 $KJmol^{-1}$ [18]. These contrasting results between the theoretical and experimental studies can be explained by considering the absence of Al in the MgH_2 phase at high hydrogenation temperatures. Based on the results shown in Table 5-3, the amount of Al in the magnesium hydride at 350°C was negligible. The long duration involved in achieving the equilibrium conditions during the development of the PCT curves provided ample time for Al to diffuse out of the hydride phase. Thereby the magnesium hydride produced during PCT experiments contained only the equilibrium level of Al, which is quite low [112]. Hence the bond strength between Mg-H was not affected due to the absence of Al and thereby the enthalpy of formation/dissociation was not changed significantly when compared to pure Mg powders.

5.5 Summary and Conclusions

Pressure Composition isotherms of Pure Mg, Mg-10at%Al, Mg-8at%Al, and Mg-4at%Al were developed at different temperatures. The evolution of different phases and their fractions during the development of PCT curve of the Mg-10at%Al alloy powder was established. The results of this study reveal that the initial plateau region observed in the PCT curve corresponds to the formation of magnesium hydride. During this transformation the Al is rejected out of the hydride and into the hcp-Mg phase, which results in the formation of the intermetallic compound $Mg_{17}Al_{12}$. This intertmetallic compound hydrogenates further at a higher pressure to form a different intermetallic compound, i.e. Al_3Mg_2, and magnesium hydride. At much higher

pressures the Al_3Mg_2 phase also reacts with hydrogen to form magnesium hydride and fcc-Al. The enthalpy of formation/dissociation is not affected significantly when compared to the pure Mg powders as the magnesium hydride produced form Mg-Al alloy powders is depleted of Al and hence the magnesium-hydrogen bond strength is not affected.

Table 5-1. Hydrogen solubility and equilibrium plateau pressure of hydrides in pure Mg powders at different temperatures.

Temperature(°C)	Solubility (wt%)	Equilibrium plateau pressure (MPa)	
		Absorption	Desorption
275	0.01	0.09	0.08
300	0.02	0.18	0.16
325	0.04	0.37	0.29
350	0.09	0.7	0.48

Table 5-2. Nomenclature of different samples during the development of PCT curve.

Sample code	Condition
S1	Initial Powders
S2	Hydrogenated partially upto 2.5 MPa
S3	Hydrogenated upto maximum pressure (9 MPa)
S4	Hydrogenated to maximum pressure and dehydrogenated partially
S5	Complete 1 cycle of hydrogenation/dehydrogenation

Table 5-3. EDS compositional analysis of %Al in various phases in different samples mentioned in Table5-1

Sample	Dark	Grey	Bright
S1	-	9.9 ± 2.0	-
S2	0.8 ± 0.4 0.8 ± 0.4	-	62.8 ± 1.03 94.0 ± 1.2
S3	0.8 ± 0.5	-	93.0 ± 1.2
S4	0.5 ± 0.2	10.2 ± 0.7	39.2 ± 2.7
S5	-	5.5 ± 1.3	41.1 ± 1.2

Table 5-4. Phase fraction analysis on the samples mentioned in Table 5-1

Sample	Dark	Grey	Bright
S1	-	0.9±0.02	0.1±0.01
S2	0.82 ± 0.07 0.6 ±0.02	-	0.15 ± 0.08 0.35±0.1
S3	0.92 ± 0.02	-	0.07 ± 0.03
S4	0.77 ± 0.05 0.6± 0.06	0.13 ± 0.04 0.2 ± 0.03	0.09 ± 0.04 0.16±0.09
S5	-	0.8 ± 0.05	0.2 ± 0.1

Table 5-5. Hydrogen solubility and equilibrium plateau pressure of hydrides in electrodeposited Mg-8at%Al alloy powders at different temperatures

Temperature(°C)	Solubility (wt%)	Equilibrium plateau pressure (MPa)	
		Absorption	Desorption
350	0.02	0.73	0.63
365	0.01	0.97	0.89
380	0.03	1.33	1.23
395	0.04	1.89	1.78

Table 5-6. Hydrogen solubility and equilibrium plateau pressure of hydrides in electrodeposited Mg-4at%Al alloy powders at different temperatures

Temperature(°C)	Solubility (wt%)	Equilibrium plateau pressure (MPa)	
		Absorption	desorption
350	0.02	0.67	0.57
365	0.01	0.88	0.83
380	0.02	1.22	1.16
395	0.03	1.7	1.6

Table 5-7. Enthalpy and entropy values calculated from the Van't Hoff plot for the materials studied

Material	Process	ΔH(KJ/mol H)	ΔS(J/mol H K)
Pure Mg	absorption	-79.07±3.13	-143.12±2.8
	desorption	-79.91±2.3	-123.45±2.5
Mg-8at%Al	absorption	-72.69±2.8	-142.01±4.2
	desorption	-78.97±2.2	-133.04±3.9
Mg-4at%Al	absorption	-71.88±2.2	-111.85±3.46
	desorption	-79.17±3.77	-122.47±5.86

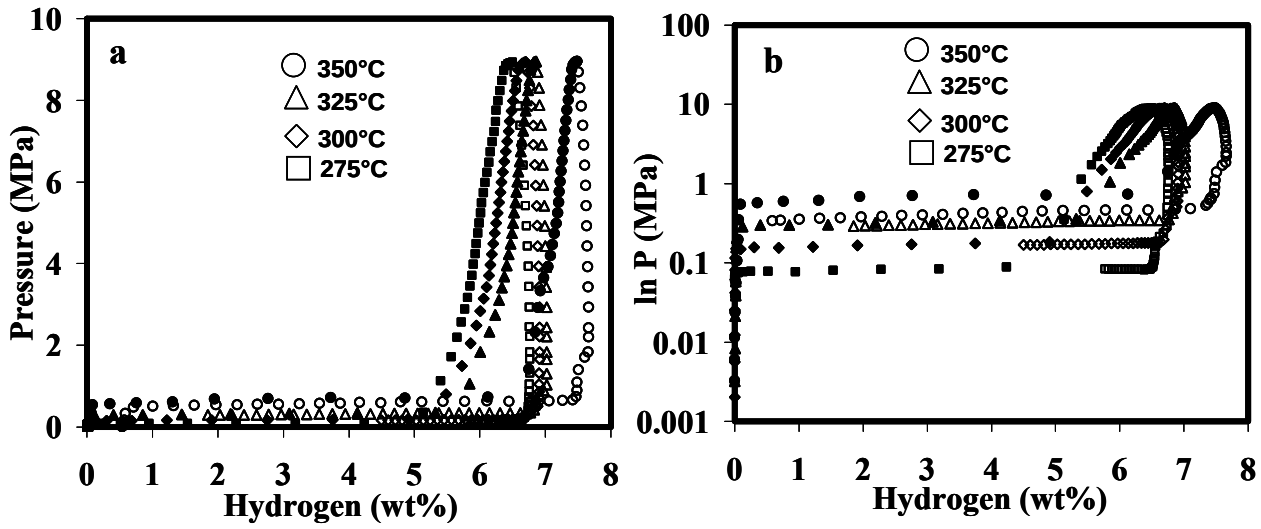

Figure 5-1. Pressure-composition isotherms developed for pure Mg powders at different temperatures (a) normal pressure axis (b) logarithmic pressure axis. The filled symbols represent the absorption curves and the unfilled symbols represent desorption.

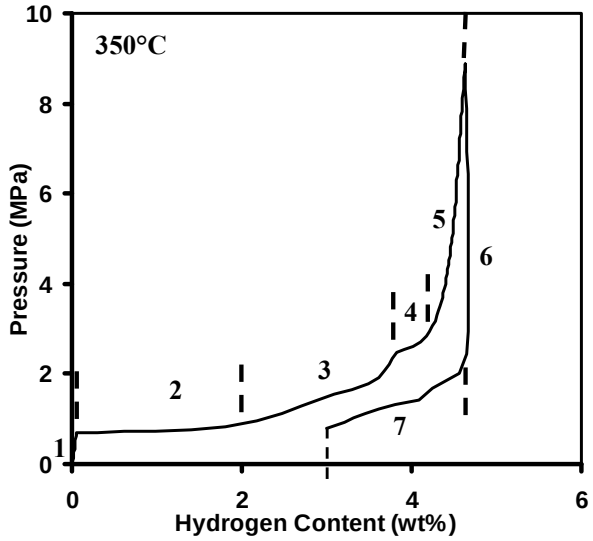

Figure 5-2. Pressure-composition isotherms developed for electrodeposited Mg-10at%Al powders at 350°C. The vertical dashed lines represent the division of stages.

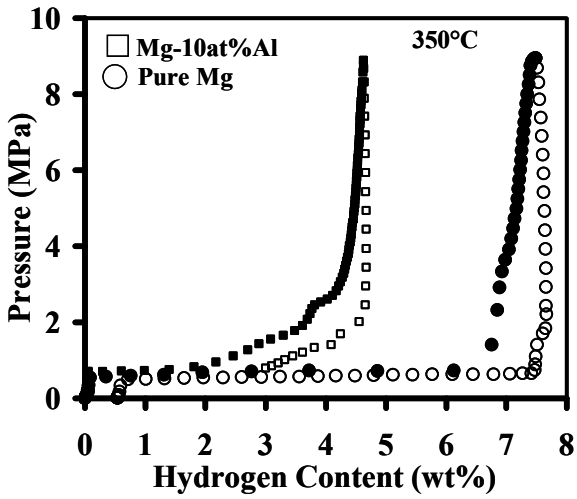

Figure 5-3. A comparison of PCT curve for pure Mg and Mg-10at%Al developed at 350°C.

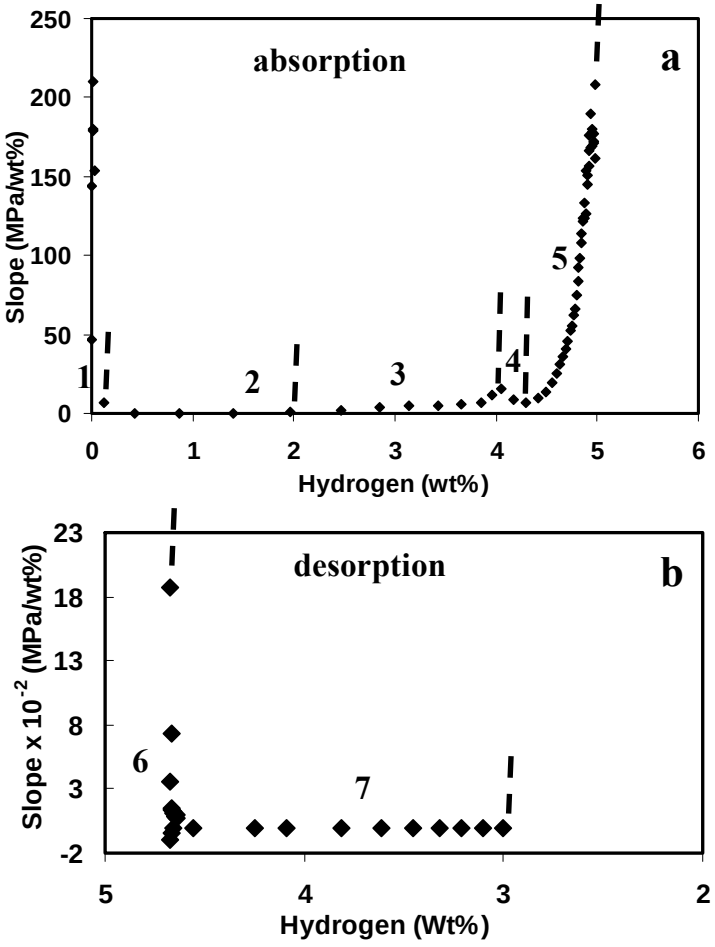

Figure 5-4. The PCT slope vs. Hydrogen wt% curves for (a) hydrogenation (b) dehydrogenation part of the PCT curve developed for Mg-10at%Al alloy powder at 350°C.

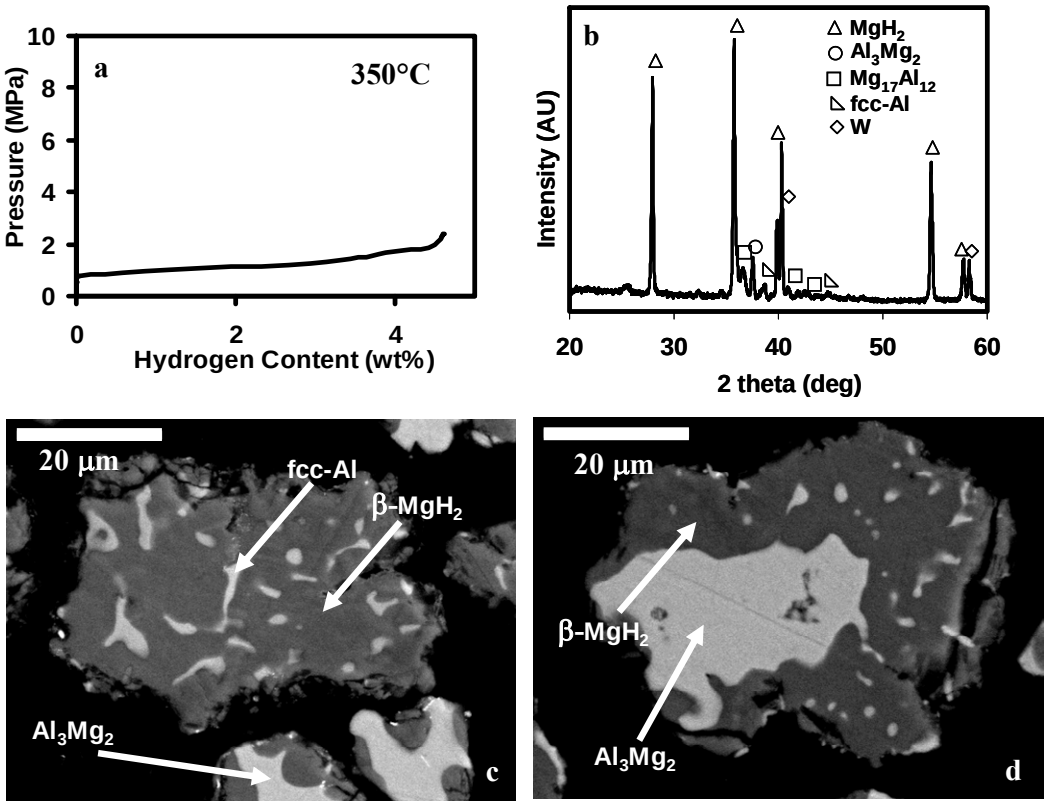

Figure 5-5. (a) The PCT curve of sample S2 developed at 350°C, (b) XRD patterns of the sample S2. Backscattered electron (BSE) micrographs of different types of particles in sample S2 revealing MgH_2 phase as "dark" and (c) Fcc-Al as "bright" and (d) Al_3Mg_2 phase as "bright" regions.

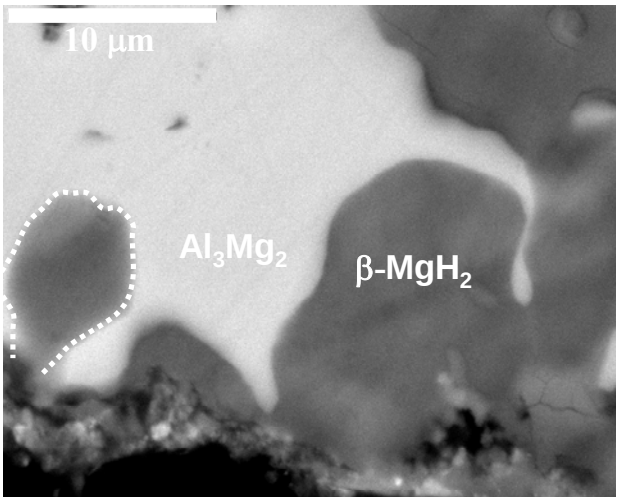

Figure 5-6. Higher magnification images of sample S2 showing the nucleation of hydride on the surface.

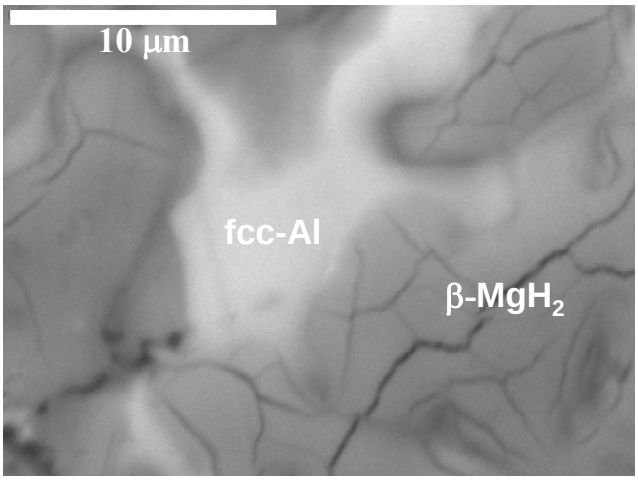

Figure 5-7. Higher magnification SEM/BSE micrograph of a particle in sample S2 showing the microstructure of MgH_2.

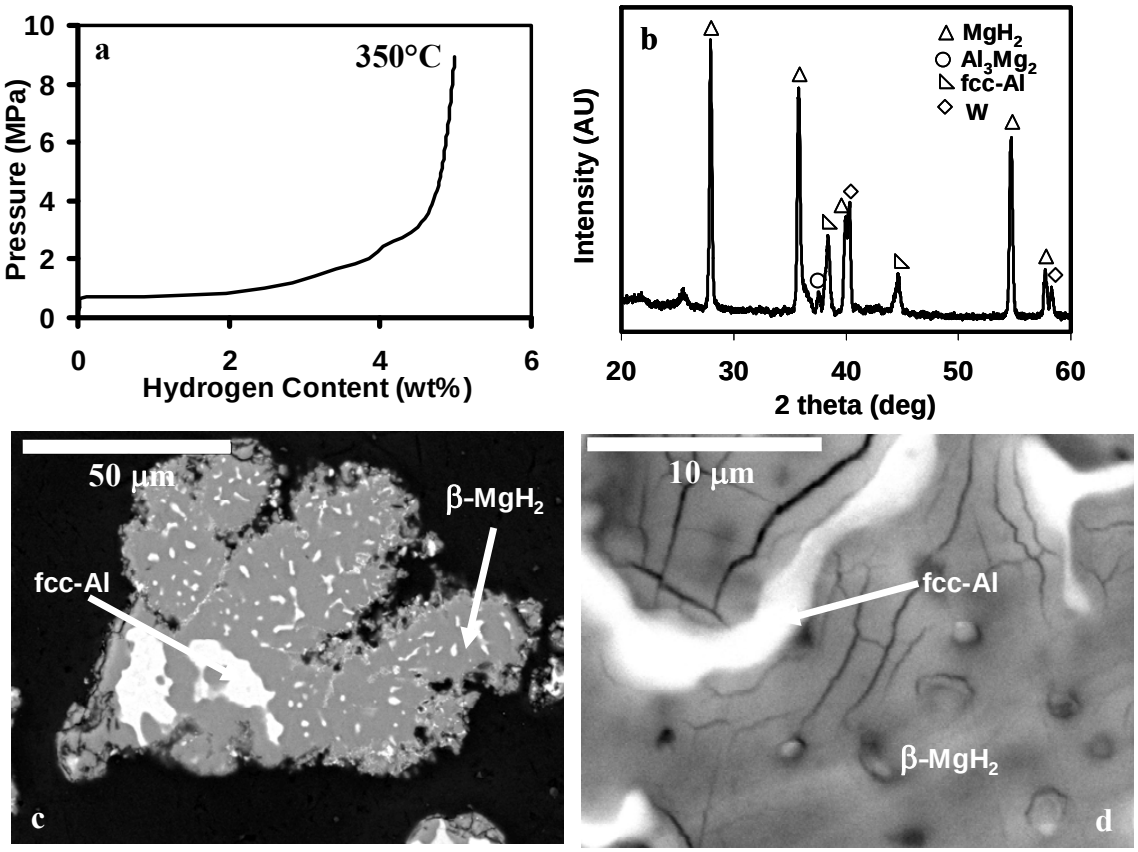

Figure 5-8. (a) The PCT curve of sample S3 developed at 350°C (b) XRD patterns of the sample S3. (c) BSE micrographs of particles in sample S3 revealing MgH_2 phase as "dark" and fcc-Al as "bright" regions. (d) Higher magnification micrograph of the microstructure shown in (c).

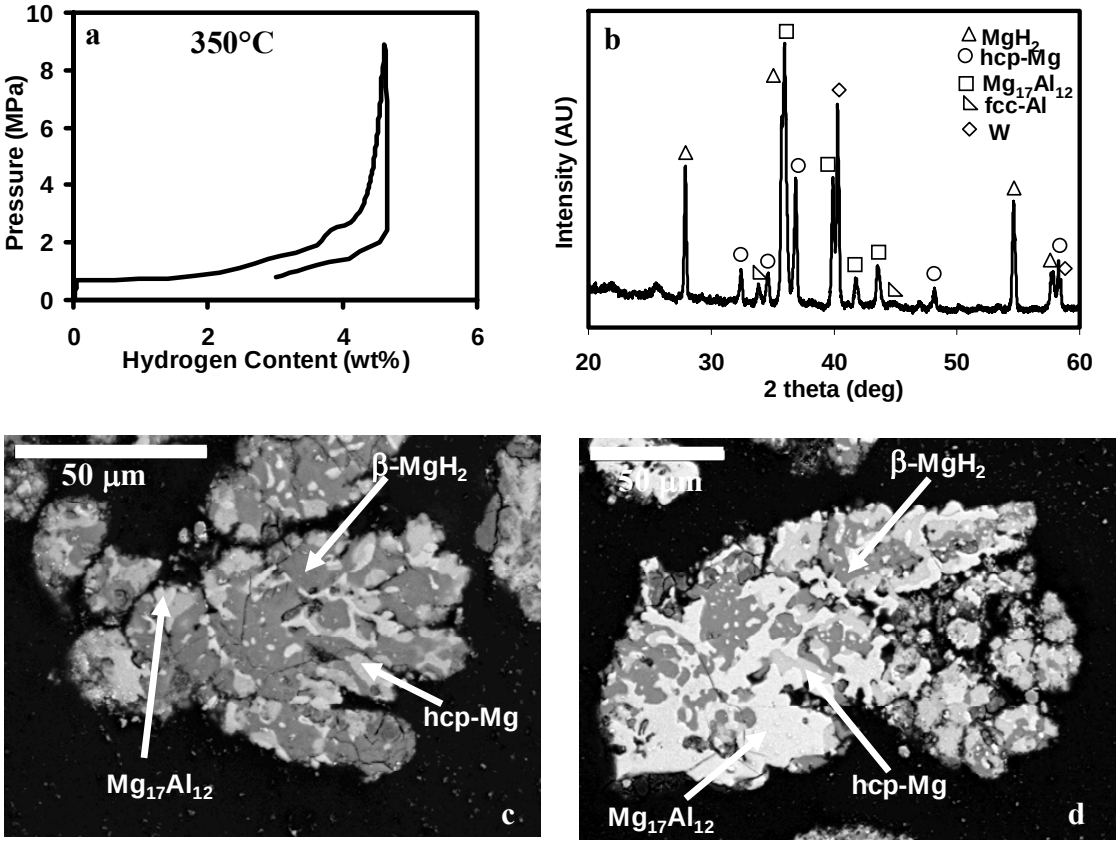

Figure 5-9. (a) The PCT curve of sample S4 developed at 350°C. (b) XRD patterns of the sample S4. BSE micrographs of different types of particles in sample S4 (c) particles with higher amount of MgH_2, and (d) particles with low amount of MgH_2.

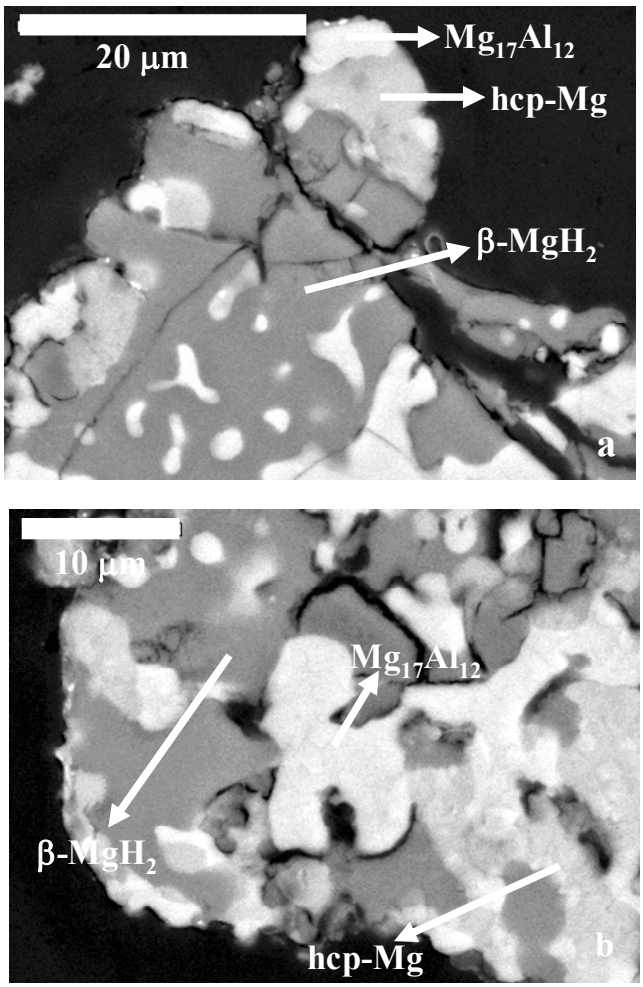

Figure 5-10. Higher magnification SEM/BSE micrographs of the partially desorbed powders illustrating (a) the phase evolution during desorption, (b) nucleation of different phases.

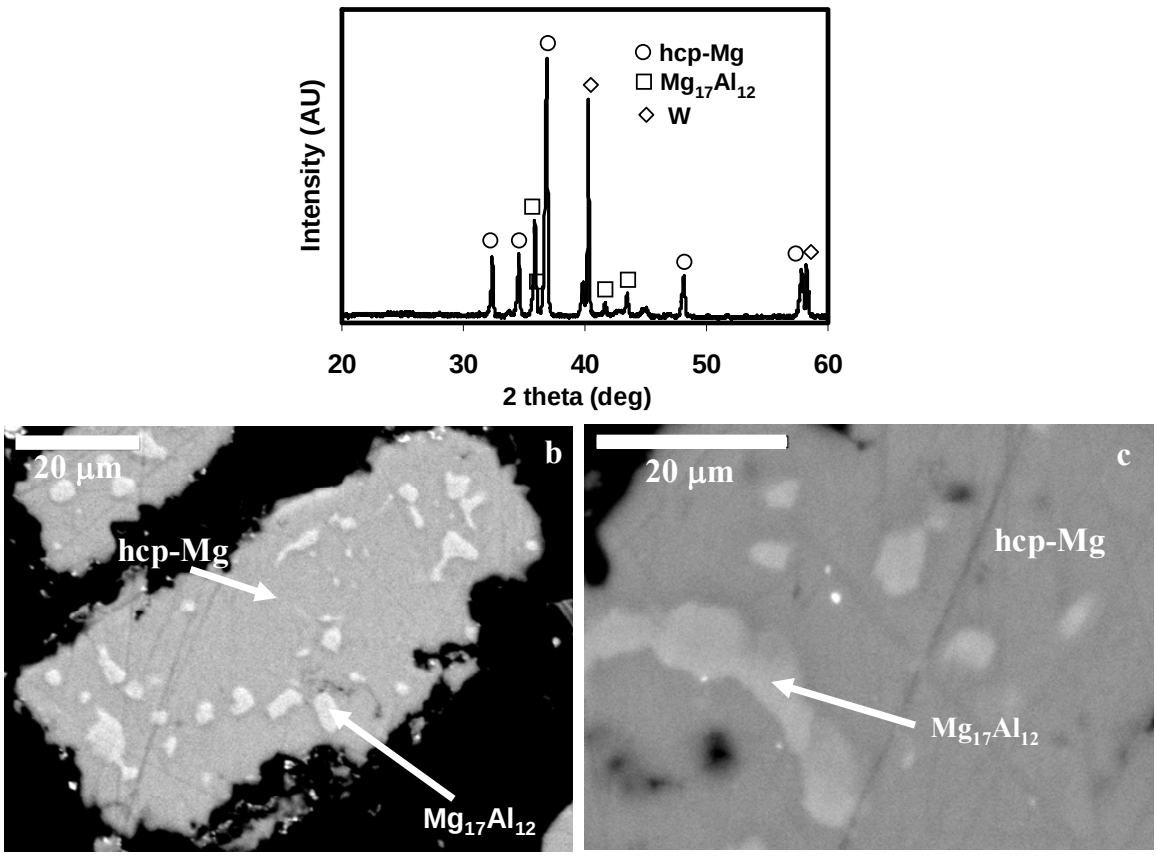

Figure 5-11. (a) XRD patterns of the sample S5. (b) and (c) BSE micrographs of particles in sample S5 revealing the presence of hcp-Mg and $Mg_{17}Al_{12}$ phases.

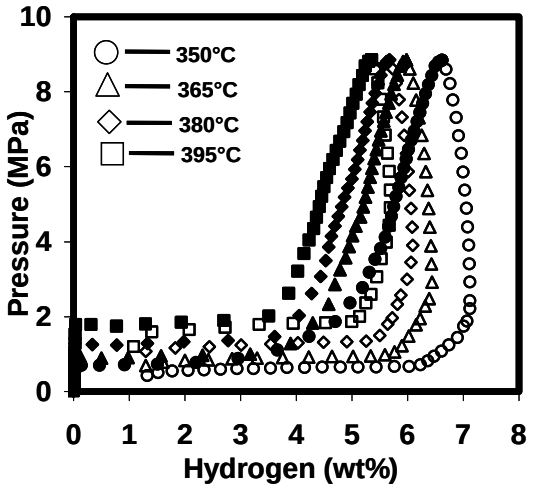

Figure 5-12. Pressure-composition isotherms developed for electrodeposited Mg-8at%Al alloy powders at different temperatures. The filled symbols represent the absorption curves and the unfilled symbols represent desorption.

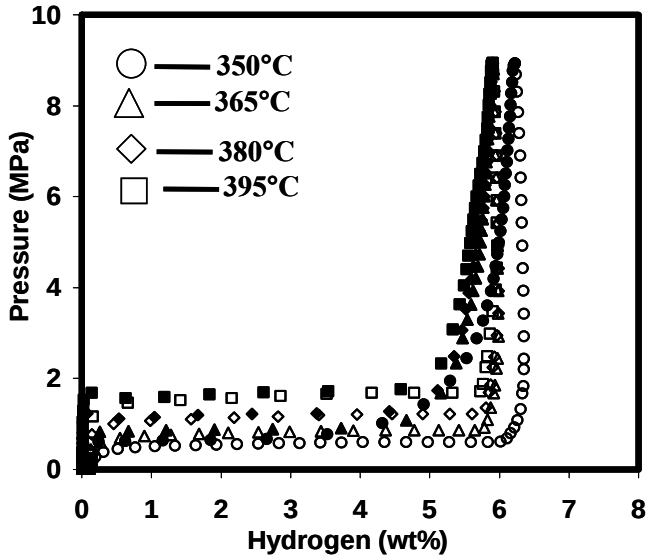

Figure 5-13. Pressure-composition isotherms developed for electrodeposited Mg-4at%Al alloy powders at different temperatures. The filled symbols represent the absorption curves and the unfilled symbols represent desorption.

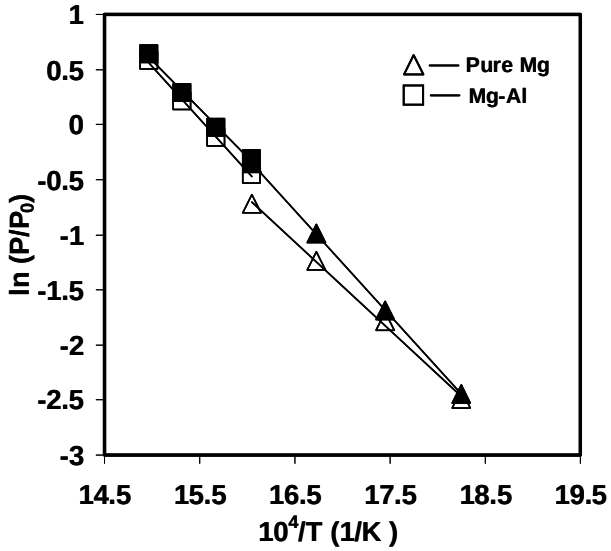

Figure 5-14. Van't Hoff plot obtained for pure Mg and Mg-8at%Al alloy powders. The filled symbols represent the plots from absorption data while unfilled symbols represent the plots from desorption data.

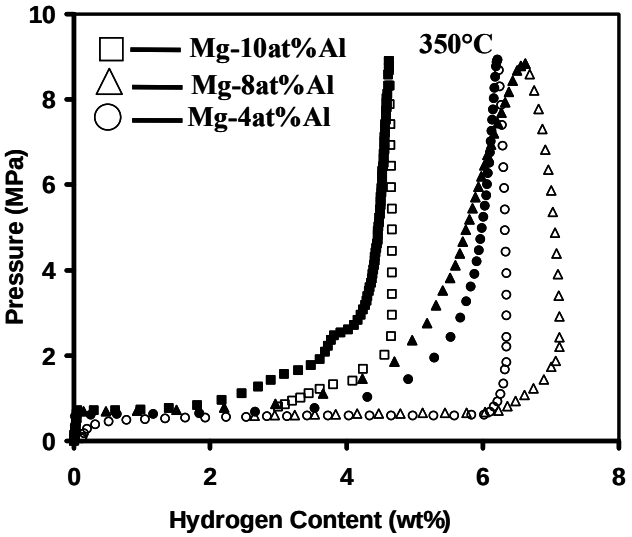

Figure 5-15.Comparison of the pressure-composition isotherms for electrodeposited Mg-10at%Al, Mg-8at%Al and Mg-4at%Al powders developed at 350 °C

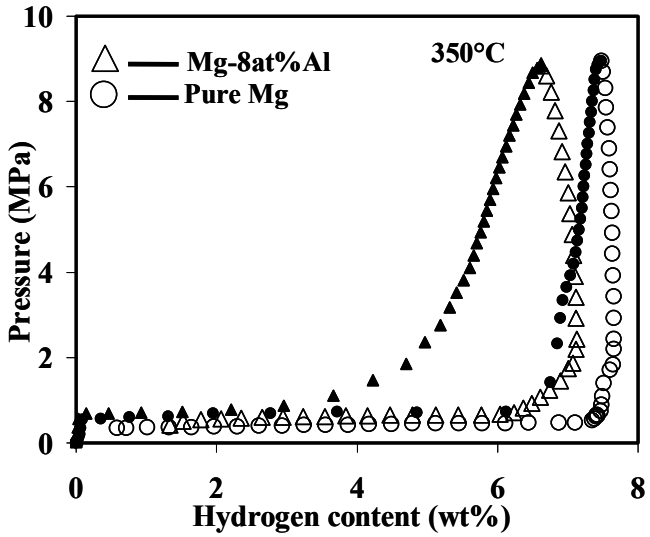

Figure 5-16. Comparison of the pressure-composition isotherms for pure Mg and Mg-8at%Al powders developed at 350 °C.

CHAPTER 6
EFFECT OF COMPOSITION AND TEMPERATURE ON HYDROGENATION BEHAVIOR OF ELECTRODEPOSITED MG-AL ALLOY POWDERS

In addition to the high thermodynamic stability of MgH_2, the Mg powders are also limited in usage due to their slow rate of hydrogen absorption and desorption. As illustrated in Section 2-5, most of the previous hydrogenation studies on the Mg-Al alloy powder had been conducted at relatively high temperatures, and have reported the β-MgH_2 and fcc-Al phases as products upon hydrogenation [28, 80]. For example, hydrogenation of ball-milled hcp-Mg alloy powders with 10at% Al at 400°C resulted in the final products consisted only of β-MgH_2. However, the hydrogenation of a powder with composition close to the $Mg_{17}Al_{12}$ intermetallic compound resulted in the formation of the fcc-Al phase as well as the magnesium hydride phase [28]. In another study, the hydrogenation of a cast and powdered Mg-30at%Al at 350°C had revealed that the amount of the $Mg_{17}Al_{12}$-phase increased during the initial period of hydrogenation and upon further hydrogenation for longer periods of time, the intermetallic phase transformed to magnesium hydride and fcc-Al [30]. Not only the hydrogenation behavior of Mg-Al alloy powders was conducted at higher temperatures, the microstructural studies of hydrogenated Mg-Al alloys has been very few [8, 114]. The investigation of a Mg alloy with 3at%Al (Alloy AZ31) using optical microscopy showed that the magnesium hydride nucleated at grain boundaries during hydrogenation at 450°C and its formation did not result in the development of the intermetallic $Mg_{17}Al_{12}$ phase [114]. On the other hand the hydrogenation of induction melt samples of Mg-10at%Al at 450°C revealed that the hydride may have nucleated inside the grains of the hcp-Mg [8].

Although a large number of studies have been conducted on the hydrogenation behavior of Mg-Al alloy powders at high temperatures (>300°C), very less attention have been given to the

hydrogenation behavior of Mg-Al alloy powders at lower temperatures that are close to the intended application. In addition, no systematic microstructural and compositional analyses have been carried out for Mg-Al alloy powders. The goal of this chapter is to evaluate the effect of Al addition on the hydrogenation behavior of Mg powders at low temperatures. Microstructural and compositional analyses were carried out to address the evolution of magnesium hydride and elucidate the presence of Al in MgH_2. To understand the effect of Al addition, pure Mg powders were also hydrogenated under similar conditions. The difference in microstructural changes due to temperature and hydrogen absorption was evaluated by comparing the microstructures of the hydrogenated powders with annealed powders that were heat treated in similar conditions.

6.1 Hydrogen Absorption Experiments

The electrodeposited nanocrystalline Mg-8at%Al, Mg-4at%Al powders and the microcrystalline pure Mg powders, after coating with Ni, were hydrogenated using the in house built hydrogenation setup. The details of the hydrogenation setup and the hydrogenation procedure are described in Chapter 3. Pressure was kept constant at 1 MPa, which is much higher than the equilibrium pressure of magnesium hydride formation from magnesium at the temperatures studied here. Each hydrogenation test described below was conducted at least twice under the same conditions for investigating the repeatability.

6.1.1 Effect of Al addition on Hydrogen Absorption Characteristics of Mg

Figure 6-1 compares the hydrogenation curves at 280°C for pure Mg and Mg-8at%Al alloy powders. The pure Mg powder exhibited a fast hydrogenation rate up to approximately 4wt% hydrogen and then the rate decreased sharply and eventually saturated at about 7.2wt% hydrogen, near to the theoretical capacity. The electrodeposited Mg-Al alloy powder initially hydrogenated very fast but the rate decreased gradually after about 0.35 wt% hydrogen. The hydrogen capacity, as defined by the approximate saturation level after 5 hours of hydrogenation,

was much lower for the Mg-Al alloy powder (Table 6-1). The X-ray diffraction profiles of both powders after hydrogenation are shown in Figure 6-2, which confirmed the formation of the β-magnesium hydride in both cases. The fcc-Al and the hcp-Mg phases present in the initial Mg-8at%Al powders were not observed after hydrogenation, while the content of the $Mg_{17}Al_{12}$ intermetallic was increased. The (110) XRD peak for the β–MgH_2 phase was fitted using a Peasron's VII function to calculate the lattice parameter, "a". The fitted peaks along with the original peaks for Mg-Al alloy and pure Mg powders hydrogenated at 280°C are shown in Figure 6-3. Similarly, the "c" lattice parameter was calculated from the fitted (101) peak. The 2 theta positions and the calculated lattice parameters presented in Tables 6-2 and 6-3, respectively, indicate that there is no significant change with the addition of Al when the powders are hydrogenated at 280°C.

The backscatterd SEM (BSE) micrographs of pure Mg and Mg-8at%Al hydrogenated at 280°C for 5 hours are presented in Figure 6-4 (a) & (b), respectively. In both powders the surface was completely covered with magnesium hydride. Pure Mg powders exhibited a small core of Mg in the particles, while the hydride in Mg-8at%Al exhibited a network like structure inside the particles. Based on compositional analysis, the bright phase observed in Figure 6-4(b) contained ~ 42 at%Al, which corresponds to the $Mg_{17}Al_{12}$ intermetallic phase. This phase was observed mostly inside the particles and in between the hydride phases. The distribution of % Al acquired from EPMA is shown in Figure 6-5. EPMA compositional analysis at multiple spots on 5 particles in this sample indicated that the amount of Al present in the β-MgH_2 is about 0.1±0.1 at%, which is very low within the accuracy of measurement. The absence of fcc-Al and Al_3Mg_2 phases suggested that $Mg_{17}Al_{12}$ intermetallic was stable under the conditions of 280°C temperature and 1MPa pressure and did not react with hydrogen. This observation was consistent

with previous studies that have shown that the $Mg_{17}Al_{12}$ intermetallic phase did not react with hydrogen below 300°C and was very stable even at high pressures of hydrogen. Also, as demonstrated in Chapter 5, the equilibrium pressure for hydrogenation of this phase at 350°C was 1.7MPa, higher than the pressure used here.

6.1.2 Effect of Amount of Al on the Hydrogenation Characteristics of Mg-Al Powders

The effect of Al content on the hydrogenation behavior was investigated by hydrogenating powders with 8at% and 4at% at 210°C and 1MPa pressure. The hydrogen absorption curves for the electrodeposited Mg-8at%Al and Mg-4at% Al alloy powders are compared in Figure 6-6 (a) and the corresponding XRD profiles are shown in Figure 6-6 (b). The Mg-4at%Al powder exhibited a slower hydrogenation rate in the first 50 minutes, but the rate did not decrease as fast as it did for the Mg-8at%Al powder. Therefore, higher amount of hydrogen was absorbed in the former powder after 5 hours of hydrogenation (Table 6-1). In addition, the hydrogenation curve of Mg-4at%Al indicated that even after 5 hours, the saturation has not been reached. From Figure 6-6(b) it can be noticed that both Mg-8at%Al and Mg-4at% powders contains hcp-Mg, fcc-Al and $Mg_{17}Al_{12}$ phases after hydrogenation. The amount of fcc-Al phase present in both the powders after hydrogenation was similar to that of the initial powder (Figure 4-9), showing that this phase did not transform during the hydrogenation process at 210°C. The XRD peaks of (110) and (101) for MgH_2 were fitted using the Pearson's VII function and the peak values are presented in Table 6-2. The corresponding lattice parameters calculated from the peak positions are presented in Table 6-3. These results indicated that the "a" parameter for Mg-8at%Al alloy powder was slightly higher than the value for Mg-4at%Al, while the "c" parameter was almost similar in both the powders.

The SEM/BSE micrographs of the Mg-4at%Al and Mg-8at%Al powders hydrogenated at 210°C are compared in Figure 6-7. In both powders the magnesium hydride was found only

along the surface but in case of the Mg-4at%Al alloy powder the surface was not completely covered with the hydride phase as indicated by dashed circles in the micrograph shown in Figure 6-7(a). The Mg-8at%Al alloy powder showed relatively finer hydride colonies in comparison to the Mg-4at%Al alloy powder. Much less $Mg_{17}Al_{12}$ intermetallic phase was found in the Mg-4at%Al powder and it was limited to the locations near the hydride phase. However, the Mg-8at%Al powder, exhibited precipitation of this intermetallic phase inside the hcp-Mg and away from the hydride phase. Figure 6-8 shows the line compositional analysis using EPMA. The compositional analyses along the line from A to B indicated that the amount of Al was increasing until the hcp-Mg/MgH_2 interface. The composition of Al decreased immediately after the interface inside the hydride phase. In addition, the formation of intermetallic compound as indicated in Figure 6-8, near the hydride and the hcp-Mg interface, suggested that the concentration of Al reached beyond the saturation of hcp-Mg. The Al content in the hydride was about 2.1at%, which was well below the concentration of Al in initial powder and these observations demonstrated that upon the formation of magnesium hydride, Al was rejected by this phase and was accumulated at the hcp-Mg/β-MgH_2 interface. Compositional measurements revealed that the Al content of the hydride decreased significantly from 2.2±0.2at% to 0.1±0.1at% with reducing the Al content of the powders from 8at% to 4at%.

6.1.3 Effect of Temperature on Hydrogenation Behavior of Mg-Al Alloy Powders

The effect of temperature on hydrogenation was evaluated by conducting hydrogenation tests at 280°C, 210°C, and 180°C for the Mg-8at%Al alloy powder. As shown in Figure 6-9, the hydrogenation temperature affected the absorption behavior of hydrogen significantly. The hydrogenation curves obtained at different temperatures revealed that the initial kinetics of hydrogenation was similar at 280°C and 210°C, while their total capacities after 5hrs were

significantly different. Reducing the temperature to 180°C drastically reduced the transformation rate initially, however, saturation in hydrogen absorption was not reached even after 5 hours. The total amount of hydrogen present in each powder is shown in Table 6-1.

The XRD profiles of the Mg-8at%Al alloy powder hydrogenated at different temperatures are presented in Figure 6-10, which indicated the formation of β-MgH_2 at all temperatures. Other than the hydride, only $Mg_{17}Al_{12}$ phase was observed in the powder hydrogenated at 280°C. For powders hydrogenated at 210°C and 180°C, along with these phases, the fcc-Al phase and a significant amount of the hcp-Mg phase were present in the structure. The peak positions (2 theta values) for β-MgH_2 was found to depend noticeably on the hydrogenation temperature of the Mg-8at%Al alloy powder. The XRD (110) and (101) peaks for β–MgH_2 produced at each temperature were fitted with a Pearson's VII function. The peaks fitted for (110) plane are presented in Figure 6-11 and their calculated positions are presented in Table 6-2. The lattice parameters of the tetragonal structure of MgH_2 were calculated from these values and are also included in Table 6-3. Interestingly, the shift in the peak positions increased with a decrease in the hydrogenation temperature. The calculated lattice parameters presented in Table 6-3 demonstrated that the "a" parameter was noticeably increased by lowering the hydrogenation temperature, while the "c" parameter remained almost constant.

Backscattered electron micrographs of the Mg-Al alloy powder hydrogenated at 280°C, 210°C, and 180°C are shown in Figure 6-12. Three different contrasts can be identified in these micrographs. The darker regions correspond to the magnesium hydride phase, the brighter regions represent the $Mg_{17}Al_{12}$ and the grey region corresponds to the hcp-Mg phase.

The average compositions of different contrasts are given in Table 6-4. The amount of Al present in the dark regions as a function of hydrogenation temperature is given in Table 6-4 and

plotted in Figure 6-13. The results indicated that the amount of Al in the dark region increases with reducing the hydrogenation temperature. It is interesting to note that parallel to this increase, the standard deviation of the measured compositions increases significantly. The lighter region in the core of the powders hydrogenated at 210°C and 180°C had a composition close to the alloy composition and is believed to consist of hcp-Mg and $Mg_{17}Al_{12}$ intermetallic phases due to the limited solubility of Al in Mg.

Consistent with the hydrogenation curves, a smaller fraction of hydride (dark phase) was found in the 210°C and 180°C hydrogenated samples. β-MgH_2 formed as a shell on the surface with a network of hydride extending through the particles hydrogenated at 280°C (Figure 6-12 (a)). However, after hydrogenation at 210°C, the hydride formation was limited to the surface layer and a non-hydrogenated core remained in the particles (Figure 6-12(b)). Furthermore, the powder hydrogenated at 180°C exhibited an incomplete shell of hydride, in addition to a core as shown in Figure 6-12(c). The brighter phase was observed in large amounts inside the powder hydrogenated at 280°C, while small precipitates of bright phase were observed at 210°C.

In order to identify the phases observed on the microstructure and investigate the partitioning of Al among various phases, compositional line analyses were conducted on several particles. The analyses for two such particles are presented in Figures 6-14. Figures 6-14 (a) and (b) represent the low magnification SEM/BSE micrographs of particles hydrogenated at 210 and 280ºC respectively. Figure 6-14(c) represents the distribution of Al along the line AB on a particle that was hydrogenated at 210°C. This region covered the three contrasts that were observed in the powder. The Al content near the $MgH_2/Mg_{17}Al_{12}$ and $Mg_{17}Al_{12}$/hcp-Mg interface changed sharply showing the accumulation of Al. Only two contrasts were observed in the powder hydrogenated at 280°C and the line composition analyses of the corresponding particle is

presented in Figure 6-14(d). These results revealed that the bright areas in the microstructure of the hydrogenated powders contained approximately 43 to 46 at% Al, which corresponds closely to the composition of the $Mg_{17}Al_{12}$ (41 at%) intermetallic compound. This phase was found in between the hydride colonies or at the interface between the hcp-Mg and the hydride in the 210°C hydrogenated powder. However, in the powder hydrogenated at 280°C, the intermetallic phase had grown significantly larger between the MgH_2 colonies due to the high temperature. The microstructure of the powder hydrogenated at 210°C contained a large amount of the Mg(Al)-phase (grey phase) as shown in Figure 6-12 (b) which is in accord with the XRD results shown in Figure 6-10. On the other hand, the microstructure and the XRD results (Figure 6-10) of the 280°C hydrogenated powder did not show detectable amount of the grey phase, i.e. the hcp-Mg phase.

6.2 Thermal Stability of Electrodeposited Mg-Al Powders

To identify the phase changes in Mg-8at%Al alloy powder due to the hydrogenation and the temperature, annealing tests were conducted on these powders. The Mg-8at%Al powder was annealed at 180, 210 and 280°C for two different time periods of 20 minutes and 5 hours. The annealing test for 20 minutes corresponds to the initial time where the powder was heated before insertion of hydrogen and the 5 hours experiment corresponds to the hydrogenation time.

The SEM/BSE micrograph of the powders heat treated for 20 minutes at 180°C, 210°C, and 280°C are presented in Figure 6-15. Other than hcp-Mg, the contrast corresponding to the intermetallic compound was not identified in powders heat treated for shorter times. At higher magnifications, very fine particles with bright contrast appeared but the composition of those particles could not be identified due to their size. The SEM/BSE micrographs of the powders heat treated for 5 hours are shown in Figure 6-16. The intermetallic compound has grown to a certain extent at 180 and 210ºC while it has grown significantly at 280ºC after 5 hours. Small

precipitates of the intermetallic compound were observed in case of the powder hydrogenated at low temperatures while large intermetallic phase was observed when annealed at 280°C. The intermetallic compound formed at 280°C was observed primarily near the surface. The larger particles and the formation near the surface indicates that the diffusion of Al at 280°C is much higher than at 180 and 210 C. The presence of $Al_{12}Mg_{17}$ inside the particle and near the defects like surfaces illustrates that the nucleation of intermetallic takes place both in continuous and discontinuous form. Previous work on Mg-9Al alloy also indicated the formation of intermetallic particles of $Mg_{17}Al_{12}$ both continuously and discontinuously inside hcp-Mg [69]. Furthermore, even in a conventional bulk alloy used in this study, the precipitate sizes after aging at 200°C for 8 hours were very fine (approximately 25 nm wide and 50 nm long). Therefore, it is predicted that the intermetallic phase present in the powder annealed at 280°C after 20 minutes is grown when compared to the powders at 180 and 210°C. However, it is not observed in the SEM/BSE micrographs due to its poor resolution at higher magnifications.

6.3 Discussion

6.3.1 Effect of Al Addition

The results of this study indicated that under relatively low temperatures the hydrogenation of Mg-Al alloy powders resulted in the formation of β-MgH_2 and $Mg_{17}Al_{12}$ phases. However, previous studies at higher hydrogenation temperatures have revealed the formation of the fcc-Al phase in addition to the hydride [28]. This difference can be attributed to the hydrogenation of the $Mg_{17}Al_{12}$ intermetallic compound at higher temperatures which resulted in the formation of magnesium hydride and fcc-Al based on equation presented in section 5.4.1. The presence of the intermetallic phase after 5 hours at 280°C at 1MPa hydrogen suggested that these conditions were not sufficient for the hydrogenation of this phase. It was also reported that the

hydrogenation of $Mg_{17}Al_{12}$ takes place at temperatures above 300°C and high pressures (5MPa) [53].

According to the equilibrium Mg-Al phase diagram [115] the maximum concentration of aluminum soluble in the hcp-Mg at 280°C is approximately 5.2at%. As shown in Figure 6-8, upon hydrogenation, magnesium hydride rejected Al and consequently Al accumulates at the hydride/hcp-Mg interface and resulted in the formation of more $Mg_{17}Al_{12}$ phase than expected from the binary Mg-Al phase diagram. This was also evident by analyzing the microstructure of the powder after annealing. A comparison of Figure 6-4(b) and Figure 6-16(c) indicated that the intermetallic phase formed during hydrogenation was much higher when compared to that formed in annealing. In addition, the quantitative metallographic analysis on annealed powder indicated that the volume % of $Mg_{17}Al_{12}$ was ~13.5% (close to that of predicted by phase diagram ~ 14.5%) but similar analysis on many particles revealed that the hydrogenated powders contained 28.4% of $Mg_{17}Al_{12}$ phase. The formation of intermetallic phase upon hydrogenation resulted in a much lower hydrogen capacity in Mg-Al alloy powders in comparison to the pure Mg-powder (Figure 6-1). However, correcting the hydrogenation curve with the total fraction of Mg available (Figure 6-17), the relative hydrogen capacity was equivalent to that for the pure Mg. Another consequence of the Al rejection by the hydride phase was the observation of a lower hydrogenation rate for the Mg-8at%Al alloy powder. This finding can be attributed to the required diffusion of Al. The diffusion coefficient of Al in hcp-Mg at 280°C is $1.869X10^{-15}$ m^2/s while that of hydrogen in hcp-Mg is $8.1475X10^{-9}$ $m^{2/}/s$ [116, 117]. From the mentioned coefficients, it can be noticed that the hydrogen diffusion is much higher than that of Al in hcp-Mg.

The difference observed in the hydrogenation behaviors of the Mg-8at%Al and Mg-4at%Al powders at 210°C temperature (Figure 6-6(a)) can be attributed to the amount of the intermetallic phase available when the hydrogenation begins. The higher intermetallic content of the former powder resulted in an initially faster hydrogenation rate but the impingement of the hydride colonies rendered a hydride layer. The formation of the hydride layer resulted in a fast reduction in the hydrogenation rate as the diffusion of hydrogen through MgH_2 was very slow. Consistently, the microstructural examinations showed that in contrast to the Mg-8at%Al powder, the Mg-4at%Al powder did not develop a continuous layer of magnesium hydride (see Figure 6-7). In summary, the addition of Al affects the hydrogenation kinetics in two opposing manners. The presence of intermetallic particles expedites the nucleation rate of the magnesium hydride, which enhances the kinetics of the hydride formation. On the other hand, the rejection of Al by the hydride phase slows down the growth of the hydride.

6.3.2 Effect of Temperature

The kinetics of absorption and the hydrogen capacity of the Mg-8at%Al alloy powder showed a strong dependency on the hydrogenation temperature (Figure 6-10). It was shown recently that the impingement of hydride colonies, which nucleate and grow from the surface of powders, causes the saturation of hydrogen absorption and any parameter that increases the nucleation rate, decreases the hydrogen capacity by reducing the thickness of the hydride [118]. The Van't Hoff plot (Figure 5-14) shown in the previous chapter suggests that the equilibrium temperature of hydride formation at 1 MPa from the Mg-8at%Al powder is 370°C and hydrogenation below this temperature and pressure will result in a higher driving force for nucleation. In addition, intermetallic particles can also act as the nucleation sites for magnesium hydride [95, 119]. The high hydride nucleation rate encouraged by the larger driving force due to low temperature cause the hydrogen saturation to be reached at a smaller hydride thickness at

210°C in comparison to the hydrogenation at 280ºC. A comparison of Figures 6-12 (a) & (b) elucidated that entire surface of the Mg-8at%Al particles hydrogenated at 210 °C was covered with the magnesium hydride phase. Similarly, microstructural evaluation indicated (Figure 6-12(c)) that the particles hydrogenated at 180°C were not completely covered and the absence of impingement of the hydride colonies was consistent with the lack of saturation indicated by the hydrogenation curve. The hydrogenation curve at 180ºC indicated that the hydrogen absorption kinetics was slower and this can be associated with the diffusion of Al, which was rejected by the hydride upon its formation [119]. The diffusion length of Al as a function of temperature in 5 hours is shown in Figure 6-18 [116]. It can be noticed that the diffusion length of Al started to decrease significantly in the temperature range of 180°C. The fine precipitate particles observed in the powder hydrogenated at 180°C also confirmed that the diffusion of Al was significantly slow at this temperature.

The compositional analysis of the dark regions formed at different temperatures indicated that the amount of Al reduces from 6.8% to 0.1% with increasing the hydrogenation temperature from 180ºC to 280ºC (Figure 6-14). While the accommodation of 6.8 at% of Al in MgH_2 was not realistic as the isotherms of Al-Mg-H developed at different temperatures suggest that there was no solubility of Al in MgH_2[112]. However, the detailed analysis of the XRD results and compositional analyses (Tables 6-2 & 6-3) showed that indeed reducing the hydrogenation temperature resulted in the entrapment of Al in the lattice and caused lattice expansion. The observation of MgH_2 lattice expansion due to the presence of Al was contradictory to the theoretical calculations performed on this system [24, 50]. On the other hand, these calculations did not consider the formation of defects and since the radius of Al cation is smaller than that of Mg cation, the lattice naturally contracts. In reality, magnesium hydride is an ionic compound

and the lattice parameter is influenced by the dopant's ionic radius as well as the amount and type of defects created in the crystal for maintaining the charge neutrality. When Mg^{+2} ions are replaced by Al^{+3} ions the charge neutrality is maintained by either creating interstitial hydrogen ions or magnesium vacancies. Both of these defect formations are anticipated to expand the lattice. However, the H^{-1} ion being very large (ionic radius = 1.53Å [120]), makes the formation of interstitial hydrogen atom improbable. The lattice expansion owing to the addition of the higher valance cations has also been reported in oxides with the flourite structure [121, 122]. The high level of Al content found in the dark region is believed to be associated with the inclusion of the $Mg_{17}Al_{12}$ precipitates. Higher magnification images of the powder hydrogenated at 180°C are shown in Figure 6-19. Figure 6-19 illustrates the submicrometer intermetallic particles present in the MgH_2. During the composition analysis the smallest beam size used in EPMA was about 1μm in diameter. Since the intermetallic particles were smaller than the beam size and were present everywhere inside the hydride region, it was impossible to eliminate them and measure the Al content in the MgH_2. The larger standard deviation in compositional analysis (Figure 6-13) at lower hydrogenation temperatures may be attributed to the statistics of the inclusion of the sparsely separated and larger intermetallic particles within the region of analysis. However, at high temperatures (280ºC) the diffusion of Al was high and the Al diffused away from hydride to form the $Mg_{17}Al_{12}$. These results suggest that the β-MgH_2 phase has very low solubility for Al under the hydrogenation conditions of this study, but under non-equilibrium conditions Al may be incorporated in this hydride.

6.4 Summary and Conclusions

In this chapter, the hydrogenation behavior in pure Mg powder, and electrodeposited hcp-Mg rich alloy powders were studied. Based on the microstructural and compositional analyses it can

be concluded that under nonequilibrium hydrogenation conditions Al can be incorporated in the MgH_2 crystal. Due to the slower diffusion of Al, its presence in the hcp-Mg reduces the hydrogenation kinetics at a given temperature in comparison to pure Mg. This phenomenon is attributed to the rejection of Al by the magnesium hydride, which slows the growth of the hydride. The presence of the $Mg_{17}Al_{12}$ intermetallic prior to the hydrogenation increases the hydride nucleation rate, which causes an initially fast hydrogenation rate but reduces the hydrogen capacity owing to the coverage of the powder surfaces with magnesium hydride in a short time. Raising the hydrogenation temperature increases the solubility of Al in the hcp-Mg phase. Thereby, the intermetallic content prior to hydrogenation at low temperatures is high. The higher intermetallic content at low temperatures of hydrogenation decreases the energy barrier for hydride nucleation significantly and enhances the hydride nucleation rate. This reduces the hydrogen capacity at low temperatures. Thermal stability studies on Mg-Al powders indicate that the intermetallic compound $Mg_{17}Al_{12}$ grows to a large extent when annealed for 5 hours and forms as relatively small precipitates inside the particle.

Table 6-1. Hydrogen capacity of the materials studied at different temperatures for both the runs.

Temperature (°C)	Material	Run 1 (wt%)	Run 2 (wt%)
280	Pure Mg	7.17	7.20
	Mg-8at%Al	4.84	4.81
210	Mg-4at%Al	4.16	4.12
	Mg-8at%Al	2.78	2.80
180	Mg-8at%Al	3.60	-

Table 6-2. Comparison of the XRD (110) and (101) peak positions of MgH_2 produced at different hydrogenation temperatures. Note that the standard value for the β-MgH_2 [123] is similar to the position found in the hydrogenated pure Mg.

Material	2θ (110)	2θ (101)
Std MgH_2	27.942	35.743
Pure Mg, 280°C	27.942	35.742
Mg-8at%Al, 280°C	27.941	35.742
Mg-8at%Al, 210°C	27.862	35.682
Mg-8at%Al, 180°C	27.842	35.722
Mg-4at%Al, 210°C	27.914	35.713

Table 6-3. The lattice parameters of MgH_2 produced in the Mg-8at%Al powder at different hydrogenation temperatures along with the standard values.

Material	a (Å)	c(Å)
Standard MgH_2	4.514	3.022
Pure Mg, 280°C	4.514	3.022
Mg-8at%Al, 280°C	4.515	3.022
Mg-8at%Al, 210°C	4.527	3.025
Mg-8at%Al, 180°C	4.529	3.019
Mg-4at%Al, 210°C	4.517	3.024

Table 6-4. Compositional analysis of various regions of the hydrogenated Mg-8at%Al particles shown in Figure 6-12

Temperature	Dark at%Al	Light at%Al	Bright at%Al
280°C	0.1±0.1	-	44±2.2
210°C	2.2±0.2	7±0.3	41±2.5
180°C	6.8±0.66	8±0.2	42.1±3.3

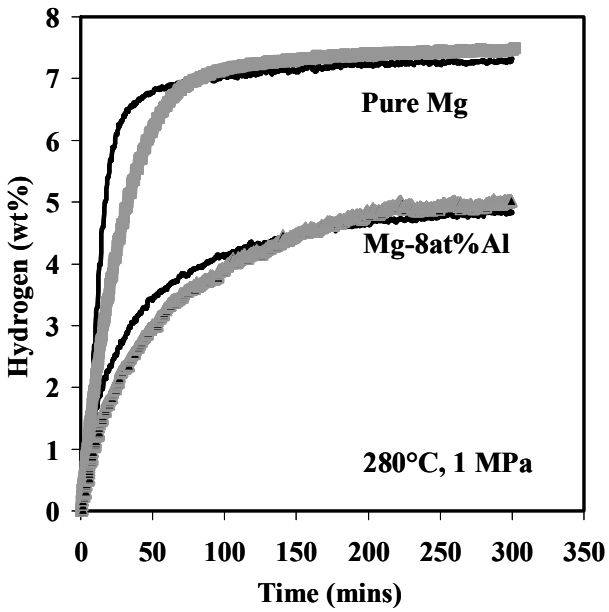

Figure 6-1. Hydrogen absorption curves for pure Mg and Mg-8at%Al powders developed at 280°C and 1 MPa pressure.

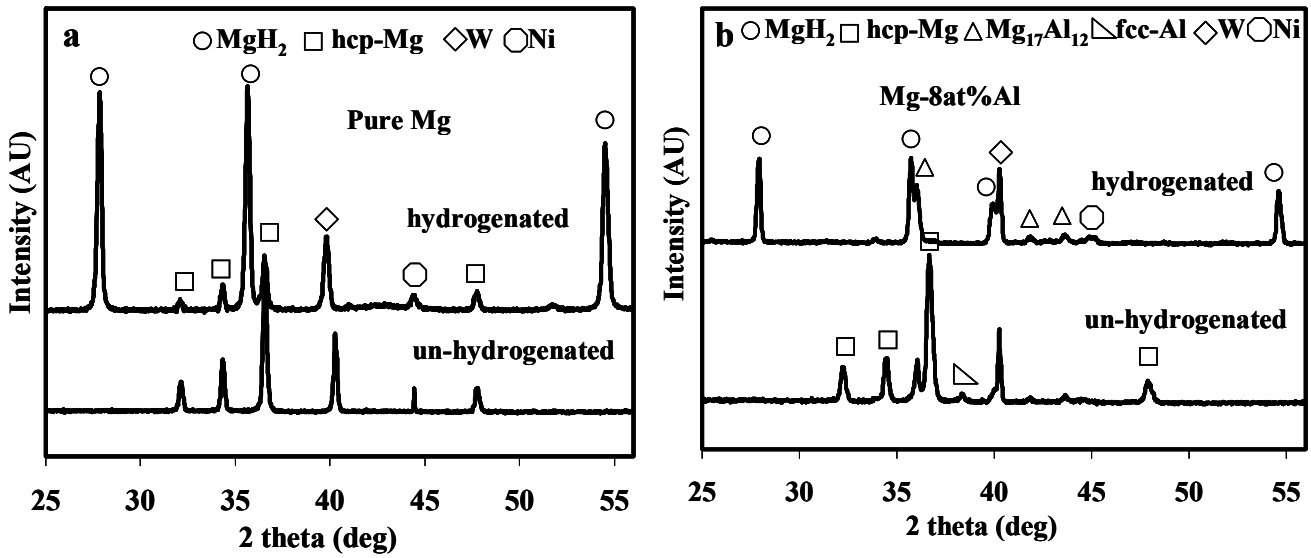

Figure 6-2. The XRD patterns of the hydrogenated and un-hydrogenated powders, (a) for Pure Mg, and (b) Mg-8at%Al powder.

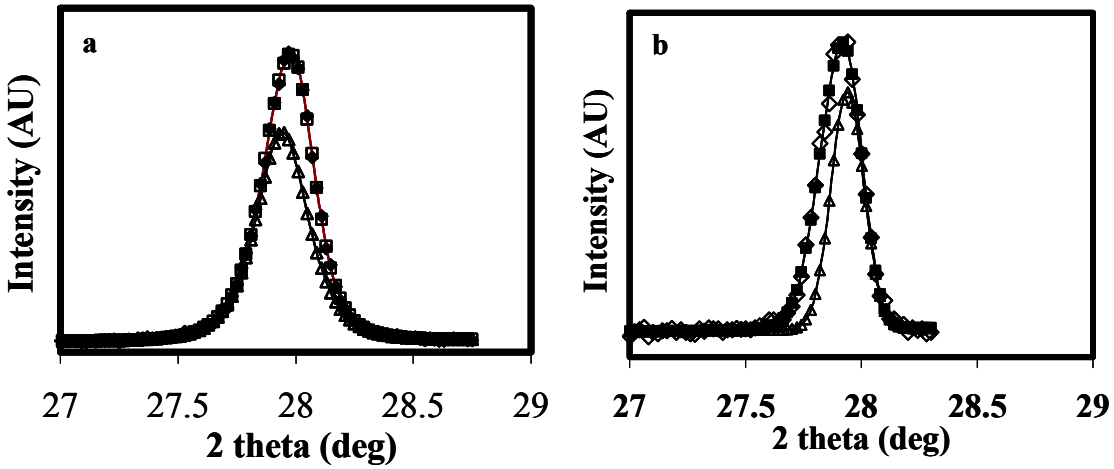

Figure 6-3. Peak fits of (110) XRD peak corresponding to (a) Pure Mg, and (b) Mg-8at%Al powder hydrogenated at 280°C

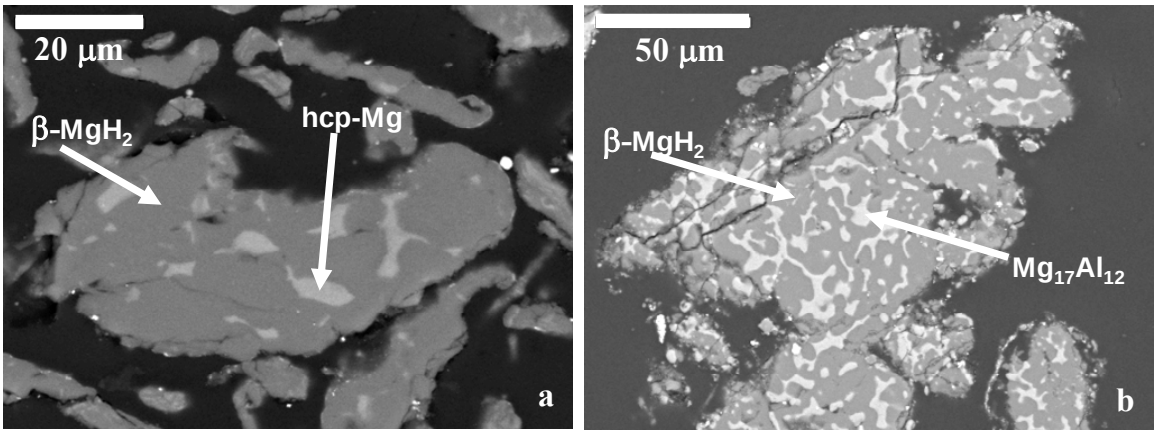

Figure 6-4. Back scattered electron (BSE) micrographs of the polished (a) pure Mg, and (b) Mg-8at%Al powders hydrogenated at 280°C.

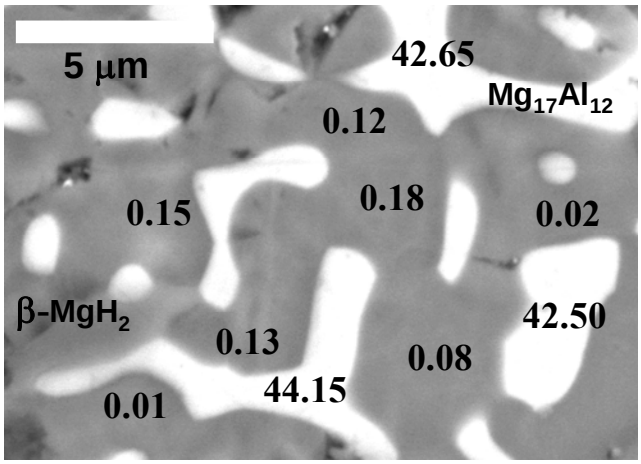

Figure 6-5. SEM/BSE micrograph of Mg-8at%Al powder hydrogenated at 280°C indicating the %Al in various phases.

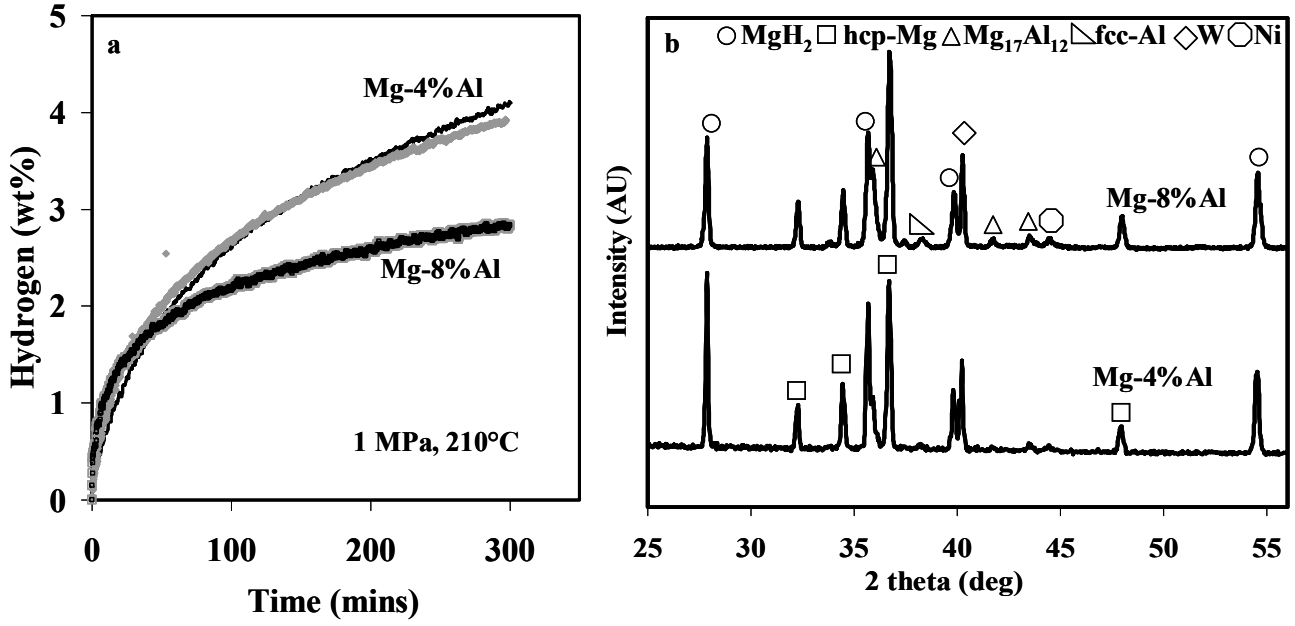

Figure 6-6. (a) Hydrogen absorption curves for Mg-8at%Al and Mg-4at%Al alloy powders developed at 210°C, and (b) the corresponding XRD patterns of the hydrogenated powders.

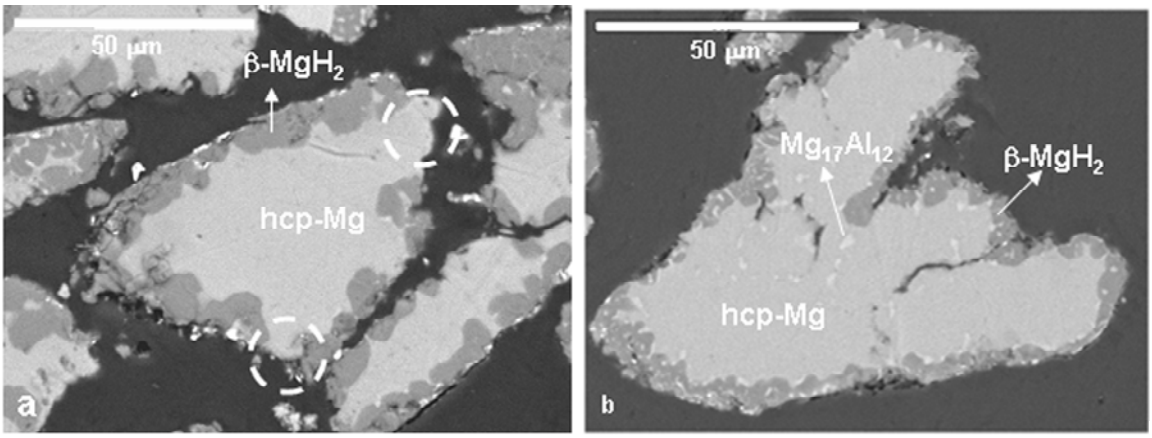

Figure 6-7. BSE micrographs of (a) Mg-4at%Al, and (b) Mg-8at%Al alloy powders hydrogenated at 210°C. Note the presence of un-hydrogenated regions, as marked by the dotted circles, on the surface of the Mg-4at%Al powder.

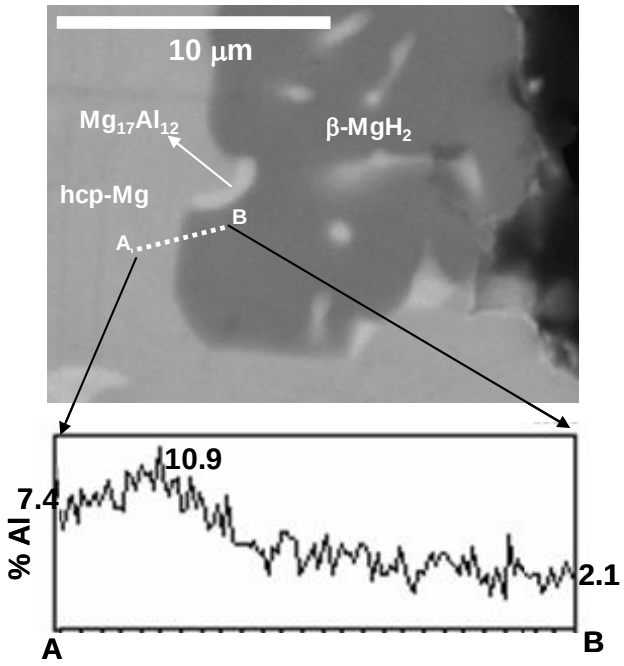

Figure 6-8. BSE micrograph of the Mg-8at%Al alloy powder hydrogenated at 210°C along with the compositional analysis along the line AB showing the accumulation of Al at the β-MgH_2/hcp-Mg interface.

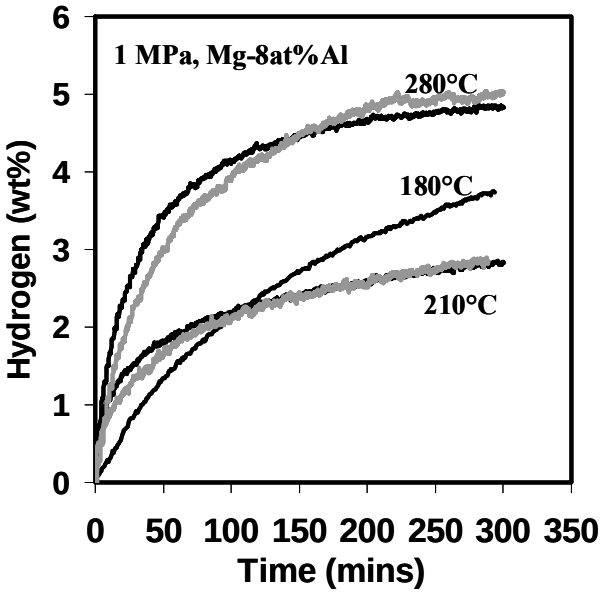

Figure 6-9. Hydrogen absorption curves for Mg-8at%Al powder developed at different temperatures and at 1 MPa pressure.

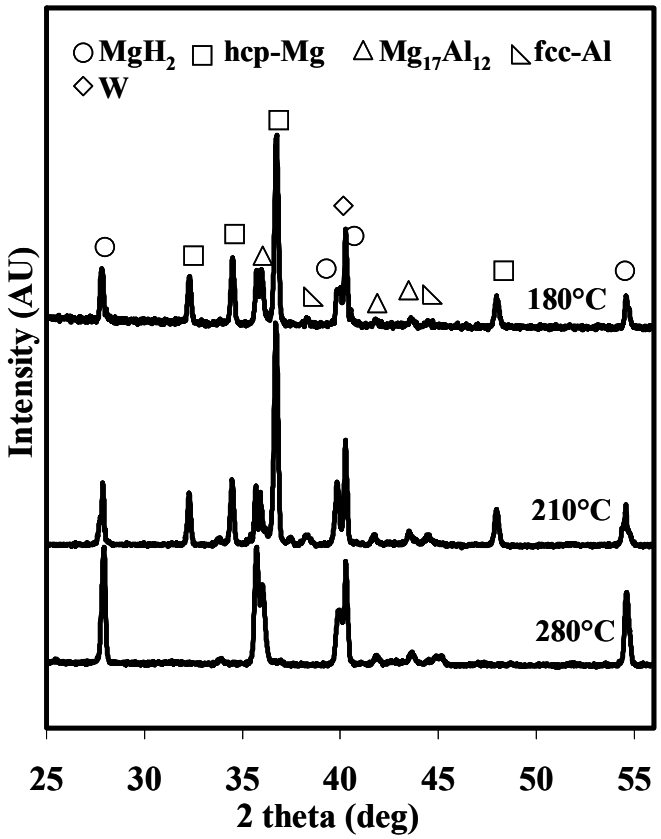

Figure 6-10. The XRD patterns of the hydrogenated Mg-8at%Al powder at different temperatures.

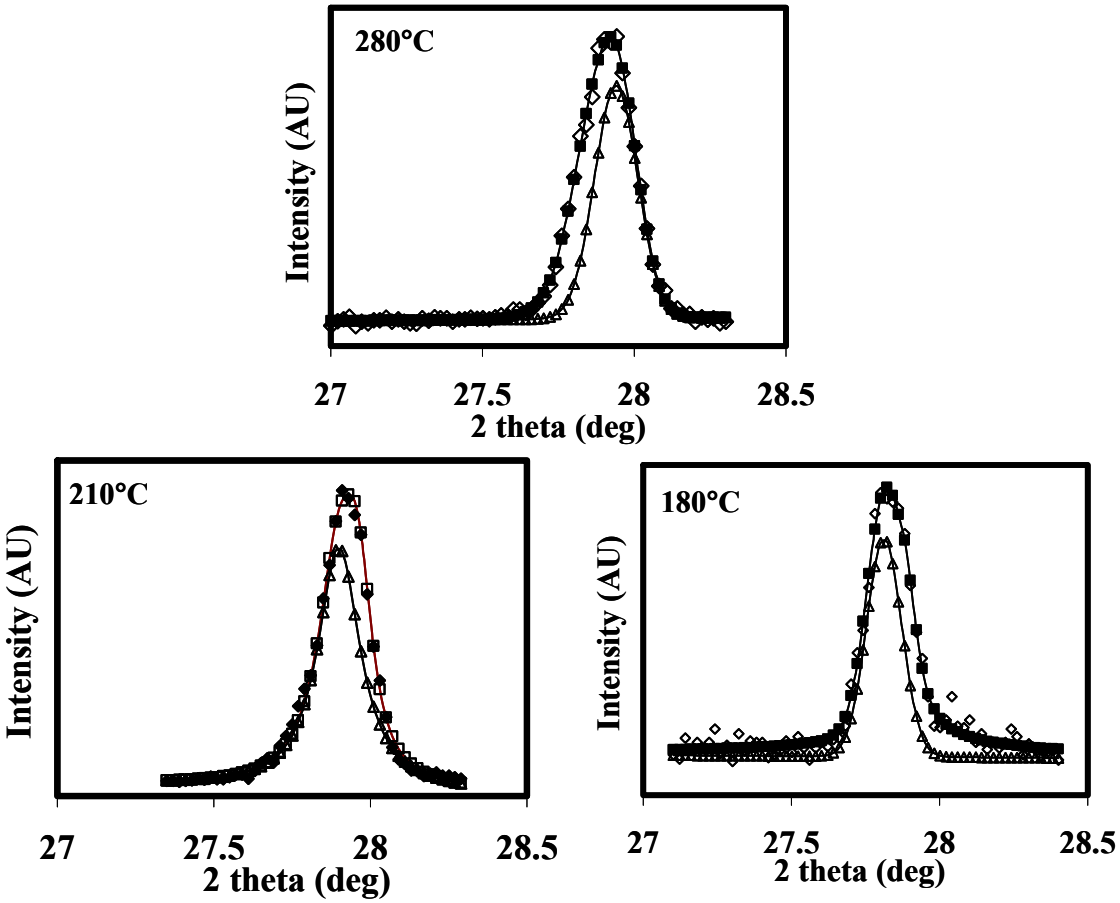

Figure 6-11. Peak fits of (110) XRD peak corresponding to Mg-8at%Al alloy powder hydrogenated at different temperatures.

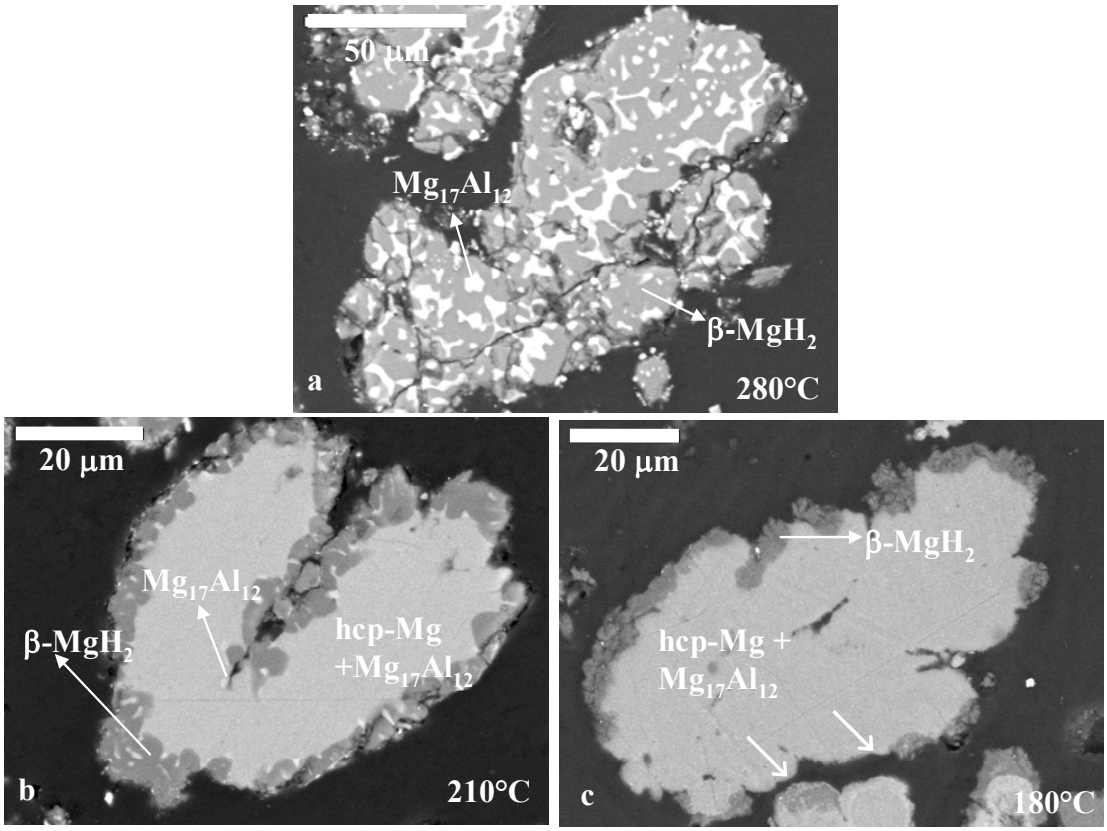

Figure 6-12. BSE micrographs of the Mg-8at%Al powder hydrogenated at (a) 280°C (b) 210°C and (c) 180°C, revealing MgH_2 phase as "dark", hcp-Mg phase as "light" and $Mg_{17}Al_{12}$ phase as "bright" regions. The arrows indicate the locations on the surface where no hydride had formed.

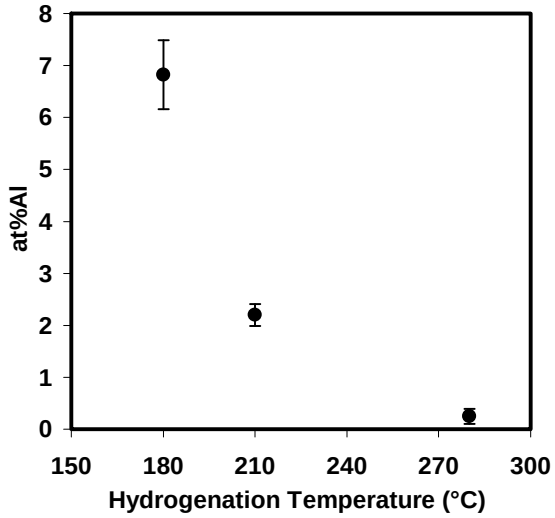

Figure 6-13. The variation of Al in the dark regions of the micrographs shown in Figure 6-12.

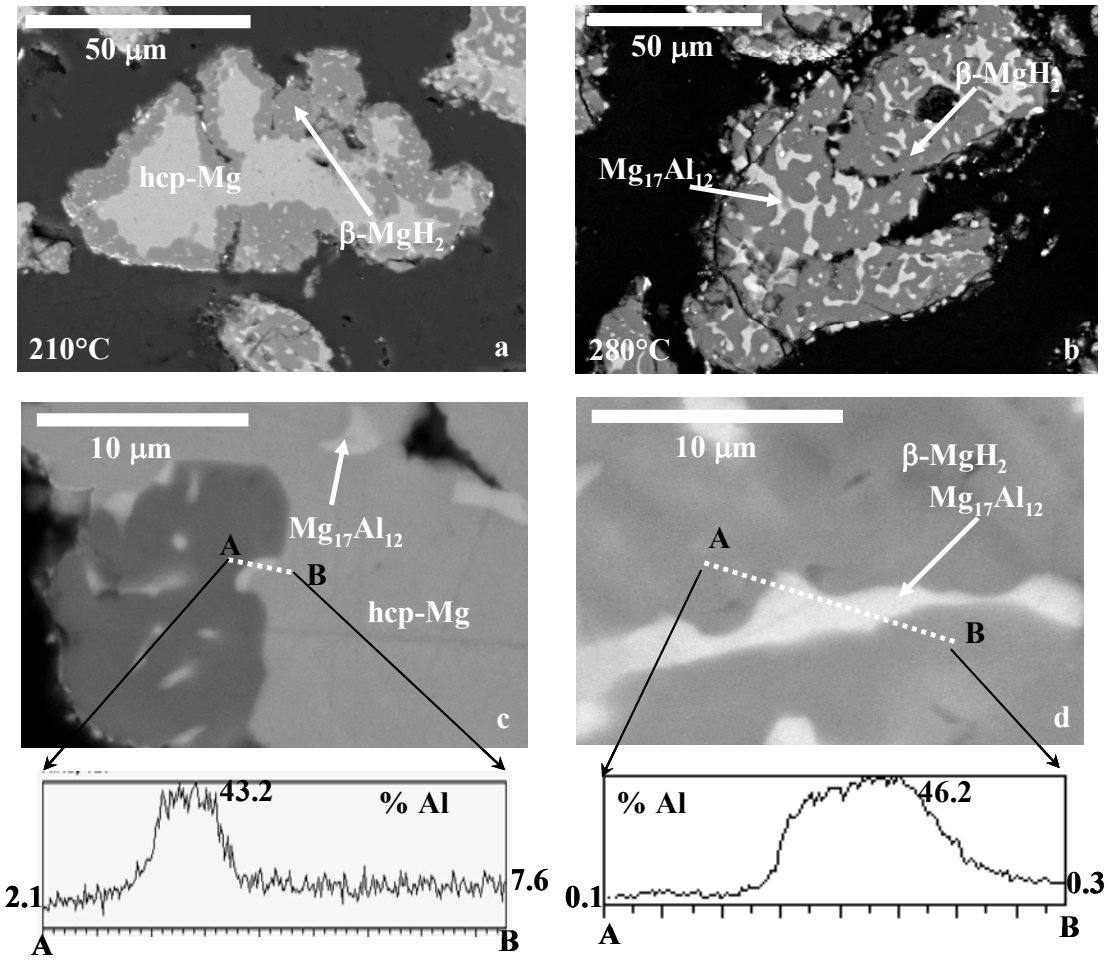

Figure 6-14. Back scattered electron (BSE) micrographs of the polished Mg-8at%Al powder hydrogenated at (a) 210°C and (b) 280°C. Higher magnification images and the corresponding variations of Al content along the AB lines developed by the EPMA method for powders hydrogenated at (c) 210°C and (d) 280°C.

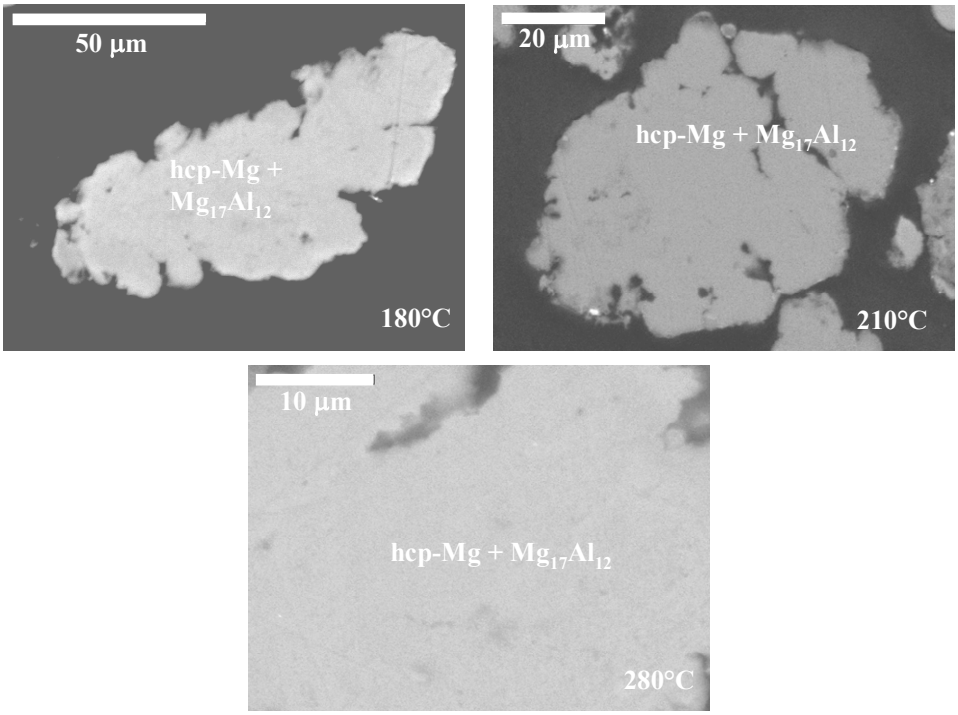

Figure 6-15. SEM/BSE micrographs of Mg-8at%Al annealed for 20 minutes at different temperatures.

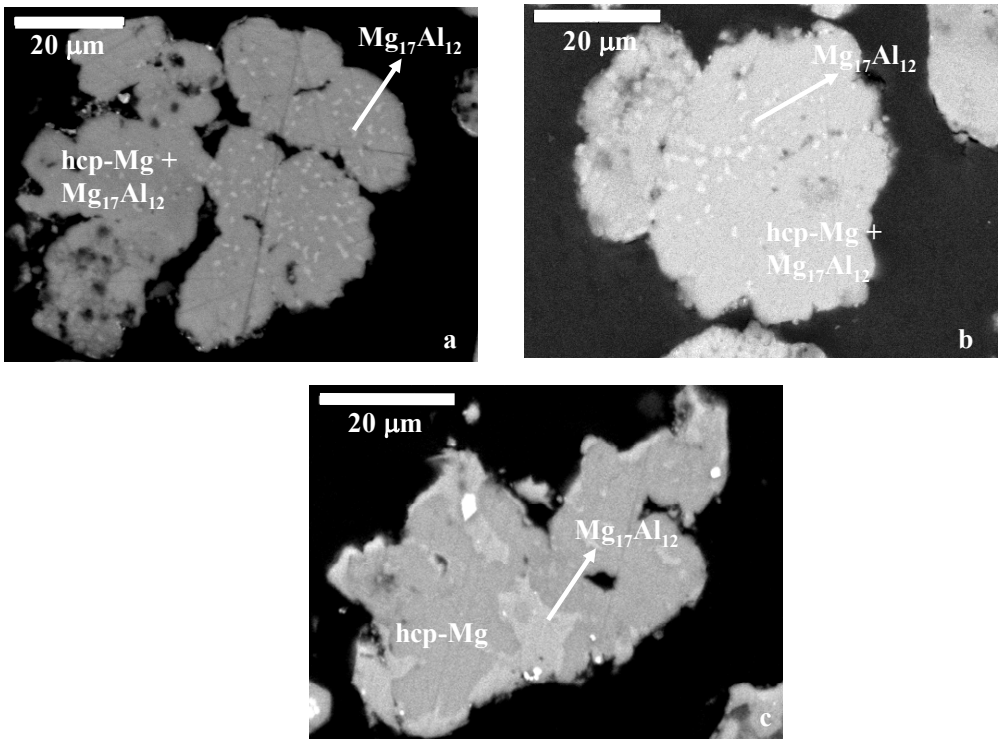

Figure 6-16. BSE micrographs of Mg-8at%Al powders annealed for 5 hours at (a) 180°C (b) 210°C (c) 280°C.

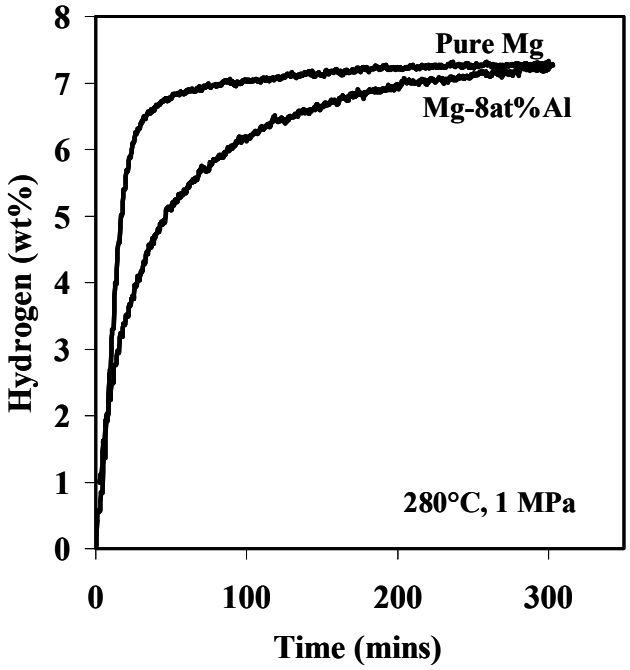

Figure 6-17. A comparison of the hydrogen absorption curves developed at 280°C for the pure Mg and Mg-8at%Al alloy powder after correction for the influence of the intermetallic phase formation.

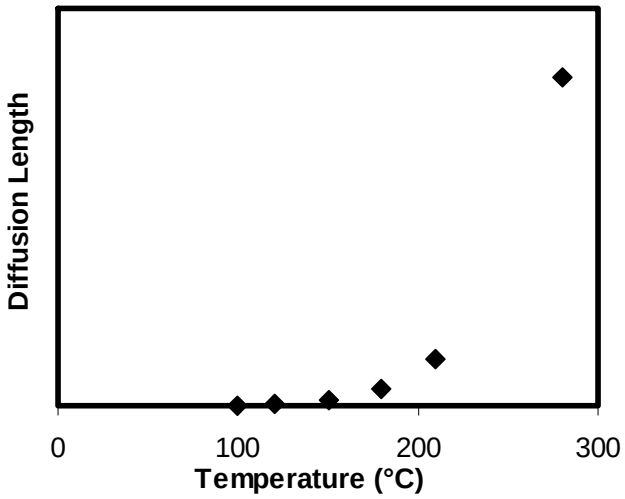

Figure 6-18. Diffusion length of Al in hcp-Mg as a function of temperature.

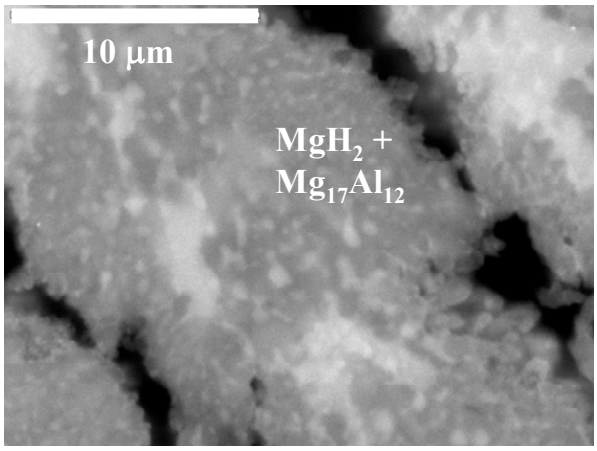

Figure 6-19. SEM/BSE micrograph of a Mg-8at%Al powder hydrogenated at 180°C showing the submicrometer precipitates in the MgH_2 region.

CHAPTER 7
DEHYDROGENATION CHARACTERISTICS OF MGH_2 PRODUCED FROM ELECTRODEPOSITED MG-AL ALLOY POWDERS

Different methods have been employed to reduce the thermodynamic stability of MgH_2. The addition of Al to MgH_2 has been predicted to decrease the stability of the magnesium hydride by reducing its enthalpy of formation. Theoretical calculations have proved that the addition of Al weakens the magnesium hydrogen bond [18, 50]. Very few experimental studies have been carried out on the desorption behavior MgH_2 produced from Mg-Al alloy powders [97, 111]. A desorption study conducted on the MgH_2-Al composite produced by ball milling of 8 mol% of Al and β-MgH_2, revealed that the kinetics of hydrogen desorption increased significantly at 300°C when compared to pure MgH_2 [97]. However, the effect of Al addition on desorption temperature of MgH_2 is not investigated and the attribution of faster kinetics of hydrogen release due to addition of Al was not very clear [97]. Other dehydrogenation experiments that have been carried out previously on hydrogenated Mg-Al powders were under equilibrium conditions as part of the PCT curve development [31].

The absorption tests described in Chapter 6 on Mg-Al powder suggested that different amounts of Al is trapped in MgH_2 crystal lattice depending on the hydrogenation conditions. The goal of the present study was to investigate the effect of the trapped Al on the stability of the MgH_2. To achieve this goal, desorption tests on MgH_2 synthesized at different temperatures from electrodeposited Mg-Al alloy powders were conducted. To understand the effect of Al addition, dehydrogenation of hydrogenated pure Mg powder was also carried out and compared with the hydrogenated Mg-Al alloy powder. Finally, the microstructural evolution during desorption was understood by analyzing the samples that were dehydrogenated partially.

7.1 Hydrogen Desorption Experiments

The desorption tests of hydrogenated electrodeposited Mg-8at%Al powders and the pure Mg powders were conducted in TGA (details of the dehydrogenation procedure were described in Chapter 3). The transformation temperatures were identified from the DSC/TGA curves by using the first deviation and extrapolated tangent method as described in ASTM E967-03 [124]. In this method the temperature where the weight loss curve deviates from the base line for the first time was reported as onset temperature while peak temperature is calculated by drawing the tangents across the base line and the heat flow curve. Each dehydrogenation test described below was conducted at least twice under the same conditions for investigating the repeatability.

7.1.1 Effect of Al Addition on Hydrogen Desorption

Figure 7-1 compares the hydrogen desorption curves (TGA) for pure Mg and Mg-8at%Al alloy powders that were hydrogenated at 210°C. Figure 7-1(a) reveals that the hydrogen was released in two stages from hydrogenated Mg-Al powders while it was released in a single stage from hydrogenated pure Mg powders. The first stage of hydrogen release was observed to occur in the temperature range of 100-150°C for Mg-Al alloy powders while the second stage occurred in the temperature range of 200-350°C. The transformation temperatures of both the pure Mg powder and the Mg-Al alloy powders are presented in Table 7-1. The hydrogen release temperatures (peak) from hydrogenated Mg-Al powders were about 115 and 327°C while for hydrogenated pure Mg powder was about 350°C. From these results it can be noticed that the hydrogen release temperature was low in hydrogenated Mg-Al powders.

The fraction of hydrogen released from both the hydrogenated Mg-Al and pure Mg samples as a function of temperature is plotted in Figure 7-1(b), which showed ~ 12% of the total hydrogen was released in the first stage for hydrogenated Mg-Al alloy powder. However, the total hydrogen present was released in 1 stage for hydrogenated pure Mg powder. The amount of

the hydrogen content in the hydrogenated samples and the hydrogen release during the dehydrogenation tests are shown in Table 7-2. These values in the table suggest that the total hydrogen present in the powders was released.

The XRD profiles of both powders after the dehydrogenation are shown in Figure 7-2. The dehydrogenation products of both the powders showed the presence of hcp-Mg phase. In addition to the hcp-Mg phase, $Mg_{17}Al_{12}$ phase was also observed in the Mg-Al alloy powders. A comparison of these XRD profiles with that of the initial powders before hydrogenation (Figure 4-6 and 4-10) revealed that the fcc-Al present in the initial powders was completely transformed into $Mg_{17}Al_{12}$ or dissolved in hcp-Mg and the 2θ position of the hcp-Mg increased (for Mg-Al, (initial 2θ = 36.662 and after 1 cycle 2θ=36.850). This increase in 2θ position for Mg-8at%Al indicated that the fcc-Al was dissolved in the hcp-Mg lattice and caused the reduction in the lattice parameter. Since the initial phases of the Mg-Al powder were not altered significantly, this powder can be cycled for more number of absorption and desorption experiments, similar to the pure Mg.

The above results indicated that the addition of Al to hcp-Mg reduced the hydrogen release temperature from MgH_2. However, the release of hydrogen in two stages from the Mg-Al alloy powder was not clearly understood and further investigations were carried out on the Mg-Al alloy powders.

7.1.2 Effect of Hydrogenation Temperature on Hydrogen Desorption of the Mg-Al Alloy Powders

Figure 7-3 shows the hydrogen release curves of the Mg-8at%Al alloy powder hydrogenated at 180, 210 and 280°C. The release of hydrogen was observed to take place in 2 stages when the Mg-Al samples were hydrogenated at 180 and 210°C, but not at 280°C (Figure 7-3(a)). The temperatures of hydrogen release for these samples are presented in Table 7-3.

These temperatures indicated that the sample hydrogenated at 280°C released hydrogen at a much higher temperature than the samples hydrogenated at lower temperatures. The transformation temperatures corresponding to the 2 stages were observed to be similar in powders hydrogenated at 180 and 210°C. Figure 7-3 (b) presents the fraction of hydrogen release in the samples hydrogenated at different temperatures. It can be noticed that the fraction of hydrogen released in the 1st stage increased with decreasing the hydrogenation temperature. Approximately, 35% of the total hydrogen was released in the first stage for sample hydrogenated at 180°C while only 10% was released when hydrogenated at 210°C. However, it was not confirmed whether the hydrogen release in the first stage was due to the dissociation of MgH_2.

7.1.3 Phase Evolution during Desorption of Mg-Al Powders

The evolution of phases during desorption of powders was evaluated using the High temperature X-ray diffraction unit. The Mg-8at%Al powder hydrogenated at 180°C was placed in the sample holder of the XRD and was heated in air at 5K/min. The XRD profile of the sample was collected as a function of temperature (and time) and is shown in Figure 7-4. As marked by dashed lines on this figure, it can be noticed that there is a drop in intensity of the (110) peak of MgH_2 (2 theta = 28.59) with respect to the other peaks in the temperature range of 100-150°C. The drop in intensity of MgH_2 peak indicated that hydrogen was released from the MgH_2, but upon further heating it was observed that the intensity of this peak increased. This analysis was not very conclusive for the release of hydrogen from MgH_2 as an analysis of peak ratios of Mg to MgH_2 varied with temperature (Figure 7-5). Figure 7-5 indicates that the peak intensity ratio of Mg to MgH_2 decreased initially with the increase in temperature till the temperature reaches 200°C and remained constant.. It can be noticed that the intensity of MgH_2 peak varied with temperature and this can be attributed to the displacement of sample holder during the heating

process. This displacement affects the sampling volume of the grains present in the surface of the powder. It was reported earlier that XRD peak intensities do change because of the displacement of sample holder at high temperatures [125]. Therefore, the intensity of the peak depends on both the phase transformation and the displacement of sample holder.

Consistent with the TGA results, the hydrogen release from the powder was observed to start around 250°C. The intensity of the MgH_2 peak decreased from 250°C until the hydrogen in the powder was completely released and at this point the peak diminished. Further increase in temperature caused the appearance of a peak corresponding to that of MgO, indicating that the hcp-Mg was oxidizing under these conditions. In addition, the peak corresponding to the $Mg_{17}Al_{12}$ phase was observed to decrease in intensity in the temperature range of 300-400°C. From this analysis it may be suggested that the hydrogen was released from MgH_2 in stage 1 as well as in stage 2. However, the reasons behind the two distinct stages of hydrogen release need further investigation.

7.1.4 Microstructural Analysis of Hydrogenated Mg-Al Powders

The SEM/BSE micrographs of the Mg-8at%Al powder hydrogenated at 180°C are presented in Figure 7-6. Two kinds of particles were observed in the hydrogenated condition with different amounts of hydride present in them. These particles were categorized as Type I and Type II. The Type I particles showed significant amount of MgH_2 as shown in Figure 7-6(a) and (b). In comparison to the other particles, Type II particles exhibited a lower amount of MgH_2 as presented in Figures 7-6(c) & (d). As indicated by the arrows on the micrographs, the surface of the particles was not completely covered with MgH_2 and there by the volume fraction of the hydride in the powders was observed to be lower. A volume fraction analysis on many particles in the powder revealed that the hydride content in the particles followed a bi-modal distribution

as shown in Figure 7-7. Majority of the particles exhibited lower amount of magnesium hydride (20-40%) content.

In order to understand the reasons behind the 2 stages, a sample hydrogenated at 180°C was desorbed partially till the end of the first stage (see Figure 7-3, till 200°C) and its microstructure was analyzed. The SEM/BSE micrographs of the particles from this powder are shown in Figure 7-8. Most of the particles exhibited similar amounts of MgH_2 and the volume fraction of the MgH_2 in these particles was about 20-45% (Figures 7-8(a) and (b)). Furthermore, it is to be noted that some particles, as illustrated in Figure 7-8(c), did not show the presence of MgH_2 at all. A volume fraction analysis on 45 particles of this sample indicated that the hydride fraction in this sample followed a normal distribution (Figure 7-9). Figure 7-9 compares the volume fraction of magnesium hydride in the particles between the

Based on the volume fraction analysis it is concluded that two kinds of particles existed in the hydrogenated powder which were termed as Type I and Type II. Upon desorption the Type I particles released hydrogen in the temperature range of 100-150°C (stage 1) while Type II particles released the hydrogen at higher temperatures. The primary difference in Type I and Type II was the amount of hydride present in the particles. The volume fraction analysis of the hydride predicted that the weight loss in the temperature range of 100-150°C could be due to release of hydrogen from MgH_2.

7.1.5 The Effect of Catalyst on Desorption of Mg-Al Powders

The effect of catalyst on desorption process was investigated by coating the Mg-8at%Al powder with two levels of Ni content. Different amounts of the catalyst on the powder was achieved by changing the proportion of the organometallic Ni to the Mg-Al alloy powders during the Ni coating procedure described in Chapter 3. A Mg-8at%Al powder is coated with half the amount of catalyst was synthesized (0.295g of organometallic Ni was used instead of 0. 59 g for

5 gms of Mg-Al powder) and hydrogenated at 180°C under 1 MPa pressure of hydrogen for 5 hours.

The hydrogen desorption curves for samples with two different amounts of Ni coating are presented in Figure 7-10. The desorption curves indicated that hydrogen was released in 2 stages from both samples (Figure 7-10(a)). However, the total amount of hydrogen released in the sample with less content of catalyst Ni was interestingly much lower. The hydrogen release temperatures of these samples are presented in Table 7-4. It can be noticed that the transformation temperatures did not change by reducing the amount of Ni.

Figure 7-10(b) illustrates the fraction of hydrogen released in different stages. The amount of hydrogen released in each stage was changed significantly by varying the content of catalyst. Only 12% of the total hydrogen present in the powder was observed to release in stage 1 (Temperature range 100-150°C) when the catalyst content was reduced to half. However, Mg-Al alloy powder with the high amount of Ni on the surface of the particles have illustrated that approximately 33% of the total hydrogen is released at low temperature. From these observations it can be concluded that the amount of Ni covering the particle played an important role in the dehydrogenation behavior of the Mg-Al powder. These results suggested that the high amount of Ni on the surface of the powders may result in higher fraction of particles with Al trapped in the MgH_2. Hence, larger fraction of MgH_2 was destabilized due to the presence of Al trapped and released hydrogen at low temperatures. It was also observed previously that the increase in the amount of catalyst led to higher amount of hydrogen release in less time at the same temperature. However, the faster kinetics in those cases was attributed to the lower diffusion distances of hydrogen on the surface to recombine into hydrogen molecule [86].

7.2 Microstructural Evolution during Desorption of Hydride

To understand the microstructural evolution during desorption of hydrogen from the hydrides, samples were partially dehydrogenated and analyzed using the SEM and XRD. The 210°C hydrogenated Mg-8at%Al powder was heated at 5 K/min in the TGA till the temperature of 290°C was reached and then the sample was cooled rapidly at 50 K/min to freeze the microstructure present at 290°C. Figure 7-11(a) illustrates that the hydrogen was released from the surface as evidenced by the elimination of the dark hydride phase and the formation of the grey hcp-Mg. A higher magnification micrograph shown in Figure 7-11(b) revealed the formation of the hcp-Mg phase on the surface of a particle. The intermetallic phase, similar to the microstructure of the hydrogenated phase (see Figure 7-11(b)), was found next to the magnesium hydride. Figure 7-11(c) shows that the hydrogen was not released uniformly from the whole surface in some particles. As demonstrated in the high magnification picture presented in Figure 7-11(c), hydride grains/colonies still existed un-hydrogenated on the surface of the particles. The inhomogenity of the dehydrogenation process may be hypothesized to be associated with the nucleation of the hcp-Mg phase, however this phase was present next to the hydride phase in all the particles and hence the nucleation will not explain the observed phenomena . Therefore, the inhomogenity of the dehydrogenation process can be attributed to the non-uniformity in the Ni distribution on the surface of particles. The dehydrogenation process requires the formation of hydrogen molecules from the hydrogen dissolved in the hcp-Mg, which, similar to dissociation process, was enhanced by the presence of a catalyst. It should be noted that during hydrogenation, Mg can diffuse into Ni (or vise-versa) and any change in the interfacial structure between Ni and hcp-Mg can possibly affect the dehydrogenation kinetics.

Figure 7-12 illustrates the phases and the microstructure of the powders after complete dehydrogenation. The sample was cooled from the dehydrogenation temperature to room

temperature at 10 K/min. The XRD profile of the dehydrogenated powder is shown in Figure 7-12(a). Hcp-Mg along with the $Mg_{17}Al_{12}$ phase was observed in the powder while the peak corresponding to the fcc-Al present in the initial powder was absent. It can be concluded from this analysis that during the dehydrogenation processes the fcc-Al was dissolved in the hcp-Mg phase at high temperatures and precipitated as $Mg_{17}Al_{12}$ during cooling to room temperature. The microstructure after complete dehydrogenation presented in Figure 7-12(b) is similar to the initial microstructure of the powders with hcp-Mg. The contrast corresponding to the $Mg_{17}Al_{12}$ phase was not observed indicating its presence as very fine particles. These results suggest that the microstructure of the powder was not changed significantly and can be recycled.

7.3 Discussion

The results of this study indicated that MgH_2 produced from the electrodeposited Mg-Al powders released hydrogen at much lower temperatures when compared to the MgH_2 produced from pure Mg powder. In addition, hydrogenation temperature played a significant role in desorption of hydrogen from Mg-Al alloy powders. MgH_2 fabricated from Mg-Al alloys at low hydrogenation temperatures was observed to release hydrogen at low temperatures. During hydrogenation, higher diffusion of Al in hcp-Mg at high temperatures caused Al to diffuse away from the MgH_2. Hence the MgH_2 synthesized at high temperatures like 280°C was depleted of Al and the hydrogen release temperature was observed to be very high in this case. So, the decrease in desorption temperature can be attributed to the presence of Al in the MgH_2 crystal lattice. From the results presented in the Chapter 6, it was concluded that Al was trapped in MgH_2 crystal when the Mg-Al alloy powder was hydrogenated at low temperatures. The presence of Al in the MgH_2 lattice reduced the magnesium hydrogen bond strength. In addition, it should be noted that for every two Al atoms present in the lattice, a vacancy is created to maintain the charge neutrality. These defects created destabilize the MgH_2 to a significant extent.

Earlier studies on defects in the MgH_2 have shown that desorption temperature of MgH_2 is decreased by the increase of these defects [61]. The reduction in the bond strength and the formation of defects leads to the release of hydrogen at lower temperatures. These results confirmed the theoretical calculations performed on MgH_2-Al system regarding the destabilization of Mg-H bond [18, 50, 97]. It has been predicted that when 8 mol% of Al is added to MgH_2, the bond energy between the magnesium and hydrogen is lowered and the enthalpy of dissociation was reduced from -76 kJ/molH_2 to -28kJ/mol H_2 [97]. The equilibrium temperature of hydrogen release from MgH_2 at 1 atm pressure of hydrogen is 288°C. From the results observed in this study it can be noticed that the desorption temperature was reduced significantly to 115°C in some particles and 260°C in the other particles when hydrogenated at low temperatures. However, the MgH_2 produced at 280°C from Mg-Al alloy powders released hydrogen at very high temperatures when compared to the pure Mg powder. The reasons behind this phenomenon are not very clear, but can be attributed to the distribution of catalyst.

Microstructural analysis of the Mg-8at%Al powder hydrogenated at 180°C for 5 hours indicated that particles were hydrogenated in homogeneously and exhibited different amounts of hydride. The variation in the amount of hydride can be attributed to the amount of Ni present on the surface of different particles. The studies carried out on the Ni distribution on the initial particles before hydrogenation revealed that the Ni distribution was not homogeneous and the total content on the particles was also not similar. Figure 7-13 presents SEM/BSE micrographs (a and c) of 2 Mg-8at%Al particles along with their corresponding SEM/BSE micrographs (b and d) after hydrogenation at 180°C. It can be noticed that from the EDS maps that the Ni distribution (green dots) was not same in both the particles. EDS Map of Ni in Figure 7-13(d) elucidates that big particles of Ni were present on the powder. A comparison of the EDS maps

illustrated that the amount and the distribution of Ni in the particles were not the same. Hence, it can be predicted that the amount of hydrogenation in both the particles will be different. As mentioned in Chapter 2, the role of the catalyst during the hydrogenation process is primarily to break the hydrogen molecule into two hydrogen atoms [85]. Therefore, the particles with higher content of Ni absorb hydrogen at a higher rate and the nucleation of magnesium hydride takes place at a faster rate. The fast transformation rate provides less time for diffusion of Al in the material and therefore more Al is anticipated to be trapped in the hydride phase of the particle. Thus, it can be suggested that the hydride in the particles with higher amount of Ni might have higher amount of Al in MgH_2 and it is expected that the enthalpy of dissociation of MgH_2 in these particles is decreased to a significant extent. This leads to two stages of hydrogen release observed in the hydrogenated Mg-Al alloy powders. Similar release of hydrogen in two different stages was observed in hydrogenated samples of Mg produced by equi-channel angular pressing. However, the temperature range observed in this study was higher and the two stage release was attributed to the differences in the distribution of grain size in the material [126].

Results of the present study indicate that changing the amount of catalyst affects the amount of hydrogen released due to larger fraction of particles with higher amount of Ni. These results are in agreement with the published data for MgH_2 with different amount of transition metal catalysts. In a study with 0-10at% of Ni ball milled with on MgH_2, it was shown that the 1wt% of Ni in contact with the MgH_2 surface releases less hydrogen from MgH_2 when compared to the powder with 5wt% Ni on MgH_2 surface [21].

From the above discussions it can be concluded that the destabilization of MgH_2 can be achieved by creating defects via alloying with Al and reduce the bond strength between Mg and hydrogen. The findings in the present study suggest that hydrogenation at low temperatures and

under the conditions with high growth rate of hydride can lead to the formation of MgH_2 with Al trapped inside the crystal lattice. The trapped Al inside the MgH_2 crystal creates the defects that weaken the bond strength between magnesium and hydrogen. The trapping of Al in MgH_2 contribute for the destabilization of MgH_2 and hence reducing the desorption temperature.

7.4 Summary and Conclusions

Hydrogen desorption behavior of both pure Mg powders and electrodeposited Mg-Al powders was studied using TGA and detailed microstructural analysis. The major conclusions that can be drawn from this study are as follows:

- When Al is trapped in the crystal structure, desorption temperature can be reduced to temperatures as low as 115°C.
- The release of hydrogen in the Ni coated electrodeposited Mg-Al alloy powders hydrogenated at low temperatures takes place in two stages. This phenomenon can be attributed to the existence of a bimodal distribution of hydride contents of the hydrogenated powders. The presence of this bimodal distribution is believed to be associated with the inhomogeneous distribution of Ni catalyst on the surface of particles.
- Decreasing the hydrogenation temperature increases the amount of hydrogen released in the 1^{st} stage of hydrogen release. This is attributed to the larger entrapment of Al in MgH_2 at lower temperatures due to the slower diffusion of Al in the hcp-Mg phase.
- Reduction in the catalyst content decreases the total amount of hydrogen in the powder and also the amount of hydrogen released in the 1^{st} stage.
- Microstructural analysis of partially dehydrogenated particles indicates that the hydrogen is released from the surface of the powders.

Table 7-1. Hydrogen release temperatures for pure Mg and Mg-Al alloy powders hydrogenated at 210°C.

	Stage 1		Stage 2	
	On-Set Temperature (°C)	Peak Temperature (°C)	On-Set Temperature (°C)	Peak Temperature (°C)
Pure Mg	-	-	296.75	349.91
Mg-Al	102.13	114.35	265.95	327.46

Table 7-2. The hydrogenation contents of pure Mg and Mg-Al alloy powder observed during the absorption and desorption.

	Hydrogen Capacity	
	Absorption (wt%)	Desorption (wt%)
Pure Mg	6.17	6.09
Mg-Al	2.93	2.90

Table 7-3. Hydrogen release temperatures for Mg-Al alloy powders hydrogenated at 180, 210, and 280°C.

	Stage 1		Stage 2	
	On-Set Temperature (°C)	Peak Temperature (°C)	On-Set Temperature (°C)	Peak Temperature (°C)
180	93.75	108.06	213.25	258.85
210	102.13	114.35	265.95	327.46
280	-	-	430.09	433.46

Table7-4. Hydrogen release temperatures for Mg-Al alloy powders hydrogenated at 180°C with different amounts of Ni.

	Stage 1		Stage 2	
	On-Set Temperature (°C)	Peak Temperature (°C)	On-Set Temperature (°C)	Peak Temperature (°C)
Low Ni	93.41	107.05	215.65	258.85
High Ni	93.75	108.06	213.25	265.92

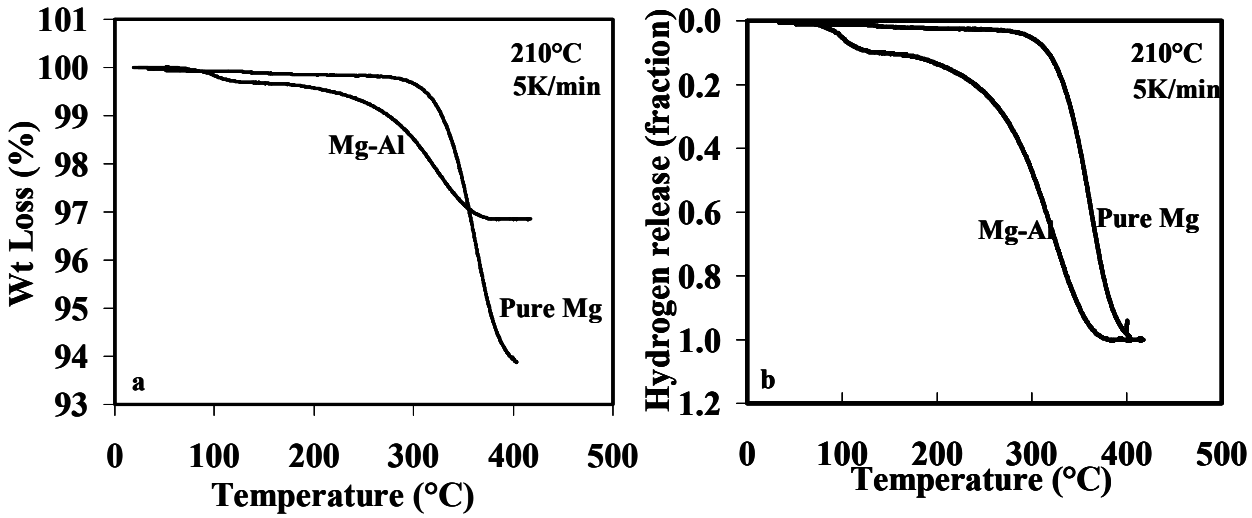

Figure 7-1. Hydrogen release curves (TGA) for pure Mg and Mg-8at%Al powders hydrogenated at 210°C, (a) represents the % weight loss, and (b) fraction of hydrogen released as a function of temperature.

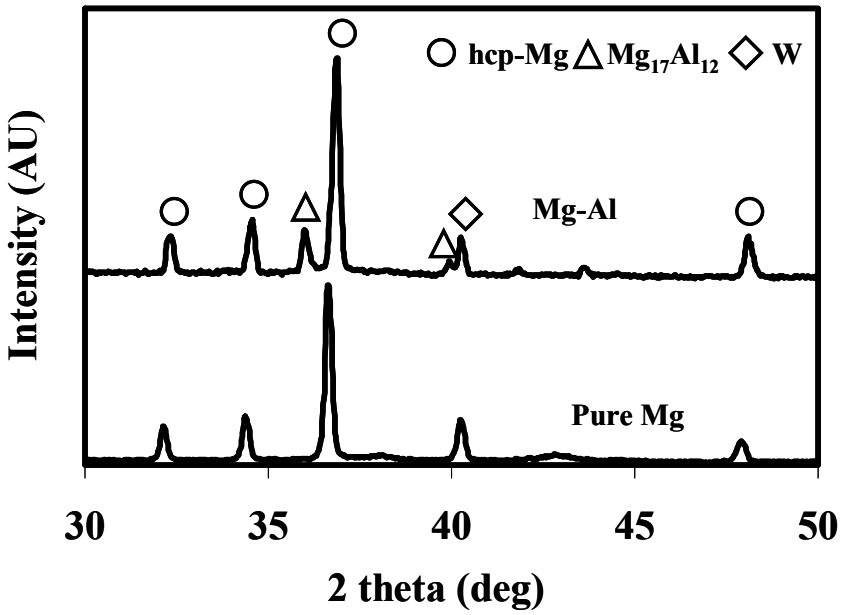

Figure 7-2. The XRD patterns of the desorbed powders for pure Mg and Mg-8at%Al powder revealing that the phases are similar to that of initial powders.

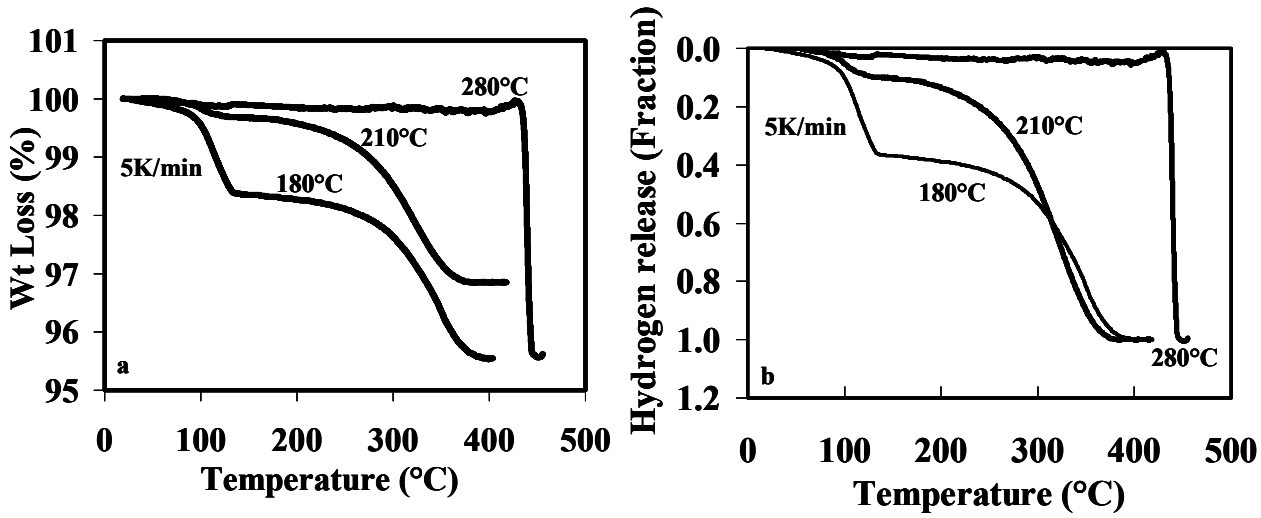

Figure 7-3. Hydrogen release curves (TGA) for Mg-8at%Al powders hydrogenated at 180, 210, and 280°C. (a) represents the % weight loss, and (b) fraction of hydrogen released as a function of temperature.

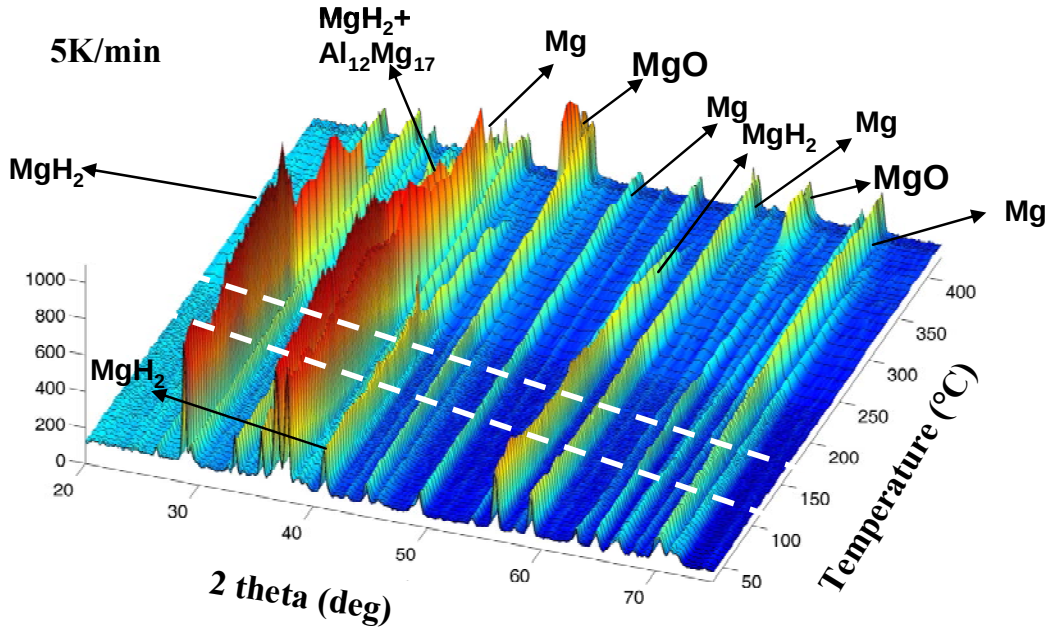

Figure 7-4. Phase evolution during desorption in Mg-Al alloy powders performed in high temperature XRD. The marked circle indicates the drop in intensity of the (110) peak of MgH_2.

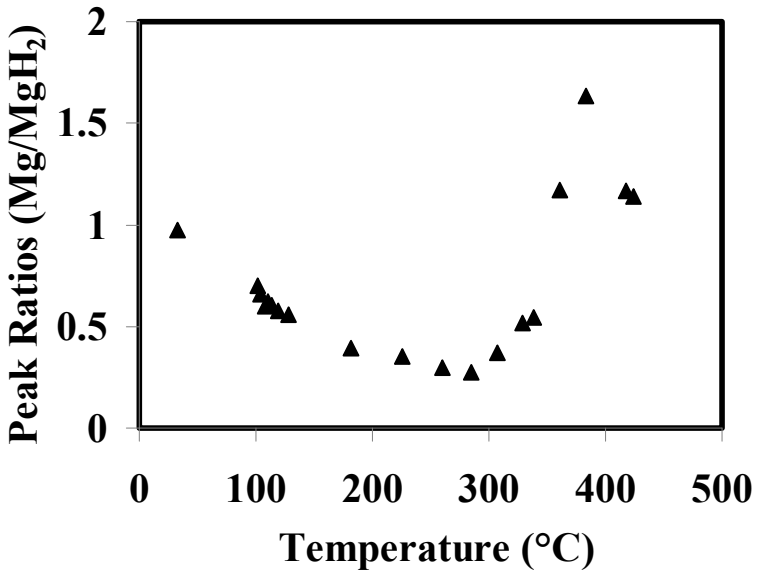

Figure 7-5. Peak intensity ratios of $Mg:MgH_2$ at different temperatures.

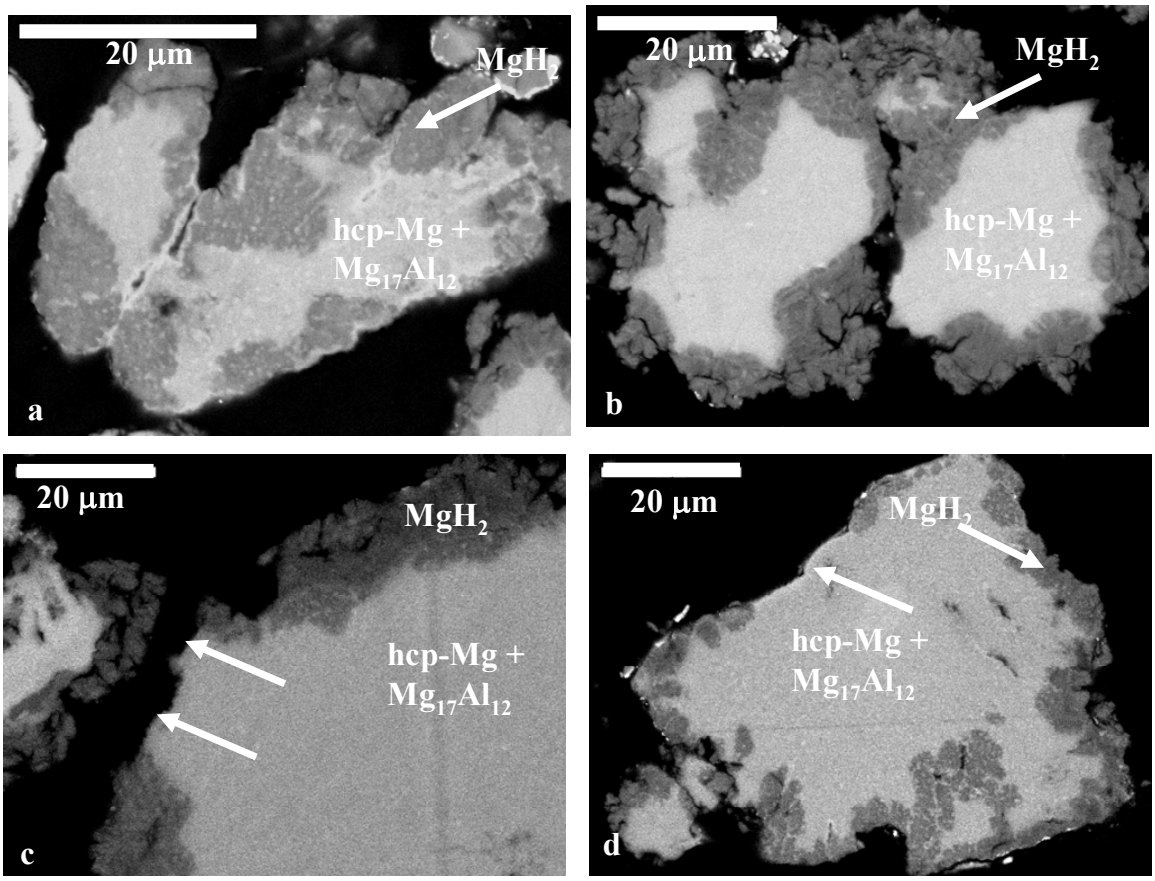

Figure 7-6. SEM/BSE micrographs of Mg-8at%Al alloy powder hydrogenated at 180°C. (a,b) Type I particles revealing higher amount of hydrides (c,d) Type II particles with less amount of hydride.

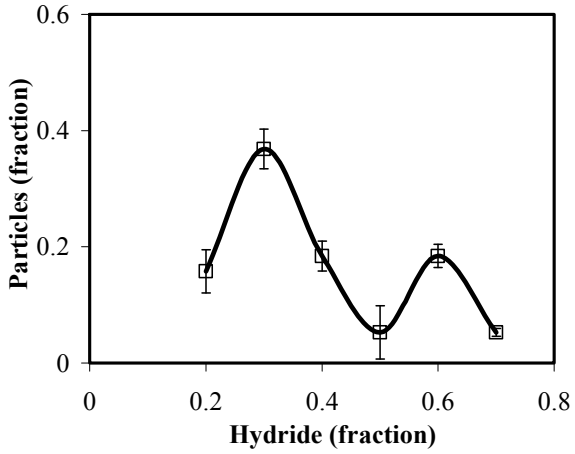

Figure 7-7. Distribution of different types of particles in Mg-8at%Al powder hydrogenated at180°C

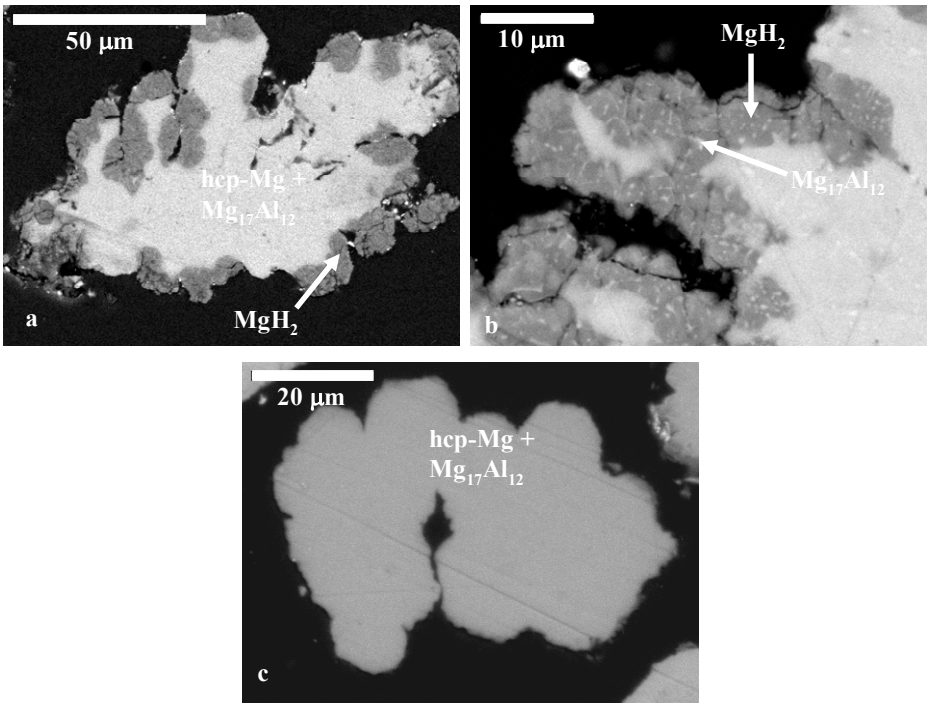

Figure 7-8. SEM/BSE micrographs of Mg-8at%Al alloy powder after the release of hydrogen in 1st stage. (a,b) particles revealing amount of hydride present. (c) particles showing the absence of hydride.

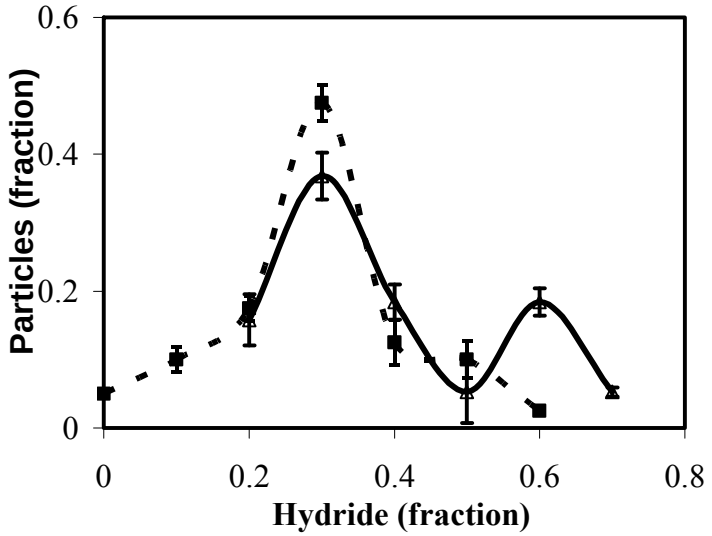

Figure 7-9. Comparison of the distribution of hydride phase between the powders in hydrogenated condition and after the 1st stage of hydrogen release

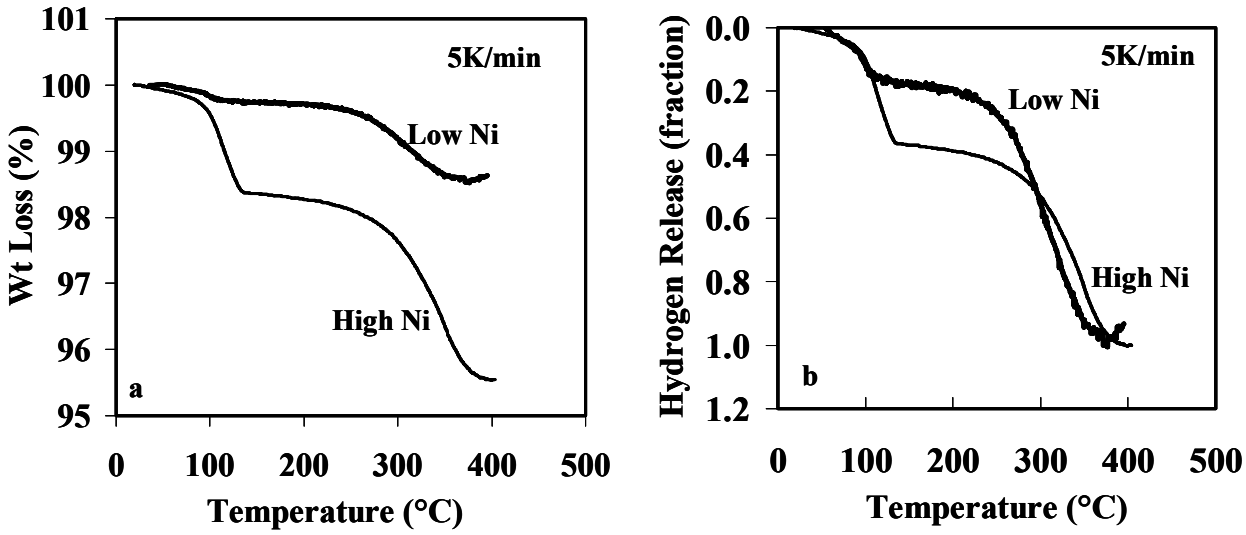

Figure 7-10. Hydrogen release curves (TGA) for Mg-8at%Al powders hydrogenated at 180°C with different amounts of catalyst, (a) represents the % weight loss, and (b) fraction of hydrogen released as a function of temperature.

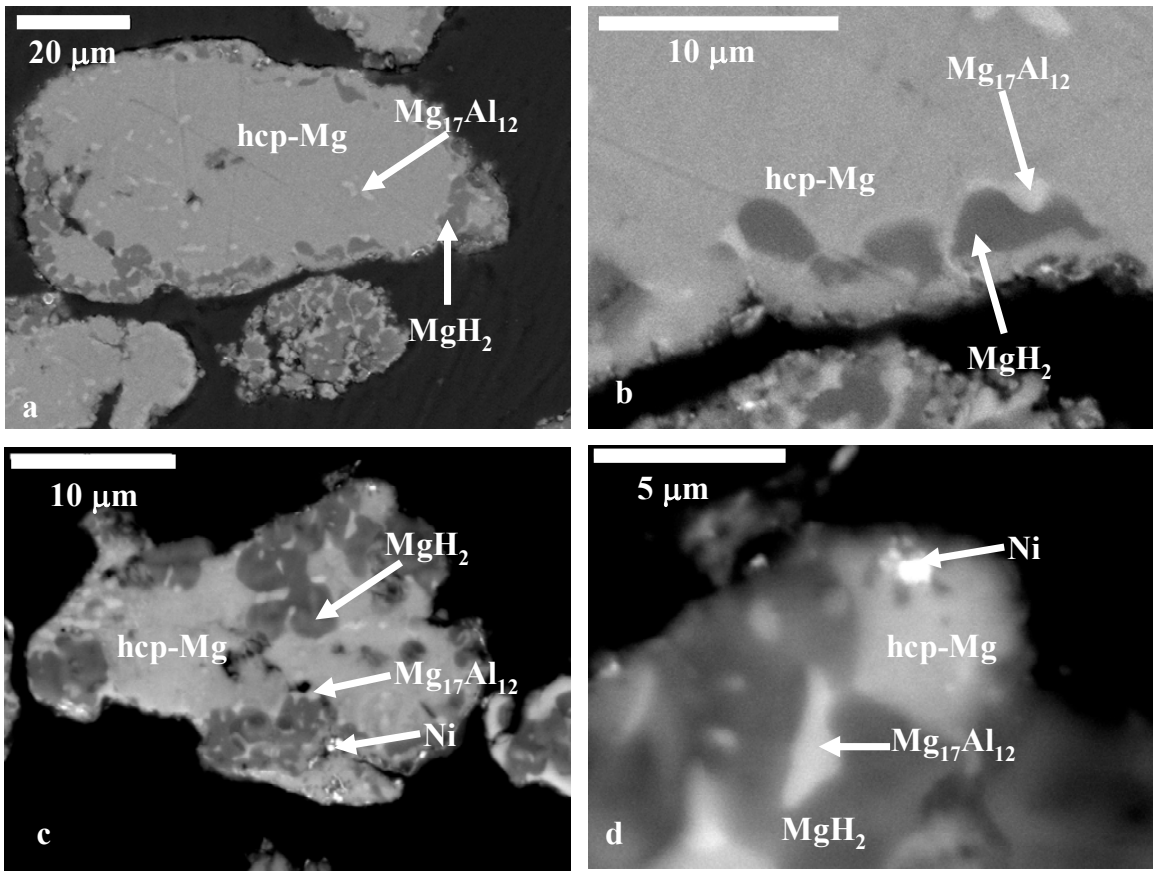

Figure 7-11. SEM/BSE micrographs of the partially dehydrogenated powders (a,c) revealing that dehydrogenation starts on the surface. (b,d) higher magnification micrographs indicating the nucleation of hcp-Mg.

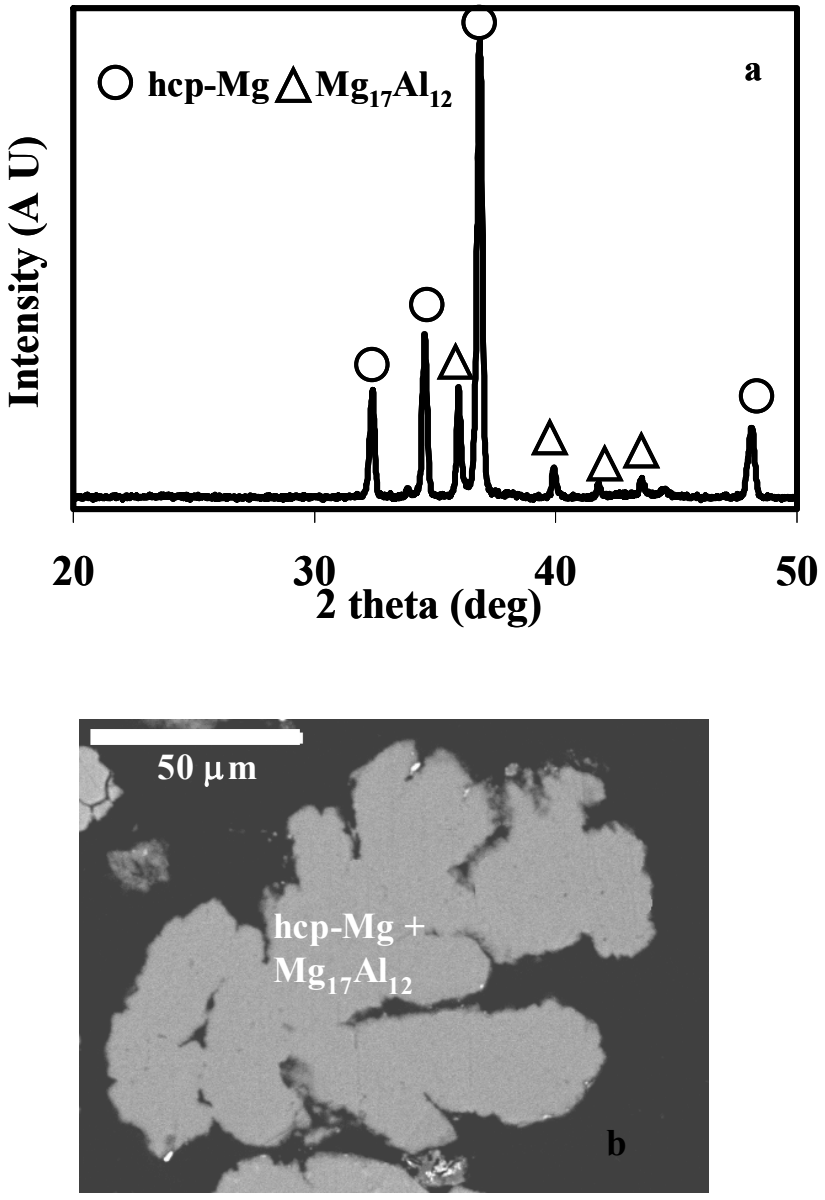

Figure 7-12. (a) XRD profile of an Mg-8at%Al powder after dehydrogenation in TGA, and (b) SEM/BSE micrograph of the un-hydrogenated particle.

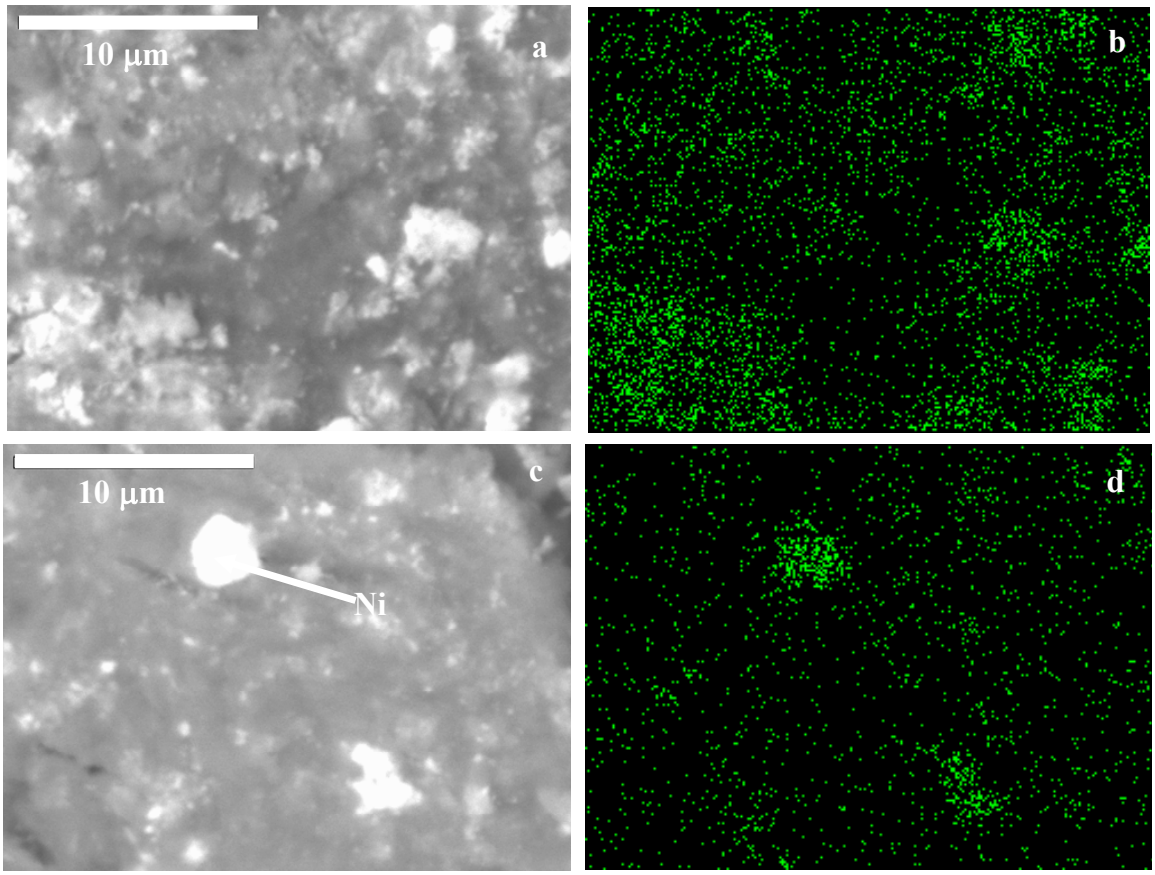

Figure 7-13. SEM/BSE micrographs and the corresponding EDS maps of Ni of Mg-8at%Al powders hydrogenated at 180°C revealing the differences in the Ni coating (amount of Ni) on different particles.

CHAPTER 8
LOW TEMPERATURE HYDROGEN ABSORPTION PHOENOMENON IN ELECTRODEPOSITED POWDERS

According to the DOE targets a suitable hydrogen storage material for PEM fuel cell technology require a gravimetric capacity of 2kWh/kg, a volumetric capacity of 1.5kWh/L and the hydrogen release temperature around 60- 80°C [127]. To achieve these requirements another class of materials, which are porous in nature, is being developed. These materials can adsorb or absorb hydrogen under high pressure and release at relatively low temperatures [128, 129]. The materials under consideration for this type of hydrogen storage are generally carbon based porous materials like carbon nanotubes, carbon nanofibers, fullerenes, graphite nanostrutctures [130]. In addition to these materials recent studies have shown that hydrogen can be physisorbed or chemisorbed into various porous metallic nanostructures like Ni nanoclusters and Pd nanostructures [131, 132]. The hydrogen absorption onto the carbon based materials is primarily attributed to their high surface area and the active bonds on the surface [130]. However, due to their low heat of adsorption, typically around 4-10kJ/mol, the adsorption can take place only at sub-zero temperatures and under high pressure of hydrogen. For example, an activated carbon is reported to absorb 7 wt% of hydrogen at 77K under a pressure of 20 MPa [129]. The maximum hydrogen absorption in carbon based materials reported at room temperature is about 2 wt% under 70 MPa pressure [133]. The major drawback of the carbon based materials is to produce ultra clean nanostructures with high surface area as the fabrication processes involves chemical routes and the absorption of hydrogen is a surface sensitive property. Furthermore, the absorption of hydrogen is possible only at subzero temperatures which is not very economic and feasible for practical applications.

Recently, metallic nanostructures have also been investigated for their hydrogen absorption properties. Nanostructures of d-block metals either supported by an organic frame work or

activated carbon are reported to adsorb 0.5-1.0 wt% of hydrogen at room temperature [134]. The mechanism for the adsorption on the metal surface is not clear. However, it is predicted that the spill over effect which describes the mechanism for catalysts could be the reason behind the absorption [134]. Similar studies have been reported in literature where the hydrogen is trapped inside the metal lattices [135]. Furthermore, in metals, it has been noticed that hydrogen can be chemisorbed into the meal lattice and can be stored near the vacancies, dislocations, grain boundaries, and at the interface of second phase particles [135, 136].

In this study, interesting observations were made during the hydrogen absorption of electrodeposited Mg-Al alloy powders at low temperatures and high pressures. Hydrogenation tests conducted at low temperatures around 40-100ºC and up to hydrogen pressure of 9MPa indicate that both the Ni coated and as deposited powders absorb hydrogen. The hydrogenation results and the possible reasons for the observed phenomenon are presented in this chapter.

8.1 Hydrogen Absorption in Electrodeposited Powders

Figure 8-1 presents the PCT curves of electrodeposited Mg-8at%Al alloy powder developed at 40 and 60°C in the as deposited form without coating with Ni. 0.02wt% hydrogen was absorbed into the material during the absorption part and even upon desorption, the material continued to absorb hydrogen till the pressure in the system reached 2MPa and the total amount of hydrogen absorbed was about 0.035wt%. This observation suggests that the Mg-Al powder was not saturated at each step during the absorption part. Below the pressure of 2 MPa, partial amount of hydrogen was released and after the PCT experiment about 0.028wt% of hydrogen was remained in the material. The PCT curve at 60°C developed after the 40°C illustrated that the hydrogen absorption increased from 0.03 wt% to 0.037 wt% and approximately 0.026wt% of hydrogen was remained in the powder.

However, in a different batch of Mg-8at%Al powders, which were prepared under similar conditions, a high amount of hydrogen (2.7 wt%) was absorbed into the material at low temperatures. Figure 8-2 illustrates the PCT curves at 40 and 60°C of the alloy powder fabricated in. Figure 8-2(a) reveals that about 2.6 wt% of hydrogen was absorbed by the powder at 40°C and 9 MPa pressure. A continuous increase of hydrogen absorption was noticed as the pressure of hydrogen increased in steps. During the initial part of desorption, 0.4wt% of hydrogen was released till the pressure in the system reached 8.5 MPa and upon further decrease in pressure hydrogen was not released significantly. Figure 8-2 (b) illustrates a PCT curve developed at 60°C. Interestingly during the absorption part of the PCT curve at 60°C, the alloy powder released hydrogen even as pressure of the system was increased. This phenomenon occurred till the pressure in the system reached 2 MPa. Approximately 1.3wt% of hydrogen was released during this part. After further increase in pressure above 2 MPa, the Mg-Al powder started to absorb hydrogen and finally the total content of hydrogen in the powder reached about 2 wt% at the maximum pressure of 9 MPa. The desorption part of the PCT curve followed a similar trend to that of the PCT curve at 40°C, where noticeable amount of hydrogen (0.3wt%) was released at high pressures followed by almost no hydrogen desorption. The results of the PCT curves at 40 and 60°C suggest that about 2-3 wt% hydrogen is absorbed into the material under high pressures and it is not released under these conditions. It should be noticed that the amount of hydrogen absorbed in a material fabricated under similar conditions exhibited much less hydrogen capacity (Compare Figures 8-1 and 8-2). Similar observations have been reported in the literature for carbon based materials. For example, in a particular study reported 65.55 wt% of hydrogen was adsorbed at room temperature and under 12 MPa pressure in graphite nanofibers [137]. However, these experiments have not been reproducible and the differences

were attributed to the varied surface conditions produced in different experiments. The inconsistency in the hydrogen absorption results of similar composition powders at low temperatures can be attributed to the surface condition of the powders.

8.2 Hydrogen Absorption in Ni coated Electrodeposited Powders

The PCT curves developed for the Ni coated Mg-8at%Al powders at 40 and 60ºC are shown in Figure 8-3. The powder employed for the Ni coating was taken from the same batch of powders fabricated to conduct the low temperature hydrogenation tests that were shown in Figure 8-1. The amount of hydrogen absorbed was approximately 0.07 wt% at 40°C and 0.075 wt% at 60°C. In contrast, to the uncoated powders, the hydrogen is released during the desorption part of the PCT curve at these temperatures. However only 0.03 wt% of the total hydrogen was released and about 0.04wt% of hydrogen remained in the material. It is noticed that same amount of hydrogen was present after the PCT curve at both the temperatures.

8.3 Discussion

The results observed in the present study suggest that electrodeposited Mg-Al alloy powders can absorb hydrogen in the temperature range of 40-100ºC. A comparison of solubility of hydrogen at high temperatures (350-400ºC, Table 5-5) and low temperatures (40-60ºC) in Ni-coated electrodeposited Mg-8at%Al powder reveals that higher amount of hydrogen is soluble in the powder at low temperatures and high pressures. However, at a constant pressure the solubility of hydrogen increased with increase in temperature. For example, at 1.89 MPa pressure (equilibrium plateau pressure of hydride formation at 395ºC), the solubility of hydrogen was about 0.02 wt% at 60ºC and 0.04wt% at 395ºC. Under the condition of low temperatures, the formation of magnesium hydride is hindered due to the high nucleation barrier and therefore, the Mg-Al alloy powder absorb continuously hydrogen at higher pressures.

However, the high amount of hydrogen absorption observed in the case presented in Figure 8-2 cannot be explained by the solubility of hydrogen. Specifically, at low temperatures, it has been reported that the hydrogen can be physisorbed on the surfaces at different active sites [134]. Further more, defects present in crystalline materials can act as hydrogen trapping sites [134]. Hydrogen atoms, due to their small size, occupy interstitial sites in the metal lattice and the diffusion of hydrogen in metals is reported to be very high [138]. For example, the diffusivity of hydrogen in vanadium is 2×10^{12} jumps per second which exceeds 15-20 orders of magnitude for interstitials like oxygen, nitrogen and hence can diffuse easily in the metal lattice [138]. In addition, the small size of hydrogen atom permits dense packing of hydrogen atoms in metal host lattices [134]. The above studies suggest that the hydrogen can be stored in various defects of the materials like dislocations, vacancies and grain boundaries. Therefore the amount of hydrogen trapped in a material depends on the microstructure, surface area, and the affinity of the host lattice towards hydrogen. Materials with large amount of defects and interfaces have been reported to absorb significant amount of hydrogen [131, 134, 139, 140]. For example, the solubility of hydrogen in the ball milled samples with high surface area, more of grain boundary area, dislocations and point defects has been reported to be higher than the conventional grain size materials [131]. In a niobium sample the solubility of hydrogen increased from 0.06H/Nb atom to 0.37H/Nb atoms when the grain size of the Nb was decreased from 200 nm to 10 nm. Therefore, the solubility of hydrogen observed in the present study can be explained by considering the microstructure of the electrodeposited material.

The hydrogen can be either physisorbed onto the surface or absorbed into the material. To verify the physisorption mechanism, the surface area of the powder was measured using the BET technique. The BET curve obtained is shown in Figure 8-4. This curve illustrates that the amount

of nitrogen absorbed at various pressures under standard conditions. By employing the molecule length of nitrogen, the total surface area is calculated. The BET surface area measurements indicated that the total connected surface area of the powder was about 1.1m^2/g. Assuming that a monolayer of hydrogen molecules was physisorbed on the surface of the powders, the hydrogen content absorbed in the experiments was calculated using diameter of the hydrogen molecule (289 $X10^{-12}$m) [141]. The amount of powder used during the PCT experiments was about 0.34 g. Using the BET surface area, the total amount of hydrogen absorbed on the powder is obtained as 0.2 wt%. The hydrogen calculated using this method is higher than the value observed in the PCT experiments for Ni coated powders. However, if the hydrogen is physisorbed on the surface, upon desorption the powder should release complete hydrogen as the activation energy for breaking the bonds in physisorption is very low. Hence, it can be concluded that the total hydrogen absorbed in the Mg-Al powder may not be due to physisorption. Furthermore, the high amount (2.5wt%) of hydrogen absorbed in uncoated powders can not be explained by this phenomenon.

Previously it was shown that the electrodeposited Al-Mg powders fabricated in our group can contain significant amount of porosity due to the deposition conditions [34]. Microstructural analysis of the electrodeposited powders conducted using TEM revealed that the Mg-rich Mg-Al powders also contain significant amount of porosity. The TEM micrographs of the Mg-Al powder investigated for these experiments are shown in Figure 8-5. The under focused and over focused micrographs in bright field mode are also presented along with the focused image to reveal the porosity of the electrodeposited powder. It can be noticed that significant amount of pores of different sizes are present in the material. The diffraction patterns corresponding to the image indicated that the material is hcp-Mg. The BET surface tests performed on the Mg-Al

powders will not include the surface area of the pores inside the material. Therefore, the physisorption of hydrogen inside the Mg-Al alloy powder may not be explained using the surface area obtained from the BET surface area calculations. The amount of closed porosity was investigated using the density measurements. The density of the Mg-Al powder was measured using the Pyknometer. The density value measured for uncoated Mg-Al powder was 1.7958 gm/cc. The theoretical density was calculated using the lattice parameter of Mg-8at%Al powder measured from XRD. The theoretical density of Mg-Al powder calculated was 1.8074 gm/cc. Even though the density values are not significantly different, the values suggest that closed pores are present in the electrodeposited powder and the volume fraction of pores was estimated to be 0.65%.

The amount of hydrogen absorbed (physisorbed) for the pore sizes noticed in TEM and in the range of observed porosity volume (0.5-1.0 % of volume porosity) are calculated. It is assumed that a monolayer of hydrogen is formed on the surface of the pore. The total surface area of the available pores in the powder was calculated and the diameter of the hydrogen molecule, as mentioned in the literature, was used to calculate the total amount of hydrogen absorbed [141]. From the TEM micrographs it can be noticed that different sizes of pores are present. The calculations carried out suggest that the maximum amount of hydrogen that can be physisorbed into the pores is about 0.06wt % for an average pore size of 30 nm with 0.65 volume % of porosity.

Initial studies on electrodeposited fcc-Al rich powders indicated that hydrogen can also be absorbed in the material. These alloy powders were prepared under similar electrodeposition conditions as that of the hcp-Mg rich alloy powders and showed extensive porosity. The hydrogenation curve of an fcc-Al rich powder at 100ºC is presented in Figure 8-6. The total

amount of hydrogen absorbed into the material was observed to be very low around 50 micro moles. The weight percent of the hydrogen was not calculated as the weight of the powder used was not known but based on our previous experiments it can be predicted that 0.4-0.5 wt% of hydrogen was absorbed in this experiment. When the temperature of the PCT experiment was increased from 100ºC to 150ºC under a hydrogen pressure of 4.6 MPa, a release of hydrogen was observed as shown in Figure 8-7. This observation, which is similar to the finding for the Mg-rich powders, suggests that higher activation energy is required to release hydrogen from the Mg-Al powder. These results suggest that the absorption of hydrogen is independent of the composition of the powders but depends on the microstructure.

Based on the results observed in this study and the calculations carried out, the unusual high hydrogen absorption capacity of the powders produced in this study at low temperatures can partially be attributed to the physisorption of hydrogen in the porous structure and the high surface to volume ratio of the electrodeposited powders. However, the further work is needed to address the large amount of hydrogen absorption and the fact that it is not released when the pressure is reduced.

8.4 Summary

The results of this study reveal that electrodeposited nanoporous nanocrystalline Mg-Al powders can potentially absorb large quantity of hydrogen (2.5wt%), i.e. beyond the solubility limit, at low temperatures and high pressures without formation of a hydride phase. The lack of repeatability of this phenomenon is consistent with previously reported studies on hydrogen absorption in high surface area materials. Such inconsistencies suggest that the surface condition plays an important role in the hydrogen capacity at low temperatures. Coating of Ni is associated with the treatment of the electrodeposited powders with chemicals and the low absorption of hydrogen may suggest that the surface of the powder is changed during this procedure. The

calculations based on the physisorption of the material did not explain the observed high capacity. The fact that hydrogen release requires thermal activation suggests that it is trapped in the material rather than physisorped.

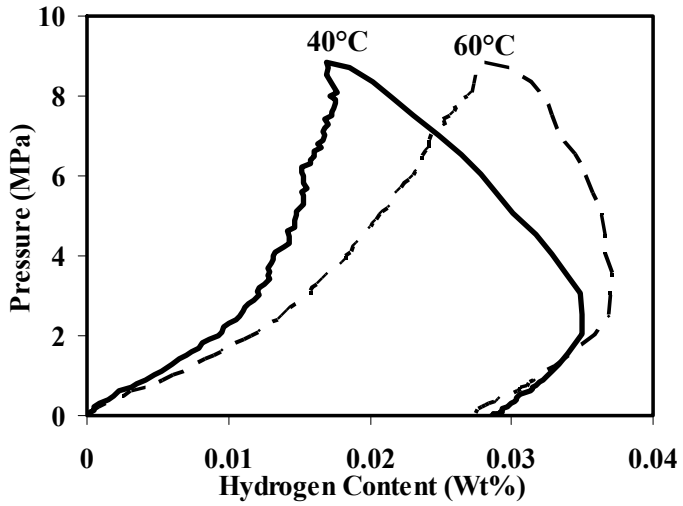

Figure 8-1. PCT curves developed at (a) 40°C (b) 60°C for electrodeposited Mg-8at%Al alloy powder without Ni coating

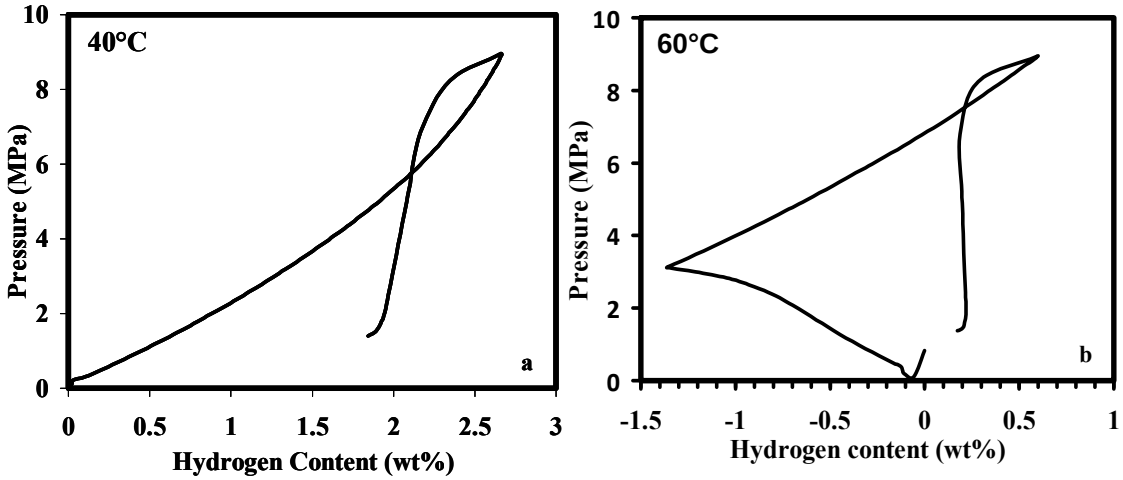

Figure 8-2. PCT curves for electrodeposited Mg-8at%Al alloy powder developed at (a) 40°C (b) 60°C from another batch of electrodeposited powders without Ni coating.

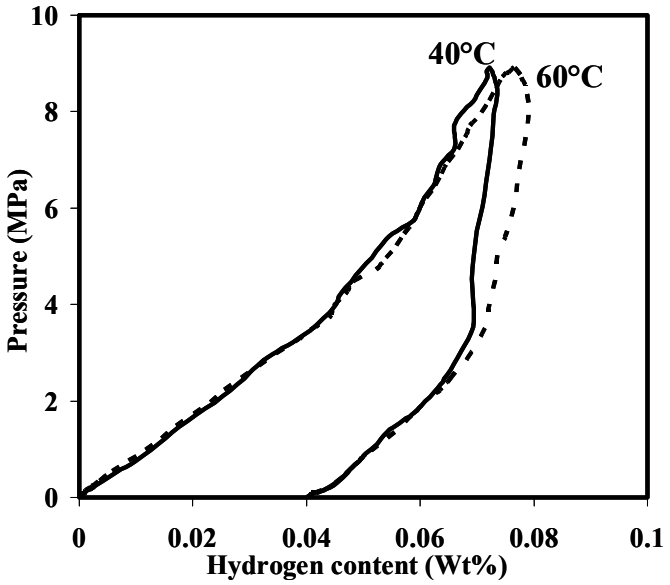

Figure 8-3. PCT curves of Ni coated Mg-8at%Al alloy powder at 40 and 60°C.

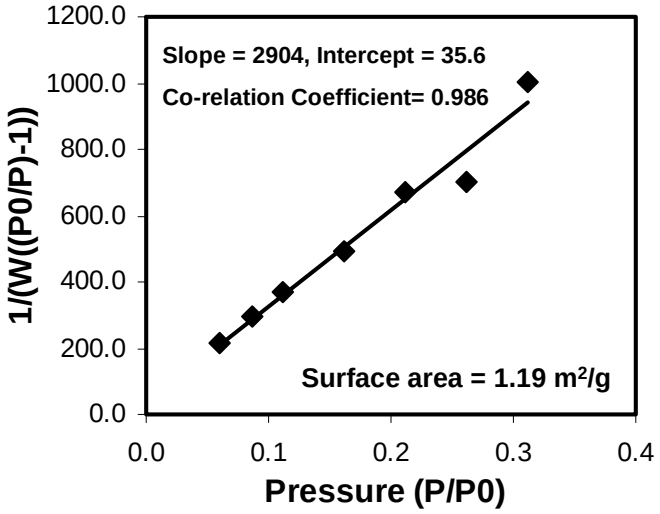

Figure 8-4. BET curve developed for measuring the surface area of the Mg-8at%Al alloy powder.

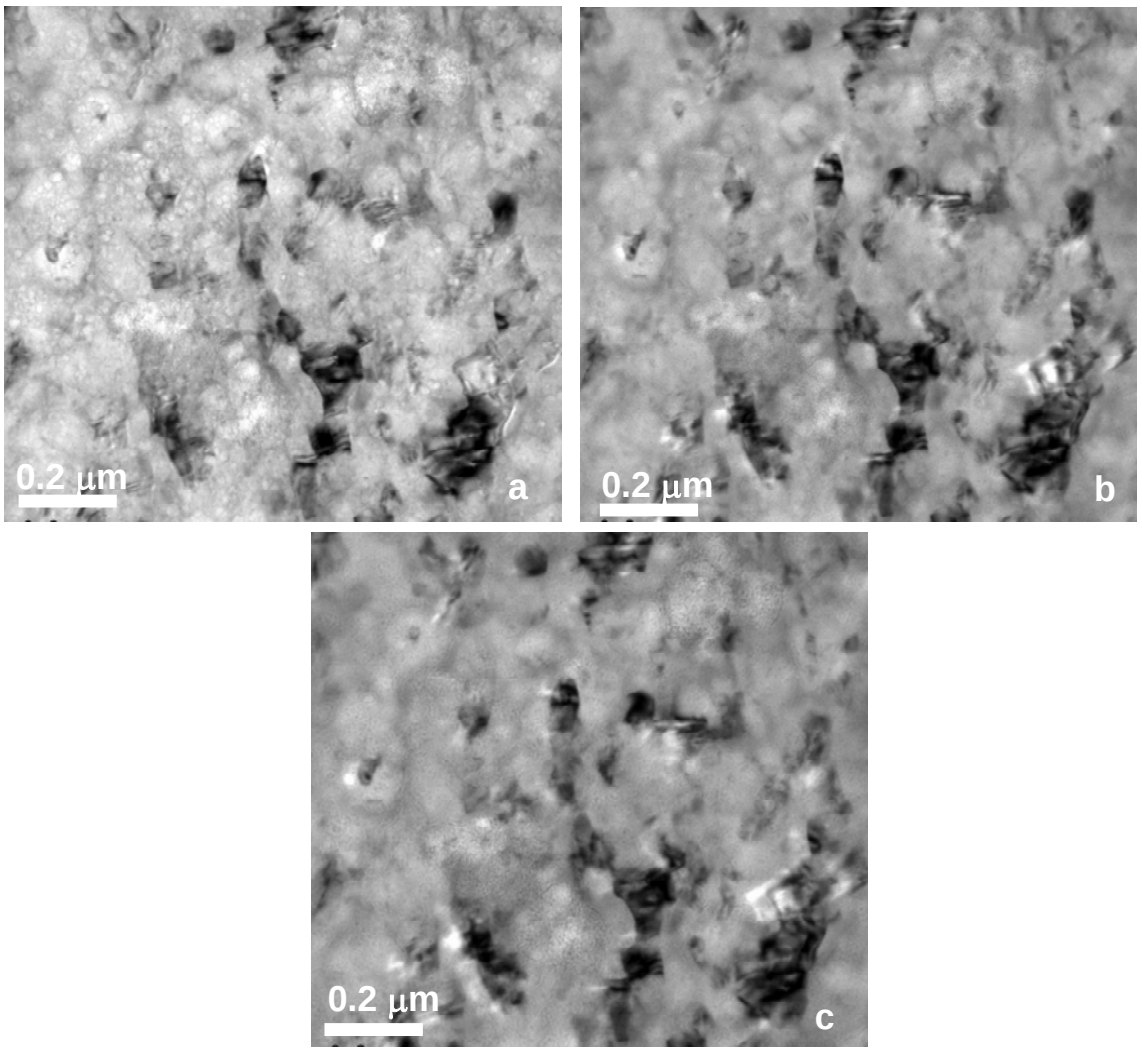

Figure 8-5. TEM micrographs of Mg-Al powder revealing its porosity, (a) underfocussed image, (b) focused image, and (c) over focused image.

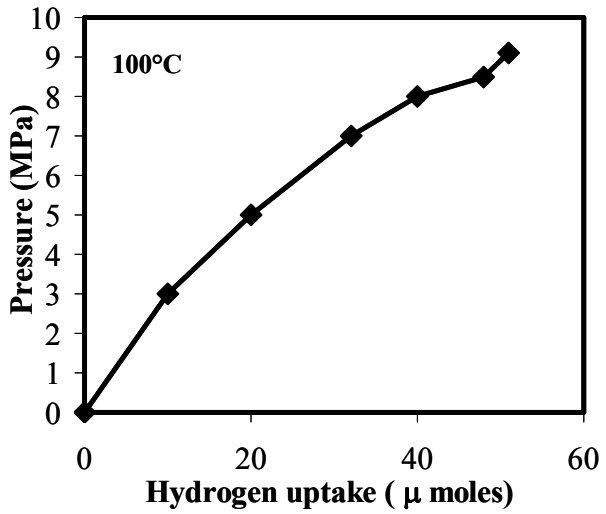

Figure 8-6. Hydrogen absorption curves of Al-Mg powder at 100°C.

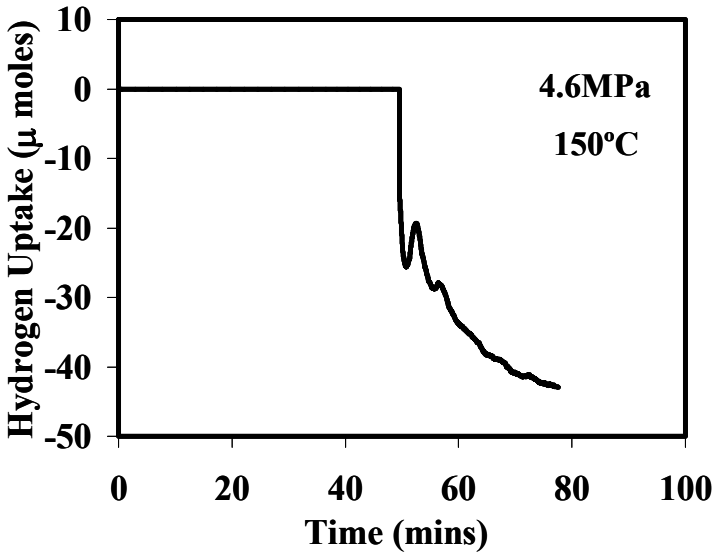

Figure 8-7.Hydrogen absorption curves of Al-Mg powder at 150°C. Hydrogen uptake vs time curve indicating the release of hydrogen at 4.6MPa.

CHAPTER 9
CONCLUSIONS AND FUTURE WORK

The hydrogenation and dehydrogenation characteristics of Mg-Al alloy powders with 0-10at% Al in hcp-Mg in the temperature range of 180-400°C were established. The Mg-Al alloy powders were fabricated using the electrodeposition technique and the amount of Al in hcp-Mg phase was varied from 4 to 12 at%. The processed Mg-Al powders were coated with Ni as catalyst to enhance the kinetics of hydrogen absorption and desorption. Even though the electrodeposition parameters were selected to produce supersaturated solid solution of Al in hcp-Mg, the formation of intermetallic compound $Mg_{17}Al_{12}$ was observed to be inevitable due to the conditions present during the powder processing and Ni coating. A commercial powder was employed for studying pure Mg.

The de/hydrogenation characteristics of the Mg-Al and pure Mg powders under equilibrium conditions were established by developing the Pressure Composition Temperature (PCT) curves in the temperature range of 275-400°C. A plateau region was observed during the absorption part of the PCT curve for pure Mg powder signifying the formation of magnesium hydride. However, instead of a plateau region an increasing slope of hydrogen absorption with pressure was found in Mg-Al alloy powders at 350°C. The sloping curve during the hydrogen absorption of Mg-Al alloy powder was due to involvement of more than 2 phases during the hydrogen absorption. The slope of the PCT curves was observed to depend on the composition and the time allowed to the reach the equilibrium during the experiments.

The PCT curves for the electrodeposited Mg-Al powders were divided into various stages based on the changes in the slope of the curves. The extent of each stage was found to depend on the composition of the powder studied. Microstructural and compositional analyses revealed that Al is rejected from MgH_2 during its formation. The rejected Al dissolves in the available hcp-Mg

and precipitates as $Mg_{17}Al_{12}$ and Al_3Mg_2 intermetallic compounds, which were observed to hydrogenate at higher pressures. The high diffusivity of Al at these temperatures and the equilibrium conditions provided during the experiment causes Al to diffuse away from the MgH_2 and precipitate as fcc-Al phase. These results show that under equilibrium conditions, MgH_2 has very low solubility for Al even at high temperatures, consistent with phase diagram predictions [112]. The equilibrium plateau pressures of magnesium hydride formation for hcp-Mg, $Mg_{17}Al_{12}$ and Al_3Mg_2 increase in that order. Interestingly it was noticed, that the hydrogenation of the powders did not take place homogeneously during the absorption process.

Desorption of hydrogen from the hydrogenated Mg-Al powders took place at a relatively constant pressure, which is consistent with the absence of Al in the magnesium hydride. The plateau pressure of dissociation of MgH_2 was lower than that of the plateau pressure of hydride formation and caused the hysteresis in the PCT curve. At a given temperature, the hysteresis was higher for pure Mg powders than that of Mg-Al powders. The observed hysteresis is believed to be due to the high energy barrier for nucleation of the hcp-Mg phase, which requires a lower pressure than the equilibrium pressure. The difference in the hydrogenation and dehydrogenation pressures at a given temperature, i.e. the degree of hysteresis, was smaller for the Mg-Al powders than that of the pure Mg powder.

Although the equilibrium pressure of formation increased at a given temperature with the addition of Al, the enthalpy of formation/dissociation of magnesium hydride, calculated from Van't Hoff plots, was found not to be affected significantly. This lack of influence, despite the theoretical prediction that Al should reduce this enthalpy by a factor of 3, is attributed to the absence of Al in the MgH_2 crystal lattice under equilibrium conditions that exist during the development of PCT curves.

Dehydrogenation of the Mg-Al powders was found to start on the surface of the powders producing hcp-Mg phase. This phase dissolved the available fcc-Al phase and formed the intermetallic compound $Mg_{17}Al_{12}$. After complete desorption, the phases and the microstructure of the powders were similar to that of the initial powders and therefore the powders could be recycled for further hydrogenation experiments.

Hydrogenation studies accompanied by detailed microstructural and compositional evaluations of Mg-Al powders in the temperature range of180ºC to 280ºC at 1MPa pressure demonstrated that the addition of Al may enhance the kinetics of hydrogenation due to the presence of $Mg_{17}Al_{12}$ precipitates which act as nucleation site for the hydride phase. On the other hand, the rejection of Al that leads to the formation of more intermetallic phase limits the total hydrogen capacity of these alloy powders.

The compositional analysis using EPMA and lattice parameter calculations using XRD showed that the MgH_2 produced at 210ºC and 180ºC at 1 MPa pressure contained Al, whose amount increased with a decrease in the hydrogenation temperature. This observation suggests that under non-equilibrium conditions Al can be trapped in the MgH_2 lattice.

The hydrogen release in Mg-Al powders was observed to take place in two stages in the temperature ranges of 90-150ºC and 250-330ºC when the MgH_2 was developed at 210ºC and 180ºC hydrogenation temperatures. However, MgH_2 produced at 280ºC from Mg-Al alloy powders released hydrogen at 430ºC. The change in the release temperature is attributed to the trapping of Al in the MgH_2 phase when produced under non-equilibrium conditions, consistent with the theoretical predictions. The two stage release behavioris believed to be associated with the inhomogeneous distribution of Ni in a batch of powders.

Suggested Future Work: In this dissertation we have shown that the hydrogen release temperature of MgH_2 can be reduced significantly by addition of Al. The results of this study demonstrate that Al can be incorporated into MgH_2 by fabricating the hydride under non-equilibrium conditions. However, several phenomenons were not completely understood to design these materials for the intended application. In order to fully understand this phenomenon, further investigations to understand the microstructure and phase transformations are required. For example, formation of intermetallic compound $Mg_{17}Al_{12}$ is inevitable during the hydrogenation/dehydrogenation processes. Hence an understanding of this formation will help in the design of microstructure. Based on the results in Chapter 7 we have shed some light on the effect of amount of catalyst and the mechanism that helps in dehydrogenation. It is worth studying the effect of different amounts of catalyst as its content should be optimized for the optimum performance. The desorption results carried out in this study indicate that the dehydrogenation temperature is reduced but no kinetic analysis was carried out. Hence, a kinetic study on desorption of the hydrogen from these materials is required to understand the various rate limiting mechanisms.

REFERENCES

[1] Gross KJ, Chartouni D, Leroy E, Zuttel A, Schlapbach L. J Alloys Comp 1998;269:259.

[2] Varin RA, T C, Z.S W. Nanomaterials for solid state hydrogen storage, 2009.

[3] Schlapbach L, Zuttel A. Nature 2001;414:353.

[4] Bowman RC, Fultz B. MRS Bull. 2002;27:688.

[5] Sandi. G. The electrochem soc Inter 2004;13:40.

[6] Dornheim. M, Klassen. T, Bormann. R. Jap Soc Prom Sci 2004:1.

[7] Chandra. D, Reilly JJ, Chellappa R. J Metals 2006.

[8] Douglass DL. Metall Trans A 1975;6:2179.

[9] Sakintuna B, Lamari-Darkrim F, Hirscher M. Int. J. Hydrogen Energy 2007;32:1121.

[10] Fukai Y, Metal-Hydrogen system, Germany, Springer series in Materials Science 2005.

[11] Stampfer JF, Holley CE, Suttle JF. J Amer Chem Soc 1960;82:3504.

[12] Zeng K, Klassen T, Oelerich W, Bormann R. Int. J. Hydrogen Energy 1999;24:989.

[13] Bogdanovic B, Bohmhammel K, Christ B, Reiser A, Schlichte K, Vehlen R, Wolf U. J Alloys Comp 1999;282:84.

[14] Klose W, Stuke V. Chemie Ingenieur Technik 1992;64:360.

[15] Stander CM. J Inorg Nuc Chem 1977;39:221.

[16] Liang GX, Wang ED, Fang SS. J Alloys Comp 1995;223:111.

[17] Liang G, Boily S, Huot J, Van Neste A, Schulz R. J Alloys Comp 1998;267:302.

[18] Song Y, Guo ZX, Yang R. Phys Rev B 2004;69:094205.

[19] Zaluska A, Zaluski L, Strom-Olsen JO. J Alloys Comp 1999;288:217.

[20] Liang G, Huot J, Boily S, Van Neste A, Schulz R. J Alloys Comp 1999;292:247.

[21] Eisenberg FG, Zagnoli DA, Sheridan JJ. J Less-Common Metals 1980;74:323.

[22] Li S, Jena P, Ahuja R. Phys Rev B 2006;74.

[23] Zaluska A, Zaluski L, Strom-Olsen JO. J Alloys Comp 1999;289:197.

[24] Song Y, Guo ZX, Yang R. Mater Sci Engg a-Struct Mater Props Microstruct Proces 2004;365:73.

[25] Mintz MH, Gavra Z, Kimmel G, Hadari Z. J Less-Common Metals 1980;74:263.

[26] Andreasen A, Sorensen MB, Burkarl R, Moller B, Molenbroek AM, Pedersen AS, Andreasen JW, Nielsen MM, Jensen TR. J Alloys Comp 2005;404:323.

[27] Binary Alloy Phase Diagrams, ASM Handbook; 3, .

[28] Bouaricha S, Dodelet JP, Guay D, Huot J, Boily S, Schulz R. J Alloys Comp 2000;297:282.

[29] Gavra Z, Hadari Z, Mintz MH. J Inorg Nuc Chem 1981;43:1763.

[30] El-Amoush AS. J Alloys Comp 2007;441:278.

[31] Bououdina M, Guo ZX. J Alloys Comp 2002;336:222.

[32] Urgnani J, Di Chio M, Palumbo M, Feuerbacher M, Fernandez JF, Leardini F, Baricco M. J Phys 2009;144.

[33] Sankara Sarma V. Tatiparti, Ebrahimi F. J. Electrochem. Soc. 2008;155:D363.

[34] Tatiparti SSV. “Fabrication Of Nanocrystalline Al-Mg Alloy Powders By Electrodeposition And Their Characterization”, PhD University of Florida, 2008. p.166.

[35] Yao XD, Wu CZ, Du AJ, Lu GQ, Cheng HM, Smith SC, Zou J, He YH. J Phys Chem B 2006;110:11697.

[36] Schlapbach L, Seiler A, Stucki F, Siegmann HC. J Less-Common Metals 1980;73:145.

[37] Suda S, Kobayashi N, Yoshida K. J Less-Common Metals 1980;73:119.

[38] Bogdanovic B, Claus KH, Gurtzgen S, Spliethoff B, Wilczok U. J Less-Common Metals 1987;131:163.

[39] Zaluski L, Zaluska A, StromOlsen JO. J Alloys Comp 1997;253:70.

[40] Zaluska A, Zaluski L, Strom-Olsen JO. Appl Phys A 2001;72:157.

[41] Noritake T, Towata S, Aoki M, Seno Y, Hirose Y, Nishibori E, Takata M, Sakata M. J Alloys Comp 2003;356:84.

[42] Bastide JP, Bonnetot B, Letoffe JM, Claudy P. Mater Res Bull 1980;15:1779.

[43] Liang G. J Alloys Comp 2004;370:123.

[44] Oskarsson F, Stier W, Camargo LG, Jonsson H. Abs Papers Amer Chem Soc 2005;229:U852.

[45] Zaluski L, Zaluska A, Stromolsen JO. J Alloys Comp 1995;217:245.

[46] Vegge T, Hedegaard-Jensen LS, Bonde J, Munter TR, Norskov JK. J Alloys Comp 2005;386:1.

[47] Huot J, Liang G, Schulz R. Appl Phys A 2001;72:187.

[48] Zaluski L, Zaluska A, Tessier P, Stromolsen JO, Schulz R. J Alloys Comp 1995;217:295.

[49] Liang G, Huot J, Boily S, Schulz R. J Alloys Comp 2000;305:239.

[50] Kelkar T, Pal S, Kanhere DG. Chem Phys Chem 2008;9:928.

[51] Bououdina M, Grant D, Walker G. Int. J. Hydrogen Energy 2006;31:177.

[52] Stander CM. Zeitschrift Fur Phys Chem 1977;104:229.

[53] Zhang QA, Wu HY. Mater. Chem. Phys. 2005;94:69.

[54] Vigeholm B, Kjoller J, Larsen B, Pedersen AS. Int. J. Hydrogen Energy 1983;8:809.

[55] Tessier P, Enoki H, Bououdina M, Akiba E. J Alloys Comp 1998;268:285.

[56] Zaluski L, Zaluska A, Tessier P, Stromolsen JO, Schulz R. J Alloys Comp 1995;227:53.

[57] Imamura H, Masanari K, Kusuhara M, Katsumoto H, Sumi T, Sakata Y. J Alloys Comp 2005;386:211.

[58] Charbonnier J, de Rango P, Fruchart D, Miraglia S, Pontonnier L, Rivoirard S, Skryabina N, Vulliet P. J Alloys Comp 2004;383:205.

[59] Asano K, Akiba E. J Alloys Comp 2009;481:L8.

[60] Gubicza J, Kassem M, Ungar T. Euro Pow Diff Epdic 8 2004;443-4:103.

[61] Borgschulte A, Bosenberg U, Barkhordarian G, Dornheim M, Bormann R. Cata Today 2007;120:262.

[62] Ebrahimi F, Zhai Q, Kong D. Scrip Mater 1998;39:315.

[63] Jovic VD, Jovic BM, Pavlovic MG. Acta Electrochim 2006;51:5468.

[64] Murray JL. Bulletin of Alloy Phase Diagrams 1982;3.

[65] El-Amoush AS. J Alloys Comp 2008;463:475.

[66] Crivello JC, Nobuki T, Kato S, Abe M, Kuji T. J Alloys Comp 2007;446:157.

[67] Yabe H, Kuji T. J Alloys Comp 2007;433:241.

[68] Gubicza J, Kassem M, Ribarik G, Ungar T. Mater Sci Engg 2004;372:115.

[69] Nie JF, Xiao XL, Luo CP, Muddle BC. Micron 2001;32:857.

[70] Crawley AF, Lagowski B. Metall Trans 1974;5:949.

[71] Duly D, Zhang WZ, Audier M. Philos Mag A 1995;71:187.

[72] Liang G, Schulz R. J Mater Sci 2003;38:1179.

[73] Qian S, Northwood DO. Int. J. Hydrogen Energy 1988;13:25.

[74] Schwarz RB, Khachaturyan AG. Acta Mater 2006;54:313.

[75] Schwarz RB, Khachaturyan AG. Phys Rev Lett 1995;74:2523.

[76] Rabkin E, Skripnyuk VM. Scripta Materialia 2003;49:477.

[77] Huot J, Liang G, Boily S, Van Neste A, Schulz R. J Alloys Comp 1999;295:495.

[78] Gross KJ, Spatz P, Zuttel A, Schlapbach L. J Alloys Comp 1996;240:206.

[79] Zhang Y, Tsushio Y, Enoki H, Akiba E. J Alloys Comp 2005;393:147.

[80] Andreasen A. Int. J. Hydrogen Energy 2008;33:7489.

[81] Fernandez JF, Leardini F, Bodega J, Sanchez C, Joubert JM, Cuevas F, Leroy E, Baricco M, Feuerbacher M. J Alloys Comp 2009;472:565.

[82] Sandrock G. J Alloys Comp 1999;295:877.

[83] Schulz R, Huot J, Liang G, Boily S, Lalande G, Denis MC, Dodelet JP. Mater Sci Engg A 1999;267:240.

[84] Pozzo M, Alfe D. Int. J. Hydrogen Energy 2009;34:1922.

[85] Fleisch T, Abermann R. J. Catal. 1977;50:268.

[86] Rivoirard S, de Rango P, Fruchart D, Charbonnier J, Vempaire D. J Alloys Comp 2003;356:622.

[87] Bazzanella N, Checchetto R, Miotello A. Appl. Phys. Lett. 2004;85:5212.

[88] Holtz RL, Imam MA. J Mater Sci 1999;34:2655.

[89] Bhat V, Rougier A, Aymard L, Nazri GA, Tarascon JM. Int. J. Hydrogen Energy 2007;32:4900.

[90] Recham N, Bhat VV, Kandavel A, Aymard L, Tarascon JM, Rougier A. J Alloys Comp 2008;464:377.

[91] Oelerich W, Klassen T, Bormann R. Adv. Eng. Mater. 2001;3:487.

[92] Barkhordarian G, Klassen T, Bormann R. J Phys Chem B 2006;110:11020.

[93] Norskov JK, Houmoller A, Johansson PK, Lundqvist BI. Phys Rev Lett 1981;46:257.

[94] Tsuda M, Dino WA, Kasai H, Nakanishi H, Aikawa H. Thin Solid Films 2006;509:157.

[95] Au M, Wu J, Wang QD. Int. J. Hydrogen Energy 1995;20:141.

[96] Gremaud R, Borgschulte A, Lohstroh W, Schreuders H, Zuttel A, Dam B, Griessen R. J Alloys Comp 2005;404:775.

[97] Shang CX, Bououdina M, Song Y, Guo ZX. Int. J. Hydrogen Energy 2004;29:73.

[98] Huot J, Liang G, Boily S, Van Neste A, Schulz R. International Symposium on Metal-Hydrogen System, p.135 1998.

[99] Gennari FC, Castro FJ, Urretavizcaya G. J Alloys Comp 2001;321:46.

[100] Huang ZG, Guo ZP, Calka A, Wexler D, Wu J, Notten PHL, Liu HK. Mater Sci Engg A 2007;447:180.

[101] Imamura H, Tabata S, Shigetomi N, Takesue Y, Sakata Y. J Alloys Comp 2002;330:579.

[102] Li.H, PhD. Gainesville 2004;University of Florida.

[103] Walsh FC, Herron ME. J Phys D 1991;24:217.

[104] Bazzanella N, Checchetto R, Miotello A, Sada C, Mazzoldi P, Mengucci P. Appl. Phys. Lett. 2006;89.

[105] Bogdanovic B. 'Method of preparing active magnesium-hydride or magnesium hydrogen storer systems' vol. US Patent 4,554,152, 1985.

[106] Checchetto R, Trettel G, Miotello A. Meas. Sci. Technol. 2004;15:127.

[107] Blach TP, Gray EM. J Alloys Comp 2007;446:692.

[108] Cullity BD, Stock SR. Elements of X-Ray Diffraction: Prentice Hall, Newyork, 2001.

[109] Klose W, Stuke V. Int. J. Hydrogen Energy 1995;20:309.

[110] Fromageau R, Hillairet J, Ligeon E, Mairy C, Revel G, Tzanetakis P. J Appl Phys 1981;52:7191.

111] Shang CX, Bououdina M, Guo ZX. Mater Trans 2003;44:2356.

[112] Palumbo A, Torres FJ, Ares JR, Pisani C, Fernandez JF, Baricco A. Calphad-Comp Coupling of Phase Diagrams and Thermochemistry 2007;31:457.

[113] Huang YC, Watanabe T, Komatsu R. Proceedings of 4th International Conference in Vacuum Metallurgy 1973:176.

[114] Takamura H, Miyashita T, Kamegawa A, Okada M. J Alloys Comp 2003;356:804.

[115] ASM Handbook 'Alloy Phase Diagrams' , vol. 3, online resource.

[116] Braszczynska-Malik KN. J Alloys Comp 2009;477:870.

[117] Schimmel HG, Kearley GJ, Huot J, Mulder FM. J Alloys Comp 2005;404-406:235.

[118] Tien HY, Tanniru M, Wu CY, Ebrahimi F. Int. J. Hydrogen Energy 2009;34:6343.

[119] Tanniru M, Ebrahimi F. Int J Hydrogen Energy 2009;Submitted.

[120] Shannon RD. Acta Crystall Section A 1976;32:751.

[121] Kim DJ. J Amer Cer Soc 1989;72:1415.

[122] Hong SJ, Virkar AV. J Amer Cer Soc 1995;78:433.

[123] American Society for Testing Materials, 35-1185 F. ASTM 1996.

[124] American Society for Testing Materials, 967-03 E. ASTM 1996.

[125] Shobit O, Eric DW, Jacob LJ, Juan CN. J Amer Cer Soc 2009;9999.

[126] Skripnyuk V, Buchman E, Rabkin E, Estrin Y, Popov M, Jorgensen S. J Alloys Comp 2007;436:99.

[127] Lennie Klebanoff, Materials Go/No-Go Decisions Made Within the Department of Energy Metal Hydride Center of Excellence (MHCoE), Oct 2007, http://www1.eere.energy.gov/hydrogenandfuelcells/news_detail.html?news_id=11721, Aug 2008.

[128] Benard P, Chahine R. Scrip Mater 2007;56:803.

[129] Jorda-Beneyto M, Suarez-Garcia F, Lozano-Castello D, Cazorla-Amoros D, Linares-Solano A. Carbon 2007;45:293.

[130] Sahaym U, Norton MG. J Mater Sci 2008;43:5395.

[131] Andrievski RA. Phys Uspekhi 2007;50:691.

[132] Zielinski M, Wojcieszak R, Monteverdi S, Mercy M, Bettahar MM. Cata Comm 2005;6:777.

[133] de la Casa-Lillo MA, Lamari-Darkrim F, Cazorla-Amoros D, Linares-Solano A. The J Phys Chem B 2002;106:10930.

[134] Pundt A, Kirchheim R. Ann Rev Mater Res 2006;36:555.

[135] Turnbull A. Corro Sci 1993;34:921.

[136] Krom A, Bakker A. Metall Mater Trans B 2000;31:1475.

[137] Chambers A, Park C, Baker RTK, Rodriguez NM. The J Phys Chem B 1998;102:4253.

[138] Volkl J, Schauman.G, Alefeld G. J Phys Chem Solids 1970;31:1805.

[139] Makenas BJ, Birnbaum HK. Acta Metall 1980;28:979.

[140] Schober T. Metall Trans 1981;12 A:951.

[141] Cheng JR, Yuan XH, Zhao L, Huang DC, Zhao M, Dai L, Ding R. Carbon 2004;42:2019.

BIOGRAPHICAL SKETCH

Mahesh Tanniru was born in 1982, at Hyderabad, Andhra Pradesh, India. He did his bachelor's degree in metallurgical engineering from Jawaharlal Nehru Technological University at Hyderabad in 2003. He received his master's degree in chemical engineering from the University of Louisiana at Lafayette in 2005. Mahesh joined the Materials Science and Engineering Department at University of Florida in Fall 2005 for his PhD and joined Dr. Fereshteh Ebrahimi's group in Summer 2006.